Explosive activity in flood lava eruptions: A case study of the 10th century Eldgjá eruption, Iceland

William Michael Moreland

Faculty of Earth Sciences
University of Iceland
2017

Explosive activity in flood lava eruptions: A case study of the 10th century Eldgjá eruption, Iceland

William Michael Moreland

Dissertation submitted in partial fulfilment of a
Philosophiae Doctor degree in Geology

Advisors and PhD Committee

Prof Thorvaldur Thordarson, Professor in Volcanology and Petrology
University of Iceland

Gudrun Larsen, Emeritus Research Professor
University of Iceland

Prof Bruce F. Houghton, Gordon A. MacDonald Chair in Volcanology
University of Hawai'i at Mānoa

Opponents

Dr Corrado Cimarelli, Faculty Staff
Ludwig Maximilians Universität, Germany

Prof Valentin R. Troll, Chair of Petrology
University of Uppsala, Sweden

Faculty of Earth Sciences
School of Engineering and Natural Sciences
University of Iceland
Reykjavik, July 2017

Explosive activity in flood lava eruptions: A case study of the 10th century Eldgjá eruption, Iceland
Explosive activity in flood lava eruptions
Dissertation submitted in partial fulfilment of a *Philosophiae Doctor* degree in Geology

Faculty of Earth Sciences
School of Engineering and Natural Sciences
University of Iceland
Öskju, Sturlugötu 7
101, Reykjavik
Iceland

Telephone: 525 4000

Bibliographic information:
William Michael Moreland, 2017, *Explosive activity in flood lava eruptions: A case study of the 10th century Eldgjá eruption, Iceland*, PhD dissertation, Faculty of Earth Sciences, University of Iceland, 92 pp.

ISBN 978-9935-9306-6-8
Author ORCID: 0000-0002-5801-1496

Printing: Háskólaprent
Reykjavik, Iceland, July 2017

Abstract

The 10th century Eldgjá flood lava eruption, southern Iceland, was the most voluminous eruption on Earth in the last 1100 years, erupting up to 21.0 km^3 of transitional alkali basaltic magma of rather uniform composition. While 19.7 km^3 was erupted as lava in the form of two extensive lava fields covering 780 km^2 in total, 1.3 km^3 (dense rock equivalent) was erupted as tephra in at least 16 explosive phases. The Eldgjá vents form a ~70-km discontinuous mixed cone-row which stretches from beneath Mýrdalsjökull to the edge of Vatnajökull.

Explosive activity took place as discrete events restricted to distinct lengths of the fissure and alternated between subglacial and subaerial until phase 10 after which all activity was subaerial. Each phase contributed a tephra unit to what became a thick composite tephra deposit over 2 m thick 10 km away from source. Eruption column heights are estimated to have reached between 11 and 18 km, well above the 10-km tropopause above Iceland. The combination of subaerial and subglacial vents lead to both magmatic and phreatomagmatic tephra being produced. Individual explosive phases have been classified as Plinian and Phreatoplinian.

Vesicle-size analysis reveals that the magma beneath all Eldgjá fissure segments had identical vesiculation histories. However, total grain-size distributions of magmatic and phreatomagmatic tephra exhibit stark differences with the magmatic having one medium lapilli mode and the phreatomagmatic having one broad peak of medium lapilli to medium ash and a narrower peak of very fine ash. Thermal granulation is suspected as having reduced lapilli-sized magmatic foam into finer particles but without adding intensity to the eruption.

Útdráttur

Eldgjárgosið á 10. öld, sem framleiddi um 21.0 km^3 af einsleitri alkalískri basaltkviku, er stærsta eldgos jarðar á síðustu 1100 árum. Rúmtak hrauna er 19.7 km^3 og gjóskan eru 1.3 km^3 (reiknað sem hraun). Gjóskan myndaðist í að minnsta kosti 16 goshrinum. Blandgígaröð Eldgjárgossins er ósamfelld og nær yfir 70 km vegalengd frá Mýrdalsjökli í suðvestri og að jaðri Vatnajökuls í norðaustri.

Sprengivirknin í Eldgjárgosinu voru einstakir atburðir (þ.e. hrina) sem afmörkuðust við ákveðna hluta gígaraðarinnar á hverjum tíma. Hver hrina leiddi til gjóskufalls sem samsvarar sérstakri einingu í gjóskulaginu. Saman mynda þessar einingar gjóskulag sem er 2 m þykkt í 10 km fjarlægð frá upptakagígum. Í fyrstu 10 hrinunum var þessi virkni ýmist í Mýrdalsjökli eða rétt utan jökulsins og skiptust því á sprengigos (freatómagmatísk virkni) í jöklinum og þeytigos (magmatísk virkni) utan hans. Síðustu sex hrinurnar voru þeytigos utan jökuls. Þessi sprengivirkni var Plínísk í eðli sínu og gosmekkirnir frá goshrinunum stigu 11 til 18 km í loft upp og vel upp fyrir veðrahvolfið yfir Íslandi.

Mælingar á blöðrumagni og blöðrustærðardreifingu Eldgjárvikurs sýnir að engin munur er á freatómagmatísku og magmatísku gjóskunni, sem bendir til þess að utanaðkomandi vatn komst ekki í snertingu við kvikuna fyrr en eftir sundrun hennar efst í gosrásinni. Verulegur munur er á heildarkornastærðardreifingu magmatísku og freatómagmatísku gjóskunnar, þar sem sú síðarnefnda inniheldur meira af fínni ösku. Leidd er rök að því að þessi fína aska myndaðist við hraðkælingu á vikurkornunum þegar gosstrókurinn reis upp í gegnum bræðsluvatn jökulsins.

Hrafn hafnarlykill var víkingur mikill;
Hrafn Haven-Key was a great Viking;

hann fór til Íslands og nam land milli Hólmsár og Eyjarár og bjó í Dynskógum;
he went to Iceland and took land between the Hólmsá and Eyjará and lived at Dynskógar;

hann vissi fyrir eldsuppkomu og færði bú sitt í Lágey.
he foresaw an eruption and moved his farm to Lágey.

Landnámabók
The Book of Settlement

Preface

The research presented here has been carried out at the Faculty of Earth Sciences, University of Iceland. The primary aim of this project has been to investigate and characterise the explosive phases of the 10th century Eldgjá eruption. Using data gathered from this eruption more general conclusions have been reached regarding processes active during fissure eruptions and subglacial eruptions. The main results are presented as papers I-III. The papers are either submitted, or in preparation to be submitted, to peer-reviewed international journals:

Paper I: **Moreland WM**, Thordarson T, Houghton BF, Larsen G *Contrasting explosive products of the 10th century Eldgjá fissure eruption, southern Iceland.* Manuscript submitted to **Bulletin of Volcanology**

Paper II: **Moreland WM**, Thordarson T, Houghton BF, Larsen G *Driving mechanism of explosive activity during the 10th century Eldgjá fissure eruption, southern Iceland.* Manuscript submitted to **Bulletin of Volcanology**

Paper III: **Moreland WM**, Thordarson T, Houghton BF, Larsen G, Miller DJ *Variation of eruption style and magma composition during a fissure eruption.* Manuscript to be submitted to **Journal of Volcanology and Geothermal Research**

Table of Contents

List of Figures

Acknowledgements

I would like to begin by thanking my supervisor. Thor first introduced me to volcanology whilst I was an undergraduate at the University of Edinburgh; first, on the beaches of the Isle of Arran while studying dykes during a 2nd year field trip, and later in the east of Iceland during my MEarthSci field course. It was soon after this that I began applying for PhD positions, one of which was to work with Thor on Icelandic volcanism. This thesis would of course not have been possible without Thor but I would like to especially thank him for teaching me the field skills that have been necessary to complete this study.

I would also like to thank my co-supervisors, Bruce and Guðrún; it has been such an experience to learn from you. Some of my most enjoyable days in the field were during our 2013 fieldwork, mapping Hekla and Eldgjá deposits in the area south of Kerlingarfjöll. Seeing you and Thor out and in your element was exactly the sort of inspiration I needed during my first field season. I didn't realise it in the beginning but having read so much of the literature now, I realise, and I am honoured to have worked with some of the most respected names in the field.

My work has benefited immensely from sharing office 146 with some terrific people over the time I've been here: Jónas, Ásgeir, Birgir, and Rob. I would like to specially thank Jónas for the insightful life wisdom he has imparted on me ever since that rainy day in 2012 at the campsite in Leirubakki when he introduced himself with a message from Thor that I had been offered the PhD position.

Over the years, I have had many helping hands for fieldwork: Jónas, Darrell, Riina, Maria, Lofty, John, Richard, Delphine, Hannah, and Kate. I enjoy rediscovering photos of all our past excursions every time I'm looking for a photo of a particular tephra section. Thank you for the company. I would like to particularly thank John Stevenson who was the first to introduce me to the joys of tephra mapping. It was at this time that John strongly influenced my later work by extolling the virtues of FOSS and the use of Python which has benefited me greatly ever since.

I have met so many fantastic people since moving to Iceland, too many to mention by name but you will know who you are: thank you. Life in Askja has been made so enjoyable by the close-knit community of geologists and biologists living harmoniously side-by-side. Thank you to the members of Folda and Flóki over the years, particularly those who made my first months in Iceland so easy but especially all the bandy players – it's been amazing!

A special thanks to Hannah. Thank you for supporting me through all of this; you've been a rock and I love rocks. It has been such a pleasure to explore Iceland with you and to experience the likes of Holuhraun side-by-side. Here's to the future.

This project was funded by the Icelandic Research Fund (Rannsóknasjóður), grant number 110077-0061, who I am grateful to for accepting our application. I am also very thankful to the South Iceland Research Fund (Háskólafélag Suðurlands) who provided additional funding for fieldwork. The final year or so was supported by a teaching assistant position sponsored by the University of Iceland and a research position in the ICAO project, thank you Ármann Höskuldsson for that.

Last and by no means least – thank you to the bank of mum and dad; I'll try to stop sponging off you now! Thank you for inspiring me and supporting me at every step. I literally could not have done it without you.

1 Introduction

1.1 Basaltic volcanism

Basaltic volcanism is the most common type of volcanism on Earth. Whilst this is mostly because around 75% of all volcanoes are located along the mid-ocean ridge system where the dominant magma type is basalt, the most voluminous eruptions on land, flood lava eruptions, are basaltic. Basaltic volcanism takes place in every tectonic environment on Earth: at divergent plate boundaries, above subduction zones, and at intra-plate hot spots such as Hawaii. Given that basaltic volcanism takes place across the full spectrum of tectonic environments, it is not surprising that it also encompasses practically all styles of volcanism. Basaltic volcanism is often seen as almost entirely effusive as a result of its low viscosity. Whilst of course basaltic magma does indeed have a low viscosity and people may immediately think to the relatively gentle lava flows of Hawaii or the like when thinking of basaltic activity, some of the most vigorous volcanic events are explosive basaltic eruptions.

An unsatisfactory consequence of both the public and scientific community considering basaltic volcanism as overwhelmingly effusive is the lack of studies on explosive basaltic volcanism. The vast majority of research on explosive volcanism since the "birth" of modern volcanology in the mid-20th century has been focused on silicic cases. As a result of this many of the processes and related models only fit the high-viscosity magma types. It is only in the past few decades that work has started to be carried out on qualifying and quantifying explosive basaltic volcanism (e.g. Mangan et al. 1993; Coltelli et al. 1998; Houghton et al. 2004; Lautze and Houghton 2007; Houghton and Gonnermann 2008; Sable et al. 2009; Costantini et al. 2010) and there is much left to learn.

Europe's reawakening to the risks of volcanic ash (with the exception of the already well-aware neighbours of Etna) after the eruption of Eyjafjallajökull in 2010 has brought subglacial volcanism to the forefront. It is an often-misconceived notion that external water is required for basaltic eruptions to be explosive. The abundance of magmatic tephra in the stratigraphic record of Iceland is evidence for the contrary. The question then arises: what is the contribution from external water to the explosivity or intensity of subglacial eruptions?

In this introduction, I will outline explosive basaltic volcanism in its many styles and explain why it is important to have a full understanding of these phenomena. I will then focus on Iceland, an incredibly volcanically active region of the world where some of the most fascinating examples of basaltic and subglacial volcanism can be found. After outlining the geology of Iceland, I will finally introduce the main subject of this thesis: the 10th century Eldgjá fissure eruption of Iceland. Whilst this eruption was a basaltic flood lava event, it also featured explosive phases which rival the likes of Hekla or Etna for volume and intensity.

1.1.1 Explosive basaltic volcanism

Fragmentation of magma occurs when exsolving volatiles expand rapidly in a magma which resists that expansion. As a result of this, silicic magma, which is up to 10 orders of magnitude more viscous than basaltic magma (Lesher and Spera 2015), is more commonly

explosive than basaltic magma. In basaltic magma, the bubbles (formed of exsolved volatiles) rise more quickly than in silicic magma, often leading to the decoupling of the volatiles from the melt, and resulting in an effusive eruption of outgassed magma. Outgassed magma may even stall in the conduit, without reaching the surface to erupt. For the system to remain coupled, resulting in a more explosive eruption, the ascent velocity of the magma must be close to that of the bubbles. This is more common in silicic magma than basaltic as the higher viscosity prevents the easy nucleation and growth of bubbles and so essentially traps them at their point of origin. In basaltic magma, the low viscosity allows the easy nucleation and growth of bubbles however the reason for the rapid ascent rates required to couple the gas and melt phases are still unclear. One suggestion is that, in some cases, the early exsolution of CO_2 at depth could increase the buoyancy of the magma enough to rapidly rise (Sable et al. 2006). Another suggestion is that decompression by removal of lithostatic pressure (e.g. a landslide; Coltelli et al. 1998) could trigger magma ascent.

The style of explosive activity depends strongly on the manner in which the volatiles ascend with or through the magma column (Figure 1.1), and can be roughly grouped into

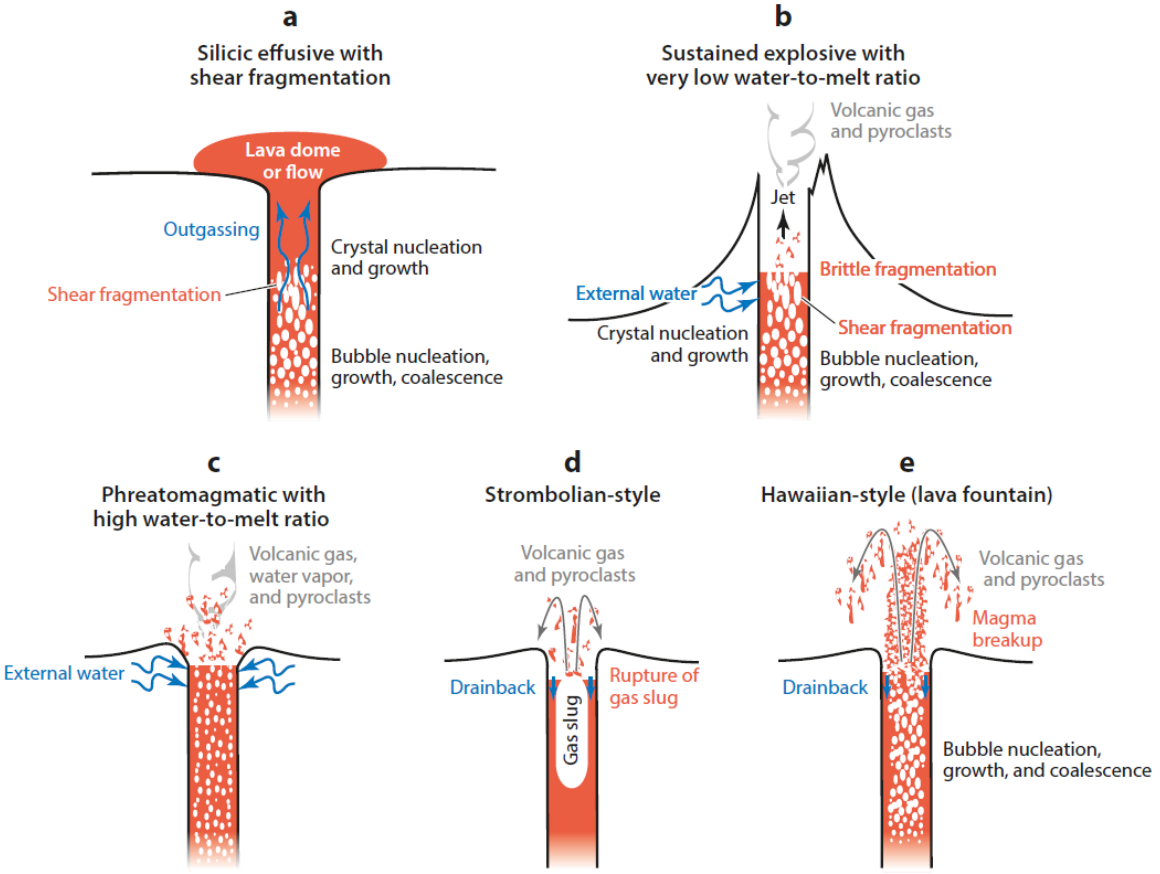

Figure 1.1 Examples of different styles of eruption. a) Effusive eruption of viscous silicic lava involving shear fragmentation along the conduit walls, not discussed here. b) Sustained eruption of magma involving either high viscosities or high shear rates, or both. c) Phreatomagmatic explosions resulting from high water-to-melt ratios and involving the explosive expansion of steam. d) Strombolian-style activity resulting from the rise of smaller bubbles and coalescence into much larger gas slugs which burst at the surface. e) Hawaiian-style fountaining due to high ascent rates maintaining coupling of the volatile and melt phases and resulting in high-powered gas jets at the surface. From Gonnermann (2015)

unsteady or sustained eruptions. At the low-energy end of the explosive basaltic spectrum are Hawaiian and Strombolian-type eruptions with basaltic Plinian eruptions at the high-energy end. One of the most common methods of classifying explosive eruptions is that of Walker (Figure 1.2; Walker 1973). This method uses two characteristics of tephra deposits, dispersal, and fragmentation indices, to group similar eruptions. The dispersal index, D, is a measure of how quickly a deposit thins away from the vent. It is measured by finding the area enclosed by the $0.01 \times T_{max}$ isopach where T_{max} is the maximum thickness of the deposit. The fragmentation index, F, is a measure of how fine-grained the deposit is and is the weight percentage finer than 1 mm, measured where the dispersal axis crosses the $0.1 \times T_{max}$ isopach. Whilst this classification scheme has been widely accepted there are few eruptions which have been classified using it, most likely due to the need for detailed fieldwork to acquire the data required. Also, because the data used in this classification is by nature time-averaged (i.e. the dispersal does not consider changes in activity over time), this classification cannot tell apart long-lived eruption styles, such as Hawaiian and Plinian, from transient eruptions like Strombolian or Vulcanian.

Hawaiian-type eruptions

Hawaiian-style eruptions are the low-energy endmember of sustained explosive volcanism, the high-energy endmember being Plinian explosions. Hawaiian-style eruptions are characterised by sustained discharge of magma through fire-fountains which can reach several hundred metres in height (Stovall et al. 2011, 2012). Although the eruption is sustained in terms of magma discharge, the intensity of the activity can greatly fluctuate; for example, during the Pu‘u ‘Ō‘ō fountaining events between 1983 and 1986 the heights of fountains varied between

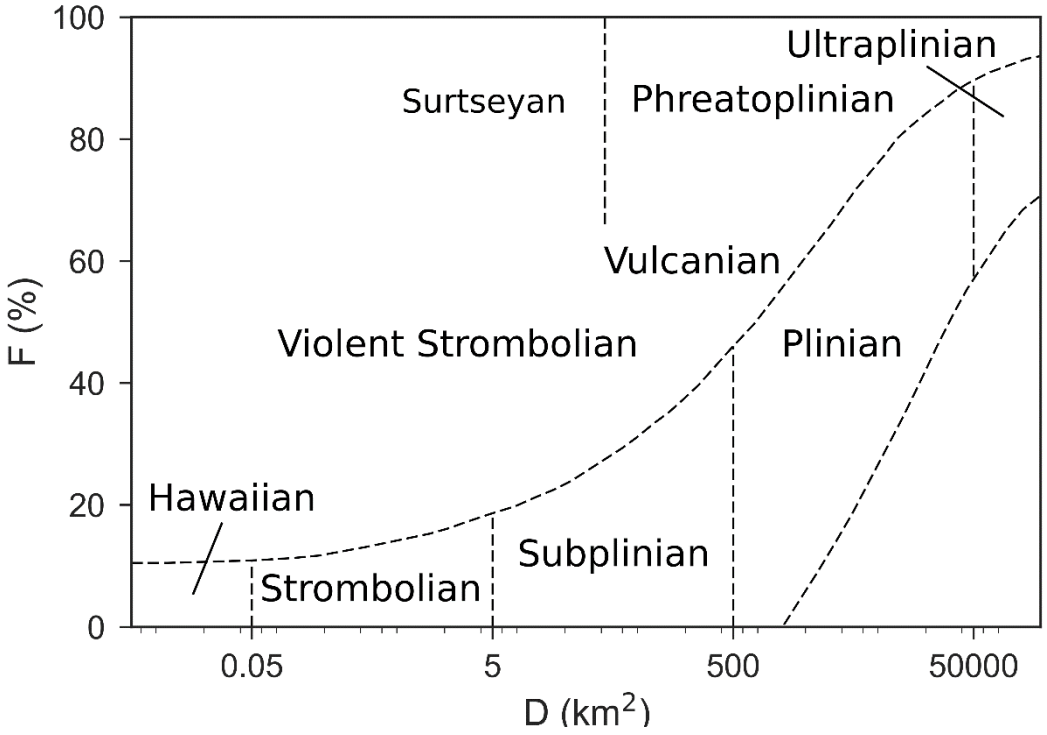

Figure 1.2 Walker’s classification of explosive volcanism (1973). D, dispersal index, is a measure of how quickly a deposit thins away from source; and F, fragmentation index, is a measure of how fine-grained a deposit. See text for full details

30 to 470 m and each episode lasted between 5 hours and 12 days (Wolfe et al. 1988). Hawaiian fountains are driven by higher gas flux rates than slug flow (below) and instead feature continuous, albeit heterogeneous, gas phases in either churn or annular flow (Figure 1.3) with annular flow requiring a magnitude higher gas flux than churn flow (Houghton and Gonnermann 2008). Fragmentation of the magma is dominantly a result of inertial fragmentation of the melt by the rapidly expanding gas phase (Namiki and Manga 2008).

Strombolian-type eruptions

Strombolian-type explosions are a common type of unsteady volcanism seen at volcanos around the world. The explosions are a result of large, conduit-filling bubbles called slugs bursting at the surface (Figure 1.1d, Figure 1.3; Lautze and Houghton 2005, 2007). These slugs are a product of low viscosity magma allowing the smaller bubbles to ascend more quickly, coalesce with other bubbles and, as a result, increase their rise rate. When a slug reaches the surface, it bursts and showers the surrounding area with blobs of magma which once made up

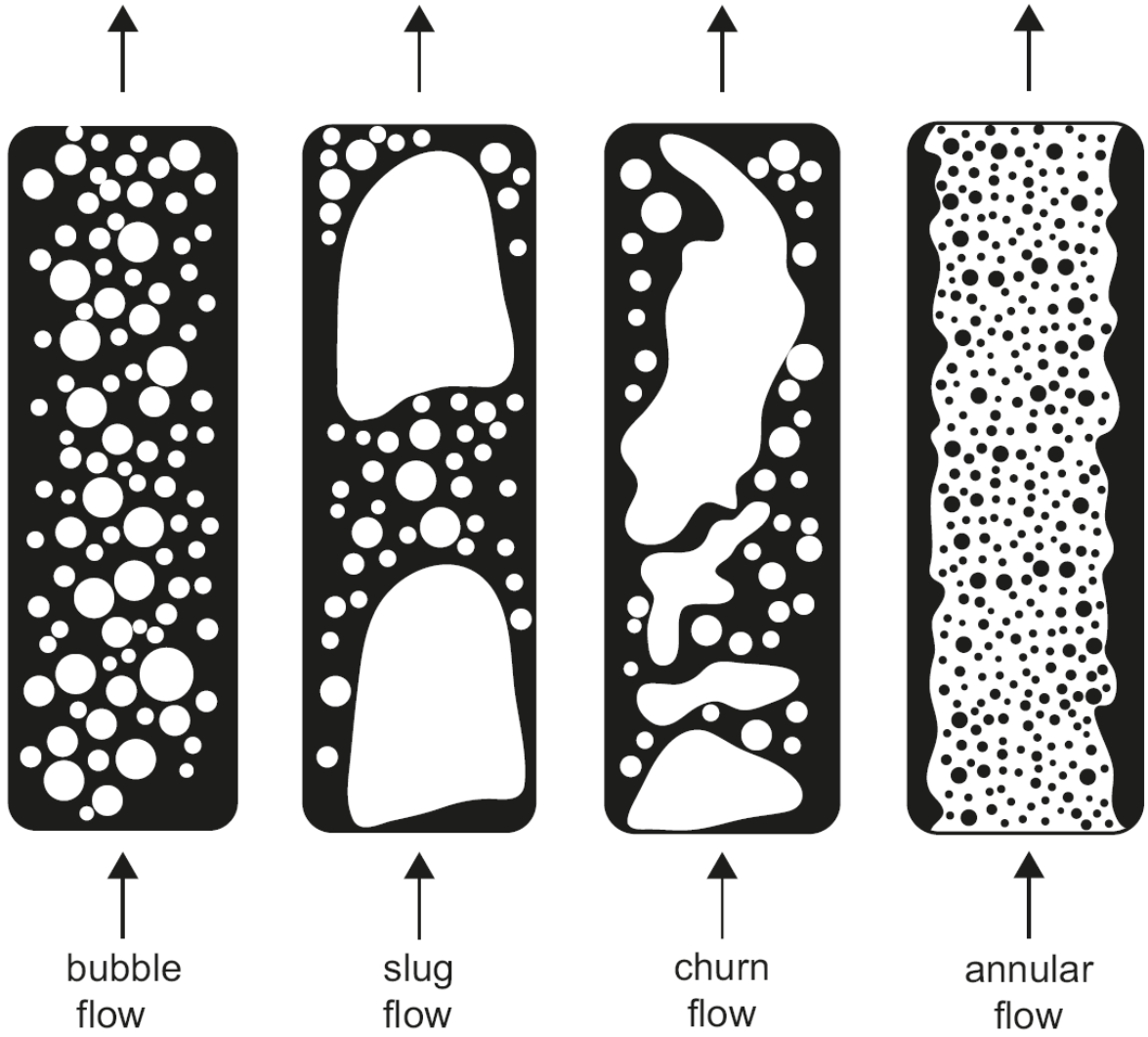

Figure 1.3 Types of two-phase flow with melt phase in black and gas phase in white. From Houghton and Gonnermann (2008)

the bubble walls. Because the accelerating slug sweeps up the conduit, amalgamating any bubbles it meets on the way, a volume of magma is left behind which is essentially devoid of volatiles. Thus, the next slug to erupt at the surface has to originate from fresh magma lower in the ascending column. It is this time delay which results in the regular periodicity exhibited by Strombolian explosions at volcanos such as Stromboli.

Subplinian and Plinian basaltic eruptions

Plinian eruptions, named after one of the observers of the 79 CE eruption of Vesuvius, are characterised by sustained eruption columns powered by pulses of explosions in rapid succession (Cioni et al. 2015). Subplinian eruptions are events of a lower magnitude but with dynamics similar to Plinian eruptions. The vast majority of known Plinian events involve silicic magma. Only four Plinian basaltic eruptions have been described in detail: the ~60 ka Fontana Lapilli and ~2 ka San Judas, both Nicaragua (Williams 1983); 122 CE Etna, Italy (Coltelli et al. 1998); and 1886 Tarawera, New Zealand (Walker et al. 1984).

The magma ascent and fragmentation processes of Plinian basaltic eruptions are not well understood. It has previously been suggested that Subplinian and Plinian eruptions are a more intense form of Hawaiian and Strombolian processes as they are dynamically indistinguishable (Parfitt and Wilson 1999). However, this is not consistent with the observation that there is a clear transition in the trend between vesicle number density and mass discharge rate (Figure 1.4). Whilst silicic magmas are capable of producing Plinian-intensity eruptions due to their high viscosity, another process must be invoked for the lower-viscosity basaltic cases (Papale 1999). The eruptions of 122 CE Etna and 1886 Tarawera both involved microlite-rich magmas

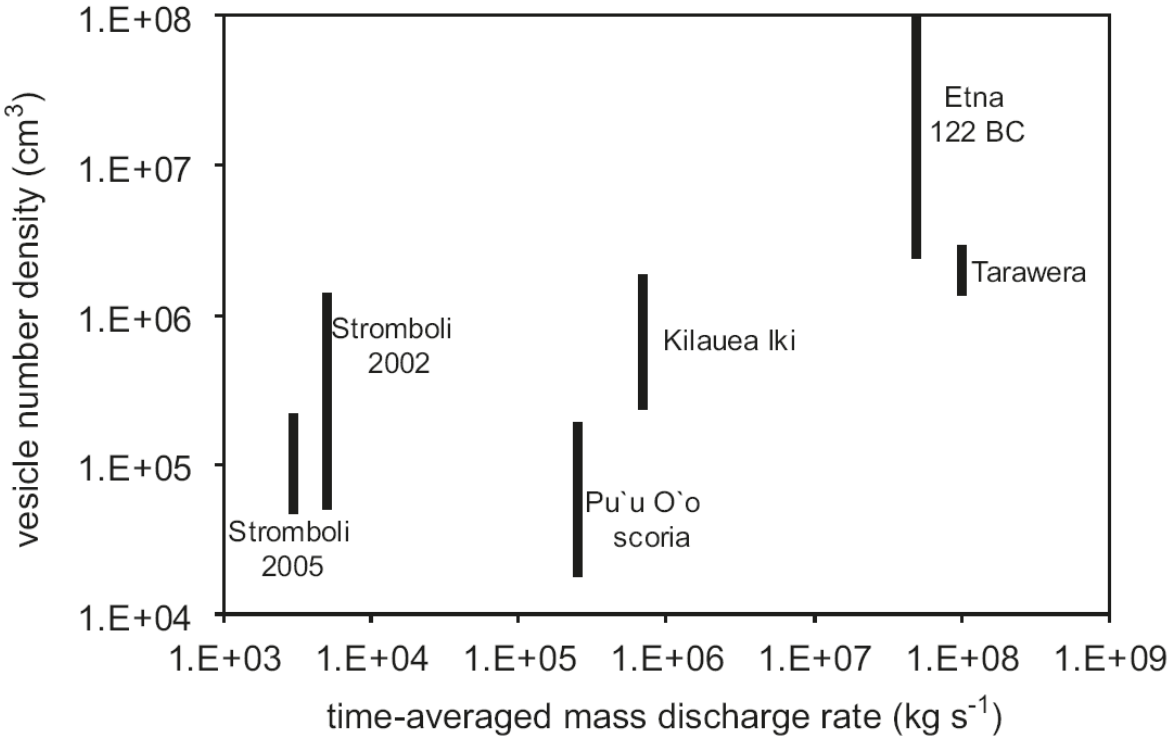

Figure 1.4 Plot of vesicle number density measurements for a range of basaltic eruptions plotted against mass discharge rate. Note the horizontal trend in the Strombolian and Hawaiian data which is offset, and much lower than the Plinian data. From Houghton and Gonnermann (2008)

where the microlites are thought to have formed as a result of late-stage degassing (Houghton et al. 2004; Sable et al. 2006). It has been suggested that this sudden growth of microlites resulted in a rapid increase in viscosity as the magma approached the surface allowing brittle fragmentation to take place (Houghton and Gonnermann 2008). However, eruptions such as the ~60 ka Fontana Lapilli (Costantini et al. 2010), and, as will be demonstrated below, the 939 CE Eldgjá eruption in Iceland, had relatively microlite-poor magmas and yet produced Plinian deposits. Vesicle number densities have been shown to correlate with ascent rates (Polacci et al. 2006; Sable et al. 2006; Stovall et al. 2012). The highest ascent rates may delay bubble nucleation so late that upon commencement of nucleation and growth the explosive decompression is violent enough to generate the strain rates necessary for brittle fragmentation in lower viscosity magma (Houghton et al. 2004).

Plinian eruption columns can reach many tens of kilometres into the atmosphere, injecting volatiles and ash into the stratosphere leading to global climatic impacts such as those seen after the 1991 Mount Pinatubo eruption (Self et al. 1996b). The eruption column is made up of three parts: the jet phase, where the plume is powered by initial momentum generated by the magma ascent rate and subsequent explosions; the convective phase, where the plume is rising by buoyant convection; and the umbrella region, where the plume overshoots its level of neutral buoyancy and begins to level out forming the stereotypical mushroom cloud (Sparks 1986).

1.1.2 Flood lava eruptions

The very name *flood lava eruption* hardly brings to mind scenes of explosive volcanism. This is understandable given that the vast quantity of material erupted during these events is indeed in the form of lava. A flood lava eruption is one which erupts between 1 and 100 km^3 of magma (Thordarson and Höskuldsson 2008). This is also the likely reason that, traditionally, research on flood lava eruptions has focused on the modes of lava emplacement (e.g. Self et al. 1996a, 1997; Thordarson and Self 1998; Keszthelyi and Self 1998), the processes involved in creating and delivering that much magma to the Earth's surface (Carlson 1991; Mahoney and Coffin 1997), or the quantity and consequence of the large volumes of climate-changing volcanic gases released during these events (e.g. Rampino and Stothers 1988; Thordarson et al. 1996; Thordarson and Self 1996; Grattan 2005; Self et al. 2005).

However, in the last two decades studies on the occurrence of explosive activity occurring during a flood lava eruption have started to appear (e.g. Németh et al. 2003; McClintock and White 2006; Brown et al. 2014). The primary interest in explosive activity in these cases is that it provides a much more efficient method of delivering the volcanic gases into the upper atmosphere where they can have much stronger and longer-lasting effects (e.g. Thordarson et al. 2003; Self et al. 2005; McClintock and White 2006). Studies have estimated mass discharge rates and found them to be similar to the maximum estimated for contemporaneous Icelandic flood lava eruptions (e.g. 1783 Laki eruption, ~4000 $m^3\ s^{-1}$, Thordarson and Self 1993; Self et al. 1998). It has also been demonstrated that, although the fissure systems of flood lava eruptions can be hundreds of kilometers long, only distinct segments of the fissure are active at any one time (Brown et al. 2014).

An additional issue associated with flood lava eruption-related explosive events is that due to the long duration of flood lava eruptions which can last from months to many years (Thordarson et al. 2003). This takes every hazard linked to explosive eruptions and then massively increases the exposure time. Thankfully, society is beginning to recognise the risks associated with flood lava eruptions as indicated by studies such as Loughlin et al. (2012) and that governments such as the United Kingdom's including fissure type eruptions in their national risk registry (UK Cabinet Office 2012)

1.2 Subglacial explosive volcanism

In Iceland, where the majority of active volcanoes are covered by glaciers, subglacial explosive volcanism dominates the eruption record, accounting for 75% of explosive events recorded in the postglacial tephra stratigraphy (Thordarson and Höskuldsson 2008). Although initial activity is confined to beneath the ice, subglacial eruptions can rapidly melt through several hundred metres of ice to become subaerial (Gudmundsson 2003).

Magma-water interaction results in phreatomagmatic fragmentation of the magma, producing a finer-grained tephra deposit compared to a purely magmatically-fragmented deposit. This fragmentation can take place at a range of intensities depending upon the ratio of magma to water, the timescales involved, and exactly when the water encounters the erupting magma.

On the lower end of the intensity scale is thermal granulation where the formation of fine-scale hydrofractures disintegrates the magma without adding explosivity to the system (Kokelaar 1986). The most intense phreatomagmatic process is molten fuel-coolant interaction. This process requires a stable steam film to insulate the hot magma from the cooler water. When this film is ruptured, the magma and water meet and the heat flux increases by two orders of magnitude (Zimanowski et al. 2015 and references therein). The water must then expand rapidly but the magma is unable to accommodate, leading to cracking of the magma and infiltration of the water. The water-filled cracks provide fresh hot surfaces with which to heat and expand the water further causing the cracks to rapidly grow. This establishes an explosive feedback loop of heating, expansion, and cracking leading to the fragmentation of the magma at timescales in the order of milliseconds.

1.3 Geology of Iceland

Iceland is situated on the Mid-Atlantic ridge at the junction between the Kolbeinsey Ridge to the north, the Reykjanes Ridge to the south and the Greenland-Iceland-Faeroe Ridge to the east and west (Figure 1.5). This region of oceanic crust, known as the Iceland Basalt Plateau, rises 3000 m above the surrounding ocean floor (Malinverno 1990) and is the product of a mantle anomaly, commonly referred to as the Iceland mantle plume (e.g. Lawver and Müller 1994; Bjarnason 2008), located approximately beneath Vatnajökull in southern Iceland (Figure 1.5). Iceland is unusual both because it is the only place on Earth where a mid-ocean ridge is exposed above sea level but also because, for the last 65 million years (Saunders et al. 1997), a mantle plume has been interacting with this spreading centre and supplying more magma to the surface than would otherwise be the case.

Iceland is split into three stratigraphic groups: the oldest Tertiary Basalt formation, the Plio-Pleistocene formation, and the Upper Pleistocene formation. Within the Upper Pleistocene formation lies the neovolcanic zones within which all recent volcanism has taken place. Within the neovolcanic zones are into the Western (WVZ), Eastern (EVZ), and Northern volcanic zones (NVZ) which contain the majority of currently active volcanic systems on Iceland and which delineate the path the mid-Atlantic Ridge takes across Iceland. Other areas of active volcanism on Iceland are the Snæfellsnes Volcanic Belt (SVB), Mid-Iceland Belt (MIB) and Öræfi Volcanic Belt (ÖVB). A transform fault, the South Iceland Seismic Zone (SISZ) connects the Western and Eastern volcanic zones in the south whilst the Mid-Iceland Belt connects them in the middle of Iceland.

Volcanic activity in Iceland is classified into volcanic systems on the basis of volcano-tectonic architecture. There are 30 currently active systems (Figure 1.5). A volcanic system

consists of a fissure swarm or a central volcano or both. A central volcano, when present, is the focus of volcanic activity in the system and has lifetime of between 0.5 and 1.5 million years (Jakobsson 1979). Fissure systems are the surface expressions of rifting episodes in the crust during which inject magma into vertical sheets called dykes, the majority of which do not reach the surface. When a dyke does reach the surface a fissure eruption will occur which, depending on factors such as volatile content, ascent rate, or surface water, may feature lava or tephra production, or both. The Icelandic stratigraphy, especially in the East and West of the island where uplift and erosion exposes it best, is dominated by extensive lava flows. These flows are called the plateau basalts and are the product of large volume basaltic flood lava events, similar to the style of activity which produced the likes of the Deccan or Siberian Traps.

Centennial magma output at Icelandic volcanoes has been estimated at 8 km^3 over the last 1100 years, occurring in around 20 events per century (Thordarson and Larsen 2007). Basaltic

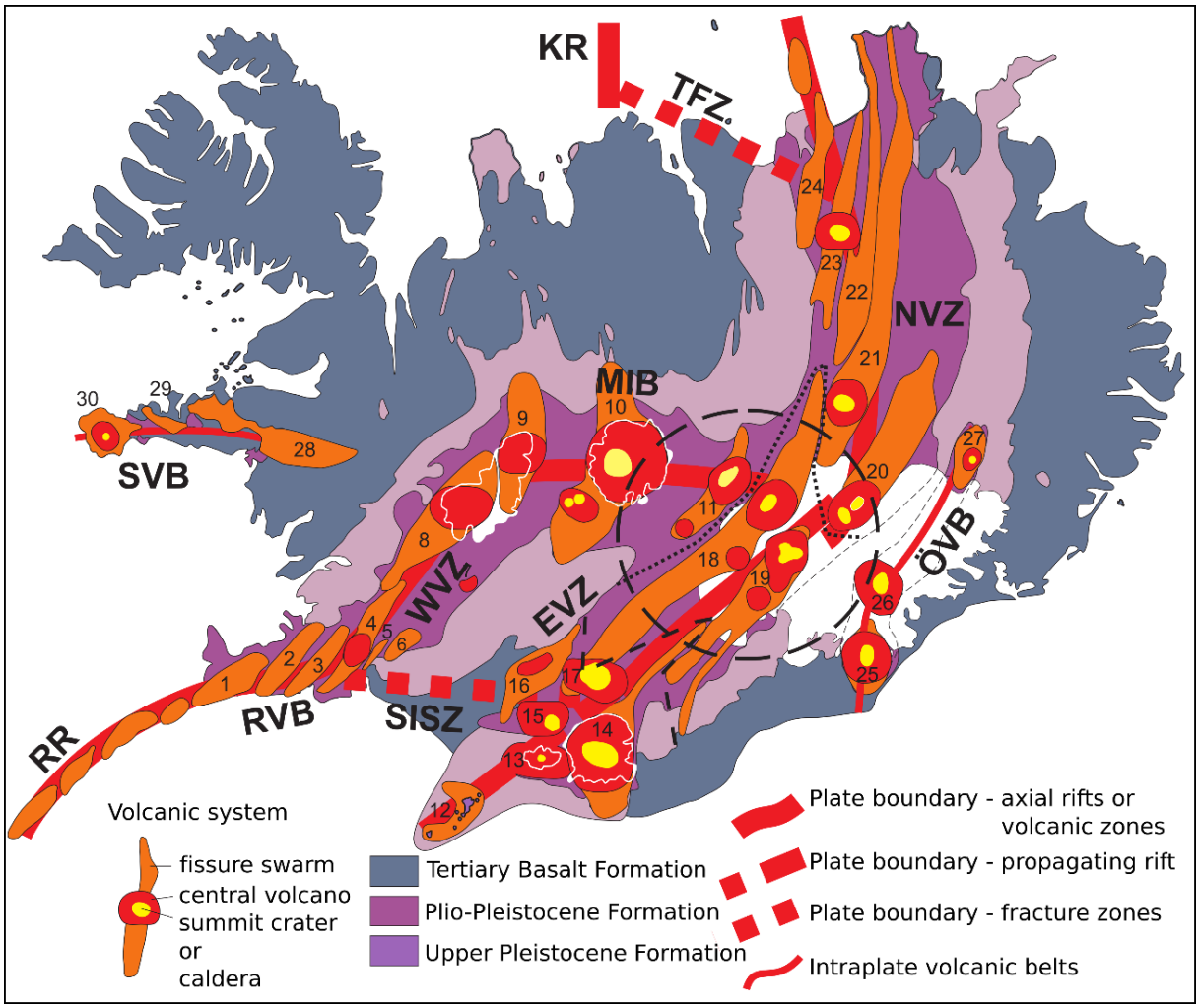

Figure 1.5 Map of Iceland outlining the locations of the volcanic belts and systems (Jóhannesson and Sæmundsson 1998). The dashed circle represents the inferred location of the Iceland mantle Plume (Wolfe et al. 1997). Abbreviations are as follows: RR, Reykjanes Ridge; RVB, Reykjanes Volcanic Belt; SISZ, South Iceland Seismic Zone; WVZ, West Volcanic Zone; MIB, Mid-Iceland Belt; EVZ, East Volcanic Zone; NVZ, North Volcanic Zone; TFZ, Tjörnes Fracture Zone; KR, Kolbeinsey Ridge; ÖVB, Öræfi Volcanic Belt; and SVB, Snæfellsnes Volcanic Belt. Numbers refer to the thirty active volcanic systems, see Thordarson and Höskuldsson (2008) for names

magma accounts for 79% of this output, with intermediate and silicic making up 16% and 5%, respectively (Thordarson and Larsen 2007). 79% of all Icelandic magma is erupted on the EVZ. This is partly accounted for by the fact that 8 of the 30 volcanic systems are located in the EVZ. The EVZ is a proto-axial rift that is propagating to the south. It is thought that it will eventually take over from the WVZ as the main plate boundary (Jakobsson 1979). Whilst the composition of magma erupted from the axial WVZ and NVZ is tholeiitic due to the high degree of partial melting at the plate boundary, the EVZ is alkali to transitionally alkali (Jakobsson 1979; Gudmundsson 1995) due to low melt fractions involved in mantle melting.

Large volume (<1 km^3) basaltic flood lava eruptions occur in Iceland with recurrence intervals of several hundred years (Thordarson and Höskuldsson 2008). Flood lava eruptions are defined as consisting of multiple eruption episodes dominated by voluminous (>1 km^3) effusive activity (>90% of the erupted material is lava) and lasting for months to years (Thordarson et al. 2003). They may also exhibit explosive phases which, in combination with the high thermal output of effusive volcanism (Stothers et al. 1986), produce eruption columns of up to 20 km (Stothers et al. 1986; Thordarson and Self 1993; Woods 1993).

1.4 The Eldgjá eruption

One example of a high-latitude basaltic flood lava eruption is the 10th century Eldgjá fissure eruption which is the most voluminous flood lava eruption to have occurred on Earth in the last 11 centuries (Thordarson and Larsen 2007). The Eldgjá vents belong to the Katla volcanic system in the Eastern Volcanic Zone of Iceland (Jakobsson 1979). The southwestern end of the vent system is inferred to be beneath Mýrdalsjökull, where radio-echo soundings have revealed the subglacial topography (Björnsson et al. 2000). Isopachs of the Eldgjá tephra layers (Larsen 2000) indicate a major source area west of Öldufellsjökull where a depression flanked by a steep ridge striking N33°E is the most prominent feature (Figure 1.6). The vent system continues subaerially in the form of a mixed cone row on a bearing of between N15°E and N45°E for ~70 km until it terminates 6 km short of Vatnajökull (Figure 1.6; e.g. Larsen 2000; Thordarson et al. 2001). The Eldgjá fissure system is one of the longest in Iceland; it is only matched by the Vatnaöldur and Veiðivötn cone rows of the Bárðarbunga-Veiðivötn volcanic system and is three times longer than the Laki fissure system of Grímsvötn volcanic system (Larsen 1984; Thordarson and Self 1993).

The Eldgjá flood lava eruption took place during the first half of the 10th century, shortly after the Katla 920 CE event but before the Hekla 1104 CE (H1) layer (Larsen 2000, 2010). The eruption has been dated to 939 CE based upon Greenland ice core records (Sigl et al. 2015), historical accounts of meteorological and astronomical phenomena (McCarthy and Breen 1997; Stothers 1998; Fei and Zhou 2006), and environmental records (Oman et al. 2006; Baillie and McAneney 2015). Unlike the 1783 CE Laki flood lava eruption, (Thordarson and Self 1993; Thordarson et al. 1996) which was a similar but 25% smaller event (with respect to volume), there is very little contemporary information on Eldgjá. It is briefly mentioned in The Book of Settlement (Landnáma) which describes lava flows forcing newly-arrived Norse settlers off their lands.

Eldgjá was dominantly an effusive eruption, producing up to 19.7 km^3 of lava (Sigurðardóttir et al. 2015) including at least 0.5 km^3 of hyaloclastite flow at Kriki (Figure 1.6; Larsen 2000). However, a significant volume of tephra was produced (1.3 km^3 dense rock equivalent, DRE; Larsen 2000) in at least 16 explosive episodes at vents along the full length of the fissure. This volume of tephra is almost an order of magnitude larger than Laki (0.4 km^3; Thordarson and Self 1993), not much less than the total volume that Hekla has produced in

subplinian-plinian eruptions in historical times (2.2 km^3; Thordarson and Larsen 2007), and on a par with the 1362 CE Plinian eruption of Öræfajökull (1.2 km^3; Sharma et al. 2008).

The first sign of activity was an explosive eruption beneath the northeast margin of Mýrdalsjökull. Successive explosive episodes occurred from ever more north-easterly sites, although activity continued at the subglacial fissure segments after subaerial activity commenced. This mixture of subglacial and subaerial activity resulted in a tephra stratigraphy composed of alternating phreatomagmatic and magmatic units (Figure 1.7). Interspersed between explosive episodes were periods of lava effusion from subaerial and subglacial fissure

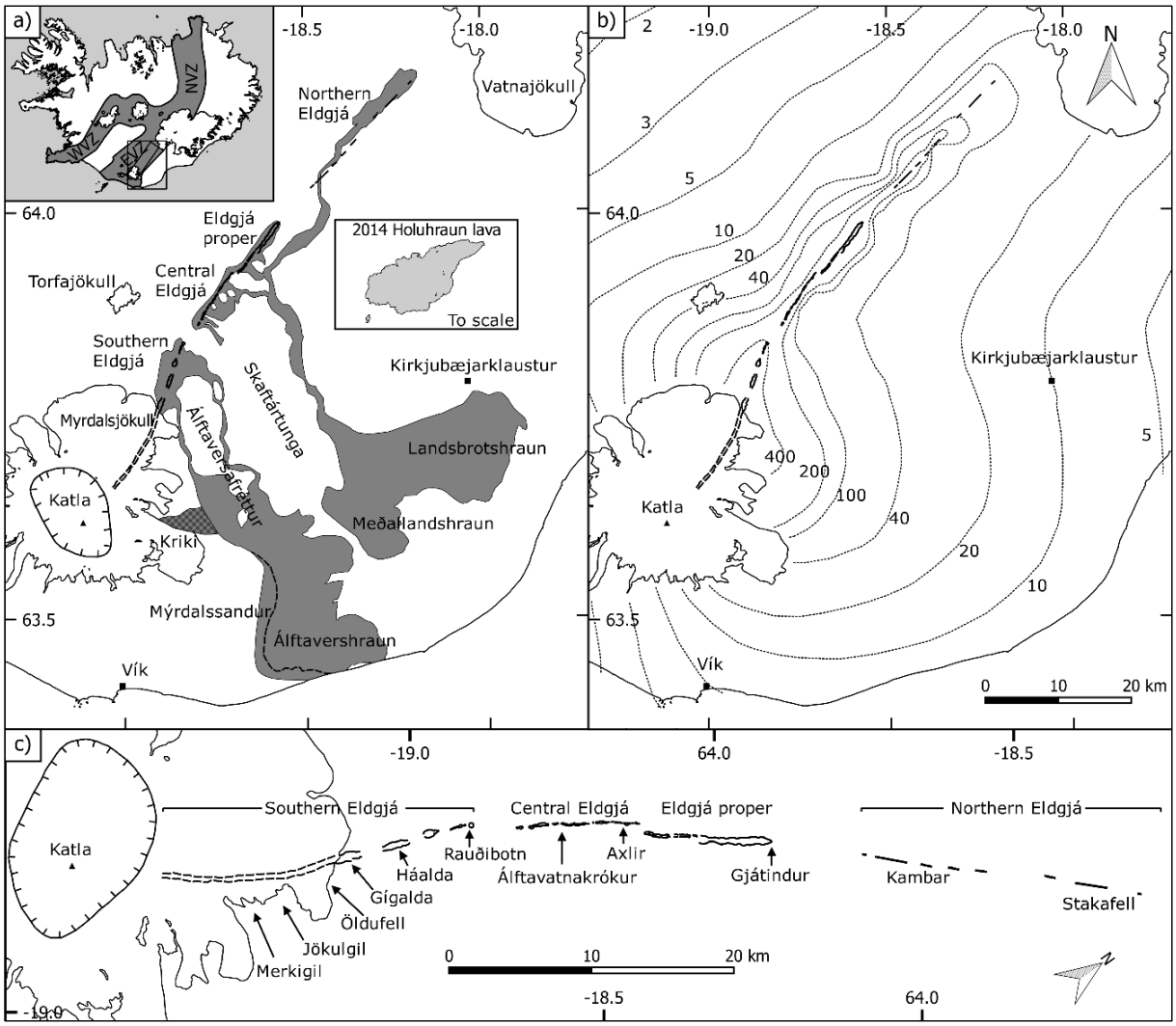

Figure 1.6 Overview map of Eldgjá a) map of the Eldgjá fissure and lava fields and the names of surrounding areas. The dashed line to the west of Álftavershraun indicates the suspected buried margin of the lava beneath Mýrdalssandur as mapped by Sigurðardóttir et al. (2015). The outline of the 2014-15 Holuhraun lava, erupted in the north of Iceland, has been overlain for comparison of size. Its volume is 1.44 km^3 (Pedersen et al. 2017) compared to 1.3 km^3 DRE for the Eldgjá tephra alone. b) Isopach map for the entire tephra deposit of Eldgjá (Larsen 2000). c) Map of the Eldgjá fissure system with locality names. Outlines of the subaerial Southern, Central, and Eldgjá proper segments are after Robson (1956). The dashed outline of the subglacial Southern Eldgjá segment is inferred from radio-echo soundings (Björnsson et al. 2000)

segments and jökulhlaups from beneath the glacier which produced extensive and thick (up to 2 m) deposits.

The exact duration of the event is not known however several sources provide suggestions. An absolute minimum duration of 6 months was calculated by Thordarson et al. (2001) by measuring the lava crust thickness at two localities and applying the method of Hon et al. (1994). The acidity peaks found in Greenland ice-cores dated to this time period indicate elevated atmospheric sulfate levels for between 3 to 6 years (Zielinski et al. 1994, 1995).

The effects of the eruption on the early settlement in Iceland must have been devastating. Scarce records show that the Eldgjá lava advanced over vast areas of productive farmland and forced many settlers from their lands, especially within the districts of Álftaver and Síða. The lava also forced the Skaftá River onto a new course. The tephra fallout from Eldgjá devastated the region of Álftaversafréttur to such an extent that it has not yet fully recovered (Larsen 2000). Furthermore, the Eldgjá event is one of the biggest volcanic pollutant events in recent history, exceeding the 1783 Laki and 1815 Tambora eruptions, by factor of two (Thordarson et al. 2001). It pumped ~200 million tonnes of SO_2 into the atmosphere and may have covered much of the Northern Hemisphere. Information in historical accounts indicates that the eruption had a significant effect on the weather patterns in Europe and the Middle East for several years (Oman et al. 2006). However, the atmospheric impact of Eldgjá may not have surpassed that of Laki or Tambora, as it may have been a prolonged event with sulfur emissions drawn out over several years.

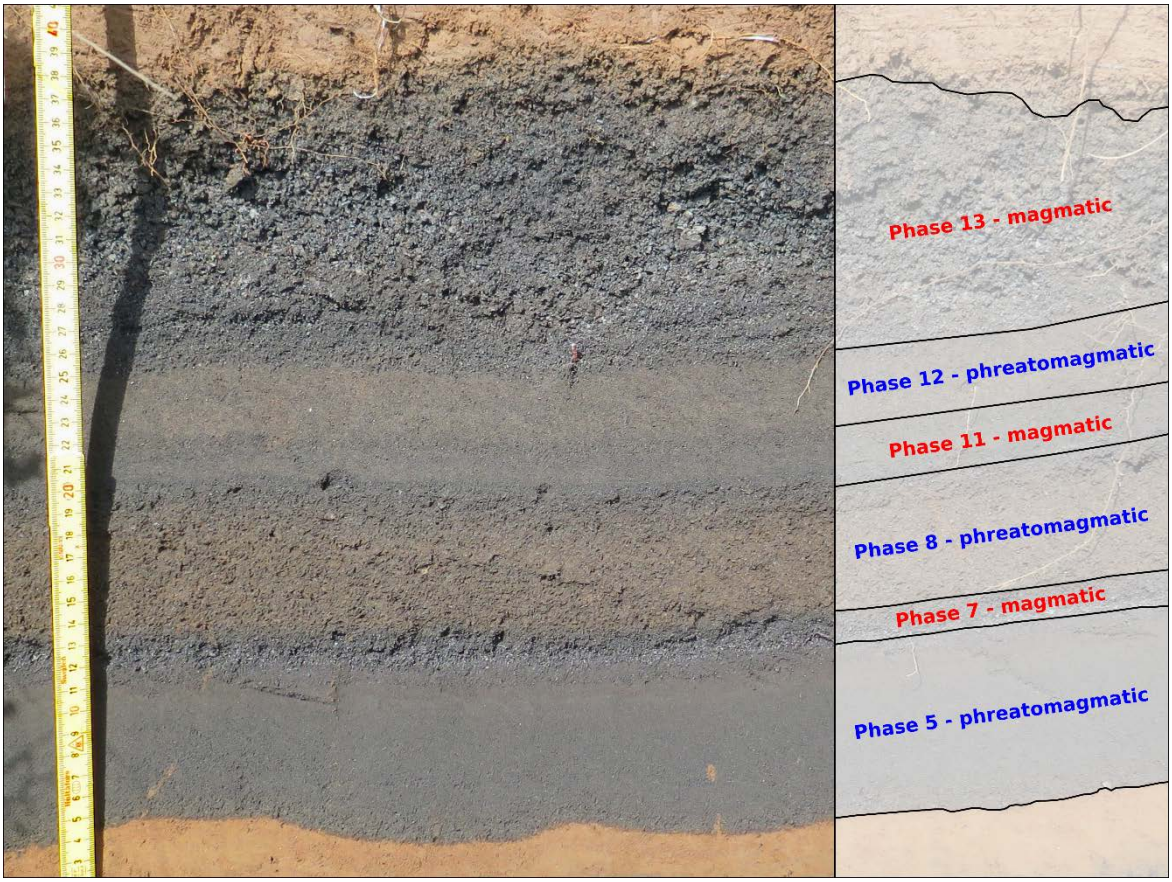

Figure 1.7 Example of the Eldgjá tephra deposit. Sample location E15-022, 63.85028°N, -18.51112°E, 13 km from fissure, 37 cm thick. Typically, the blue-black units are from magmatic phases and the brown units are phreatomagmatic. One exception to this trend is phase 5, the reasons for which are unclear

1.5 Aims of the research

The principle aim of the PhD project was to investigate the shallow conduit processes involved during the explosive phases of a basaltic flood lava eruption, using the 10th century fissure eruption of Eldgjá in southern Iceland as a case study. In addition to this, the partially subglacial location of the Eldgjá fissure allowed the effects of external water on an eruption to be constrained by using the subaerial fissure segments as a control. It should be highlighted that very few eruptions on Earth are so well positioned to examine subglacial volcanism by removing magmatic effects from the equation.

The specific objectives of this study were:

1. To compare and contrast the products of magmatic versus phreatomagmatic explosive basaltic eruptions **(Paper I)**
2. To investigate bubble nucleation processes occurring in the shallow conduit prior to an explosive phase during a fissure eruption **(Paper II)**
3. To investigate the magmatic characteristics as a function of time using detailed stratigraphic logs of the tephra deposit and major and trace element geochemistry **(Paper III)**

With the exception of the well-studied 1783 Laki eruption (e.g. Thordarson and Self 1993; Thordarson et al. 1996; Schmidt et al. 2011), there have been no studies aimed at quantifying the explosive activity at large basaltic fissure eruptions. This project provides fundamental data to the research community for enhancing the understanding of the eruption dynamics and potential impacts of even larger flood lava eruptions, which have been put forth as a possible cause for some of the main mass extinctions in Earth's history.

2 Methods

2.1 Field work

2.1.1 Mapping

The field area for this project was constrained to the area over which the Eldgjá tephra was deposited in quantities thick enough to identify individual units and roughly corresponds to the region south of the Eldgjá fissure system between Mýrdalsjökull and Vatnajökull (Figure 1.6). The tephra deposit of Eldgjá consists of many units deposited by each explosive episode (Figure 1.7). The thickness of each of these units was mapped out in detail to create isopach maps – maps upon which contours delineate lines of equal thickness. In addition to measuring the thickness, each unit was described in terms of grain-size, sorting, grading, morphological composition, and nature of upper and lower contacts with adjacent units. Units with distinct characteristics, such as unusual lithic content or distinctive grading, were used to ease the tracking of less recognisable units across the field area. These maps were then used to constrain the source of each tephra unit. Thickness measurements were taken at a total of 141 locations.

2.1.2 Sampling for grain-size analysis

At appropriately-spaced intervals, dependent upon thinning rate and change in character, samples of key units were collected at the measurement locations. The samples consisted of a bulk collection of tephra from a horizon of the deposit representative of the desired unit. The mass of the sample was determined by the approximate grain-size of the sample, ensuring that the largest pyroclast collected made up no more than 5% of the sample by mass.

2.1.3 Sampling for density analysis

Two localities, Skælingar and Stóragil, were chosen to represent the diversity of magmatic and phreatomagmatic tephra. The tephra section at Skælingar is less than 1 km south of the fissure at Eldgjá proper. It is nearly 4 metres thick and consists almost entirely of magmatic tephra. The section at Stóragil is about 10 km east of the subglacial fissure segment beneath Mýrdalsjökull. It is over 2 metres thick with nearly half being comprised of phreatomagmatic units.

Each section was logged, individual units described in detail, and sampled for both density and grain-size analysis. The density technique follows the method outlined in Houghton and Wilson (1989). Each sample consists of 100 pyroclasts between 8 and 32 millimetres in diameter collected from a horizon not more than 3 clasts thick. This size range ensures a large enough surface area in subsequent thin-sections for image analysis whilst attempting to exclude any significant post-fragmentation expansion of vesicles. The small sampling interval is used to justify the assumption that the clasts in each sample represent magma ejected from the vent during very narrow time windows.

2.2 Laboratory work

2.2.1 Clast density measurements

The samples were cleaned in a sonic bath to remove any fine particles, and dried in an oven at 40°C. The pyroclasts were weighed, wrapped in Parafilm M® to waterproof them, and weighed again, this time suspended in deionised water by a wire cage (Figure 2.1). The density of the pyroclast was then calculated using Archimedes' principle. Vesicularity is calculated from density using a value for melt density, 2850 $kg.m^{-3}$, calculated from Eldgjá glass major element concentrations.

2.2.2 Vesicle-size distribution measurements

Image acquisition and processing

Polished thin-sections were made from pyroclasts selected from the central (mean ± 0.5 × s.d.) portion of representative density distributions. Nested images of the thin-sections (Figure 2.2) were acquired over four magnifications following the method outlined in Shea et al. (2010). The first level of magnification (c. 4.5x) was collected on an ordinary desktop scanner. Backscattered electron images at 50x, 100x, and 250x magnification were collected on a Hitachi TM3000 SEM. The images were processed, decoalesced, and made binary in the free and open-source raster graphics editor GNU Image Manipulation Program.

Image analysis

The binary images are analysed using the free and open-source image processing software ImageJ (Schneider et al. 2012). Each vesicle in the reference area is counted and measured for area. ImageJ results for each magnification level were collated in a spreadsheet to give the total bubble count and the reference area in each image. The area of each vesicle was then converted to a diameter of an equivalent circle. A minimum vesicle size was imposed based on the error

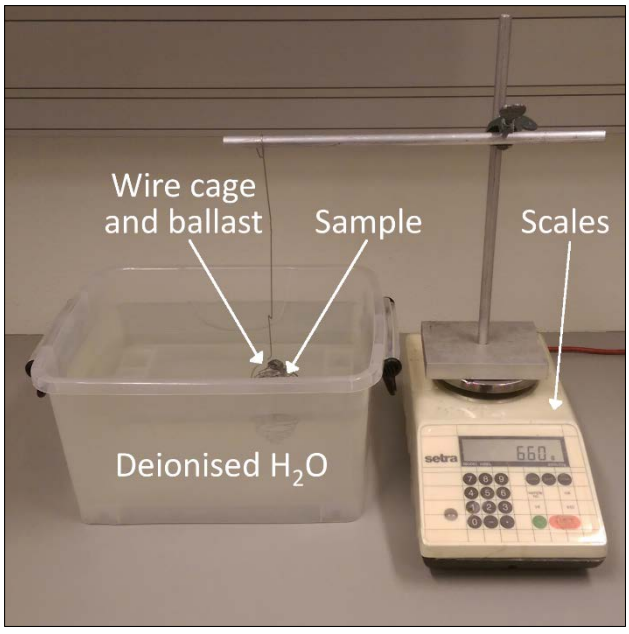

Figure 2.1 Method of measuring the density of pyroclasts using Archimedes' principle

associated with measuring circular objects represented by square pixels (Shea et al. 2010); here an 11-pixel limit was set corresponding to an equivalent diameter of 7 μm at the 250 x magnification level. The data was binned using a geometric bin size (equivalent diameter multiplied by $10^{0.1}$). The number of vesicles per unit area, N_A, was calculated for each bin in each magnification level and the results plotted against the equivalent diameter. Using this plot the transitions between magnifications were selected, ensuring a smooth transition where possible. The method of Sahagian and Proussevitch (1998) was used to convert from the number of vesicles per unit area, N_A, to the number per unit volume, N_V. This method relies upon the assumption that the vesicles are spherical which is generally true in these samples. The number per unit volume can then be corrected for vesicularity to give the number of vesicles per unit volume of melt, N_V^m.

2.2.3 Grain-size analysis

The grain-size distribution for tephra coarser than 4 Φ (Φ is $\log_2$[diameter in mm]) was determined by dry sieving samples by hand at 0.5 Φ intervals. The samples were generally split at 3 Φ (125 μm) and half were then analysed in a Micromeritics Sedigraph® III Plus Particle Size Analyzer down to 10 Φ (1 μm) using a density of 2600 $kg.m^{-3}$ obtained using a glass pycnometer. This gave four bins of overlap with which to splice the data from the two methods which was carried out manually.

Total grain-size distributions for the two episodes were calculated using the Voronoi tessellation method of Bonadonna and Houghton (2005) with the TOTGS Matlab® script of Biass and Bonadonna (2014). The bimodal distribution of Unit 8 was deconvolved into two probability density functions using the program Decolog (Borselli and Sarocchi 2016).

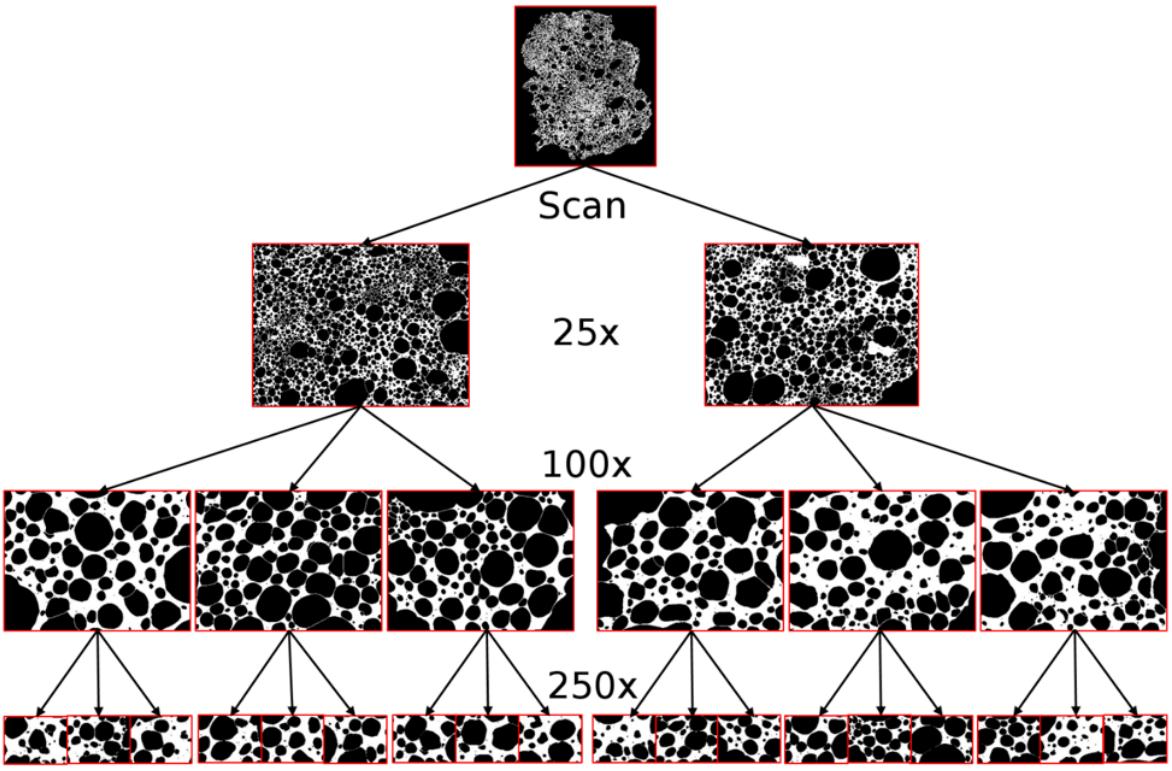

Figure 2.2 Exponential nested imaging strategy using 27 images

2.2.4 Eruption source parameters

Volume

The volume of a tephra deposit is calculated by integrating a semi-log plot of isopach-thickness against isopach-area. In an attempt to remove the effect of wind from the equation, thickness is plotted against the square root of area (Figure 2.3; Pyle 1989). There are several different methods of arriving at a volume depending on what type of curve you integrate under. In this study the methods used were: the trapezoidal (e.g. Froggatt 1982; Fierstein and Nathenson 1992), exponential (Pyle 1995), power-law (Bonadonna and Houghton 2005), and Weibull methods (Bonadonna and Costa 2013). The latter three methods were calculated using the AshCalc python script (Daggitt et al. 2014) which allows the easy comparison of the exponential, power-law, and Weibull models of volume estimation. Bulk volumes were converted to dense rock equivalent values by multiplying by (1-φ) where φ is the average vesicle fraction of the tephra in question.

Eruption column height

Methods for calculating the eruption column heights of various explosive episodes in this study include those of Carey and Sparks (1986), Mastin et al. (2009) and Wilson et al. (1978). The empirical method of Mastin et al. (2009) uses the following formula to calculate column height (H) from erupted volume (V):

$$H = 25.9 + 6.64 \log_{10}(V) \quad (1)$$

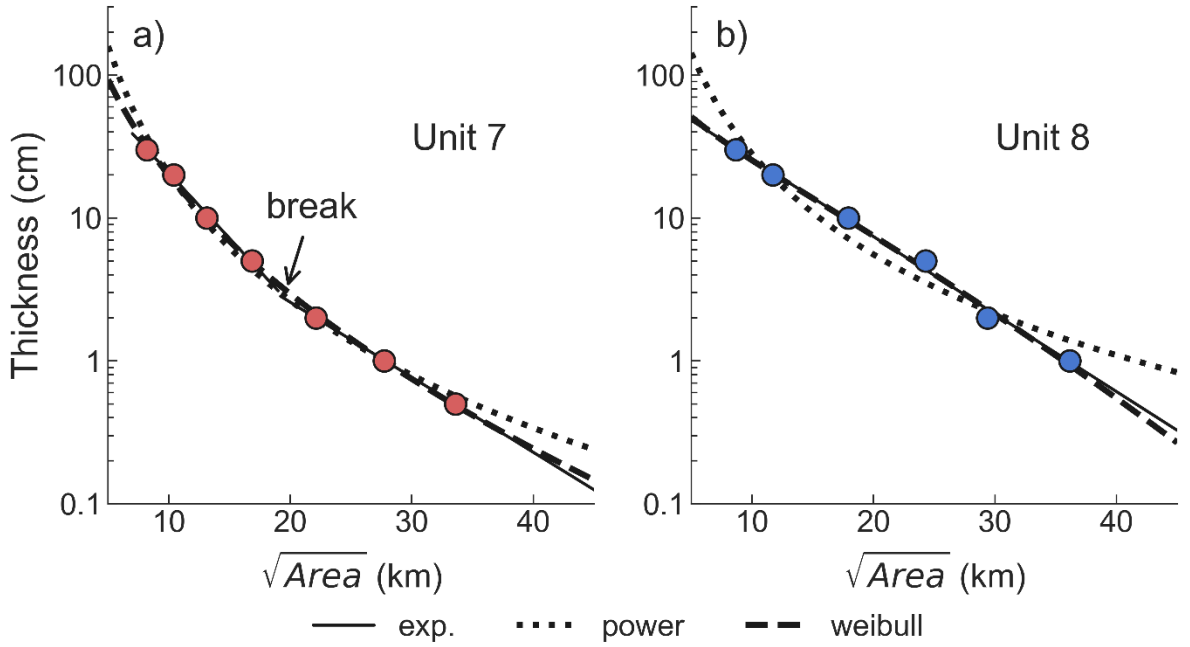

Figure 2.3 Semi-log plot of isopach thickness against the square-root of isopach area. Red data points are from Eldgjá's magmatic unit 7 whilst blue are from the phreatomagmatic unit 8. Solid lines are the exponential model fitted to the data, dotted lines are the power-law model, and dashed are the Weibull model. The exponential model fitted the unit 7 data best when two segments were used, the break in slope is labelled

The formula of Wilson et al. (1978) calculates column height from the rate of release of thermal energy at the vent (Q):

$$H = 8.2Q^{\frac{1}{4}} \quad (2)$$

where Q can be calculated by Stothers et al. (1986):

$$Q = \sigma(1 - x - y)vs_m\Delta T_f + \sigma xvs_m\Delta T_a + \sigma yvs_w\Delta T_a \quad (3)$$

where σ = magma density (2850 kg m^{-3}), x = weight fraction of tephra < 1 mm in diameter, y = weight fraction of volatiles (0.005), v = volumetric eruption rate (m s^{-1}), s_m = specific heat of basaltic magma (1100 J kg^{-1} K^{-1}), s_w = specific heat of steam (2000 J kg^{-1} K^{-1}), ΔT_f = change in temperature of tephra in the fountain (50 °C), and ΔT_a = change in temperature of tephra < 1 mm in diameter and volatiles in the plume (1150 °C).

2.2.5 Geochemical analysis

Major and trace element analysis of tephra and lava samples was carried out by X-ray fluorescence spectrometry. Samples were prepared for XRF by preparing fused glass discs for major element analysis and pressed powder pellets for trace elements. The methods used in the preparation followed those outlined by Fitton et al. (1998) with modifications noted by Fitton & Godard (2004). Analytical precision and accuracy are comparable to the values reported by Fitton et al. (1998).

3 Paper I: Comparison of explosive products

3.1 Summary

Although the Eldgjá eruption was dominantly effusive (19.7 km^3 of lava, 93% of total), there were at least sixteen explosive phases which took place along the full length of the 70-km-long fissure and produced 1.3 km^3 of tephra (all volumes are in dense rock equivalent, DRE). Explosive activity began beneath Mýrdalsjökull and subsequent phases generally took place ever more north-eastwards. Because of the subaerial and subglacial nature of the explosive activity, the composite tephra deposit of Eldgjá consists of both magmatic and phreatomagmatic tephra.

In this paper, the two styles of activity are compared in terms of physical volcanological parameters such as volume, grain-size distribution, and eruption source parameters. To this end, one magmatic unit and one phreatomagmatic unit were chosen, units 7 and 8 respectively, mapped in detail, and sampled. These units were selected due to their consecutive presence in the stratigraphy and similar distribution area which allowed fieldwork to be concentrated and carried out efficiently. They are also immediately above a highly distinctive horizon in the stratigraphy (unit 5, Figure 1.7) which aided identification.

3.2 Main results

Unit 7 is a magmatic deposit originating from a subaerial fissure segment between Gígalda and Rauðibotn (Figure 1.6). Unit 8 is phreatomagmatic, originating from beneath Mýrdalsjökull to the west of Merkigil and Jökulgil (Figure 1.6).

The volumes for each unit were calculated using several methods outlined in section 2.2.4 but the exponential method was chosen as the most representative as it fit the data most closely. Two segments were used to model unit 7 and one segment for unit 8 (Figure 2.3). The volume of units 7 and 8 are 0.024 and 0.028 km^3 respectively.

The height of the plumes during these phases is estimated to have been between 11 and 18 km, higher than the tropopause above Iceland. There was no significant difference in the plume heights between the magmatic and phreatomagmatic phases despite the preconception that subglacial eruptions are more explosive.

Using the Walker (1973) classification unit 7 has been classed as strong subplinian to weak Plinian and unit 8 as phreatoplinian.

The total deposit grain-size distribution (TGSD) of unit 7 is positively-skewed and unimodal with a mode of -2.2 Φ (Figure 3.1). Unit 8 has a bimodal TGSD with modes at 0.0 and 5.0 Φ (Figure 3.1). The fine peak of unit 8 is inferred to be the result of thermal granulation of the hot magma upon interaction with colder external water of the glacier.

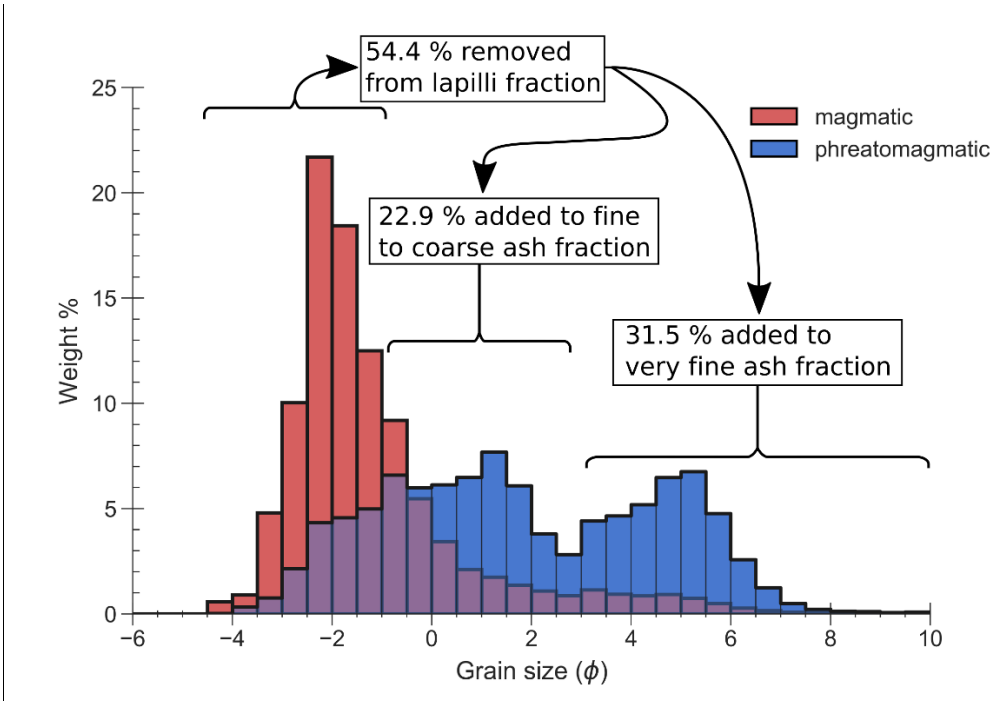

Figure 3.1 TGSD for units 7 and 8 in red and blue respectively, showing coarse, unimodal nature of the former and bimodal nature of the latter. Percentages refer to the effect of thermal granulation if the red distribution was to represent the blue prior to the blue interacting with external water

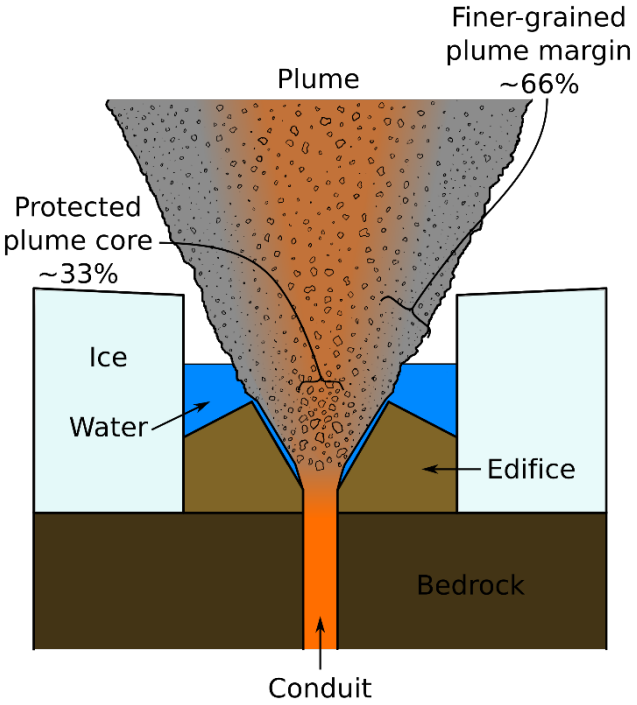

Figure 3.2 Schematic illustration demonstrating the partial interaction of the erupting magma with external water from the glacier. About half of the erupting magma undergoes full or partial thermal granulation to ash but the remaining half is essentially unaffected by water-related fragmentation

As will be discussed further in section 4, the vesiculation history of the phreatomagmatic tephra is identical to that of the magmatic tephra and that explosive phases from beneath Mýrdalsjökull would have been explosive even if no ice had been present. As such the TGSD of unit 7 can be used to represent the distribution of unit 8 had the ice not been present. Using this as a starting point it is possible to demonstrate that thermal granulation of the magmatic foam reduced about 50% of the erupting material in size (Figure 3.1). About 30% was reduced to very fine ash or finer and about 20% to between fine and coarse ash. The remaining 50% of the material was essentially unaffected by external water, suggesting that external water was only able to interact with an outer margin of the erupting column (Figure 3.2).

4 Paper II: Driving mechanisms of explosive activity

4.1 Summary

Subglacial volcanic eruptions from Iceland can have a significant impact on the atmosphere and hence on aviation and the global economy, as demonstrated by the 2010 eruption of Eyjafjallajökull (Gudmundsson et al. 2012; Dellino et al. 2012). It is thought that thermally efficient magma-water interaction (phreatomagmatism) will increase the abundance of fine ash particles present in the tephra (Kokelaar 1986; Wohletz 1986; Wohletz et al. 2013). Given the importance of fine-ash to aviation hazards and national power grids (Wilson et al. 2012) it is important to assess the role of external water in 'wet' tephra-producing eruptions.

The 10th century Eldgjá fissure eruption presents an excellent natural laboratory in which to study both magmatic vesiculation and the impact of external water for several reasons. Firstly, because the fissure had both subaerial and subglacial segments allowing ice-related effects to be isolated from the results. Secondly, the Eldgjá magma has a very narrow compositional range and so similar throughout that in terms of bulk physical properties the magma is essentially uniform. Finally, Eldgjá produced >16 voluminous and widespread tephra units which are preserved such that many can be mapped accurately and sampled for lab-based analyses and measurements with fine temporal resolution. The aim of this paper is to explore and quantify the vent and shallow conduit processes, specifically bubble nucleation, which influenced the nature of the explosive phases of Eldgjá.

To carry out this study, tephra was sampled from two key sections Stóragil and Skælingar using the methods outlined in section 2.1.3. Magmatic and phreatomagmatic tephra erupted from subaerial and subglacial fissure segments respectively were sampled at Stóragil and Skælingar for density and vesicle-size analysis. Once density measurements had been made of the pyroclasts, thirteen clasts were made into thin-sections and vesicle-size measurements were made using the methods outlined in section 2.2.2.

4.2 Main results

The vesicularity distributions (Figure 4.1) highlight a subtle difference between the magmatic and phreatomagmatic samples. The magmatic tephra feature tight, unimodal vesicularity/density distributions but a wide range of average vesicularities (61.2 to 80.4%) whereas the phreatomagmatic tephra have relatively plateau-like distributions and cover a tighter range of mean vesicularities (74.8 to 79.3%).

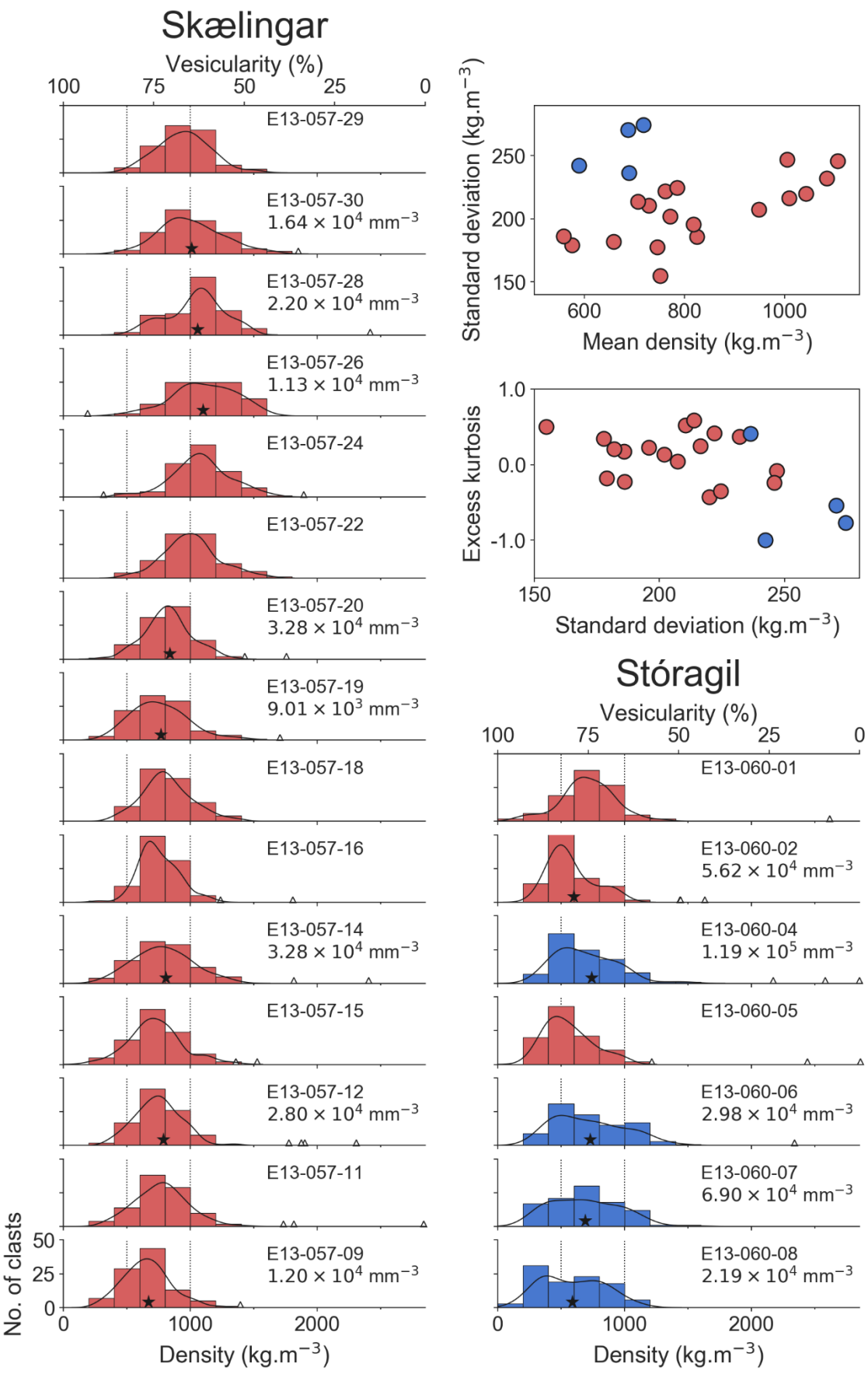
Skælingar
Vesicularity (%)
100
75
50
25
0
E13-057-29
E13-057-30
1.64 × 10^4 mm^-3
E13-057-28
2.20 × 10^4 mm^-3
E13-057-26
1.13 × 10^4 mm^-3
E13-057-24
E13-057-22
E13-057-20
3.28 × 10^4 mm^-3
E13-057-19
9.01 × 10^3 mm^-3
E13-057-18
E13-057-16
E13-057-14
3.28 × 10^4 mm^-3
E13-057-15
E13-057-12
2.80 × 10^4 mm^-3
E13-057-11
E13-057-09
1.20 × 10^4 mm^-3
No. of clasts
50
25
0
0
1000
2000
Density (kg.m^-3)
Standard deviation (kg.m^-3)
250
200
150
600
800
1000
Mean density (kg.m^-3)
Excess kurtosis
1.0
0.0
-1.0
150
200
250
Standard deviation (kg.m^-3)
Stóragil
Vesicularity (%)
100
75
50
25
0
E13-060-01
E13-060-02
5.62 × 10^4 mm^-3
E13-060-04
1.19 × 10^5 mm^-3
E13-060-05
E13-060-06
2.98 × 10^4 mm^-3
E13-060-07
6.90 × 10^4 mm^-3
E13-060-08
2.19 × 10^4 mm^-3
0
1000
2000
Density (kg.m^-3)

Figure 4.1 (overleaf) Density distributions of the Eldgjá tephra samples. Red histograms: magmatic samples; blue histograms: phreatomagmatic samples. The black curves are kernel density estimates for the density measurements. Black stars indicate the density of the pyroclasts which were used for vesicle size analysis and triangles along x-axis indicate outliers which were excluded from the statistical analyses. The vesicle number density of analysed clasts is included below the sample numbers. Vertical dotted lines are to facilitate comparisons between samples

Melt-corrected vesicle number densities for magmatic and phreatomagmatic tephra clasts are similar, both in the range 9.0×10^3 to 1.2×10^5 mm^{-3} (Figure 4.2). These values are higher than those measured in samples from Hawaiian-style fire fountaining (Kilauea Iki, Hawaii; Stovall et al. 2011, 2012), Strombolian-explosions (Stromboli; Lautze and Houghton 2005, 2007, 2008) and a basaltic Plinian eruption (Tarawera, New Zealand; Sable et al. 2009). The Eldgjá values are on a par with those measured from another basaltic Plinian eruption at Etna (Sable et al. 2006).

Both magmatic and phreatomagmatic samples present unimodal vesicle volume distributions with the mode indicating a significant nucleation event (Figure 4.3). Vesicle volume distributions for the magmatic and phreatomagmatic show no difference between the two indicating that all samples experienced similar bubble nucleation histories. The median vesicle size remains relatively uniform throughout all samples; between 0.192 and 0.340 mm for magmatic and 0.198 and 0.241 mm for phreatomagmatic.

Within both magmatic and phreatomagmatic tephra, domains of either microlite-rich or microlite-poor were found. The domains exist either as entire clasts or as microlite-rich domains within a clast of microlite-poor material. Both domain types feature ~3% plagioclase laths by area which are around 20 µm long. The microlite that make up the microlite-rich material are between 30 and 50% by area and are around µm long. The contact between domains is sharp and convoluted. Vesicle-size distributions across both are essentially identical and appear to have grown coincidently with the fine fraction of microlites. The microlite-rich domains are interpreted as recording a velocity gradient across the conduit.

Strings of vesicles have been found which are between 0.2 and 1.0 mm wide and up to 30 mm long. Whilst the process of their formation is not understood, the consequence of the strings is suggested as leading to a mesh-like network with a cell-size close to medium lapilli in diameter. These networks form planes of weakness which, when the foam fragments, determines the modal size of the fragments, hence the modal size fraction in magmatic total grain-size distributions.

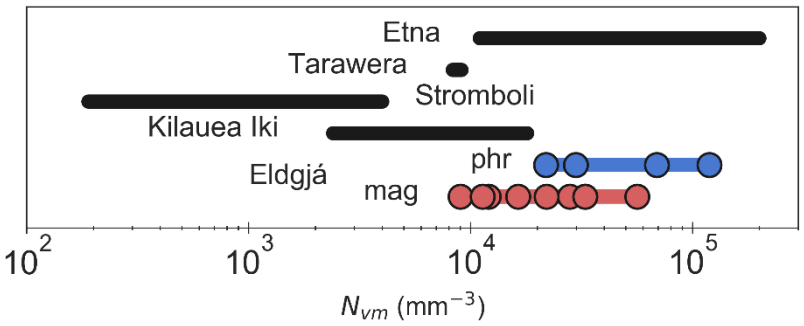

Figure 4.2 Eldgjá magmatic and phreatomagmatic vesicle number densities compared with those of other basaltic eruptions determined by the same methods (Etna 122 CE, Sable et al. (2006); Tarawera 1886, Sable et al. (2009); Stromboli 2002, Lautze and Houghton (2005, 2007, 2008); Kilauea Iki 1959, Stovall et al. (2011, 2012)

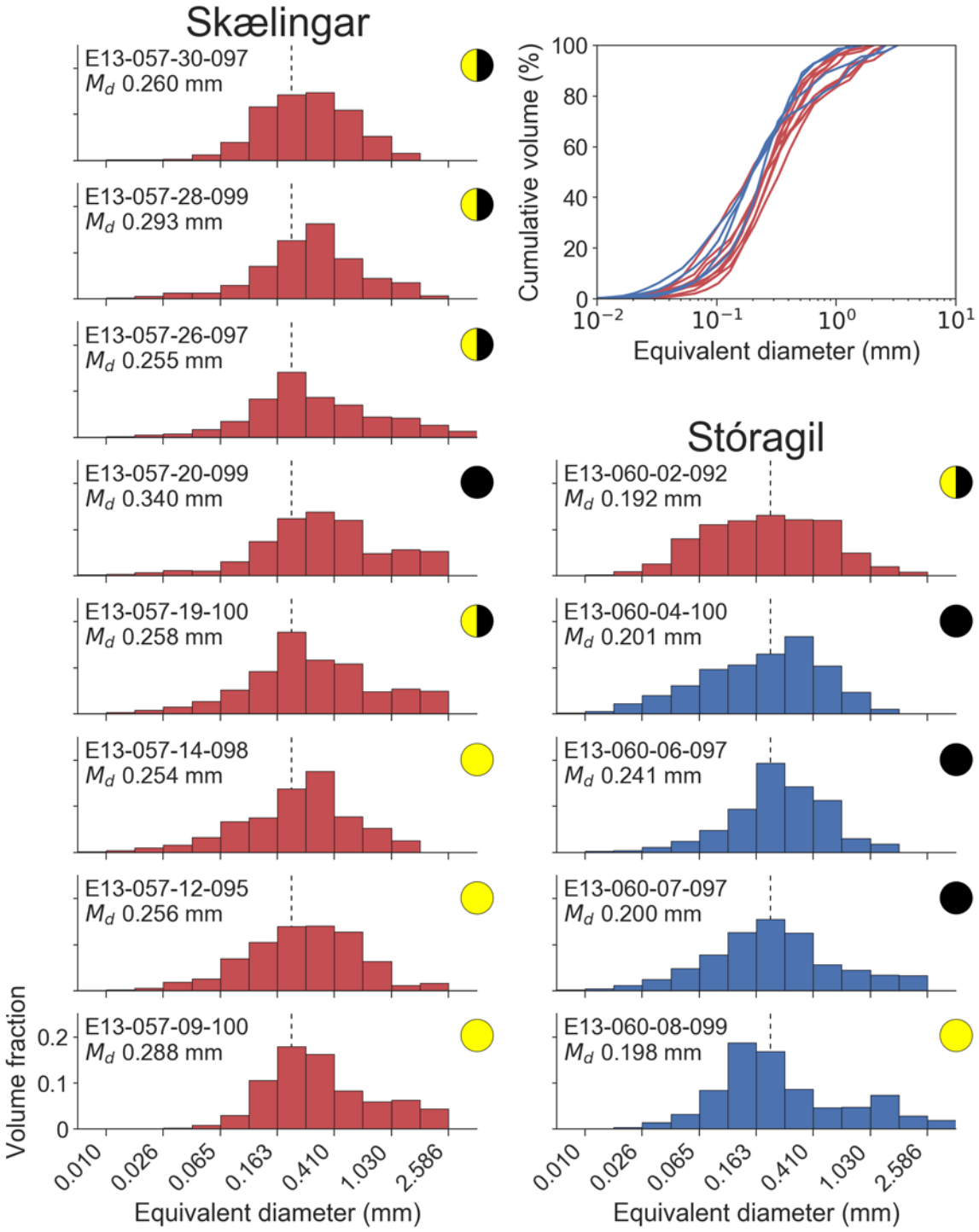

Figure 4.3 Vesicle volume distributions for the Skælingar and Stóragil tephra sections. Red plots are magmatic samples and blue phreatomagmatic. Each plot is labelled with the sample number and median vesicle diameter (M_d). The black dotted line is to aid comparison between distributions and is located at 0.2 mm equivalent diameter. Yellow or black circles indicate pyroclasts with only microlite-poor or -rich domains respectively, with yellow and black circles representing clasts containing both domain types. Inset is a cumulative vesicle volume plot summarising all sample data and highlights how similar each sample's nucleation history is

5 Paper III: Variation of style and composition

5.1 Summary

The 10th century Eldgjá eruption erupted nearly 20 km^3 of magma making it the most voluminous eruption of the last 2000 years. At least 1.3 km^3 (dense rock equivalent) of this magma was erupted as tephra in at least 16 explosive phases. By mapping and chemically analysing the composite tephra deposit of Eldgjá a data set can be constructed which would record both spatial and temporal changes in eruption style and chemical composition. This would be informative of both lower and upper crustal (i.e. upper conduit) processes active during the Eldgjá eruption. Eldgjá may also be used as an analogue of the much large Earth-altering flood lava eruptions which have formed the likes of the Deccan and Siberian Traps, and Columbia River Basalts.

To complete this objective, it was necessary to have as detailed a timeline of events during the Eldgjá eruption as possible. A key part of this was the order of explosive phases as recorded in the stratigraphy (Figure 5.1).

5.2 Main results

The tephra stratigraphy revealed that the explosive phases of Eldgjá took place in discrete segments of the fissure segment. These discrete segments were not active simultaneously, nor were they active in a linear geographic order. Instead activity seemed to fluctuate between subglacial and subaerial fissure segments either side of the edge of Mýrdalsjökull, by Öldufell (Figure 1.6). During and after phase 11 activity finally progressed fully to the northeast taking advantage of pre-existing graben structures at Álftavatnakrókur and Eldgjá proper.

The magma composition evolved with time with whole-rock MgO in early tephra units between 5.6 and 5.7 wt.%, and dropping to almost 4.5 wt.% with time while TiO_2 increased from 4.4 to 4.6 wt.%. The incompatible trace element concentrations also increased with time; for example, Ba increases from 168 to 193 ppm, an increase of 15%.

The ratio of Zr to Nb is effectively constant throughout the Stóragil stratigraphy, varying between 6.8 and 7.1. This demonstrates that the observed compositional range in the major and trace elements must be a result of fractional crystallization, and not magma mixing as that would require mixing a high MgO magma with a low MgO magma with both having identical incompatible element ratios.

The data do not support a model of magma extraction from a chemically stratified magma chamber in which case the earliest products would be the least primitive. Instead, a source from relatively deep which supplied primitive magma directly to beneath the region of Öldufell is suggested. This conduit was established and then magma began to migrate north-eastwards to the rest of the fissure system.

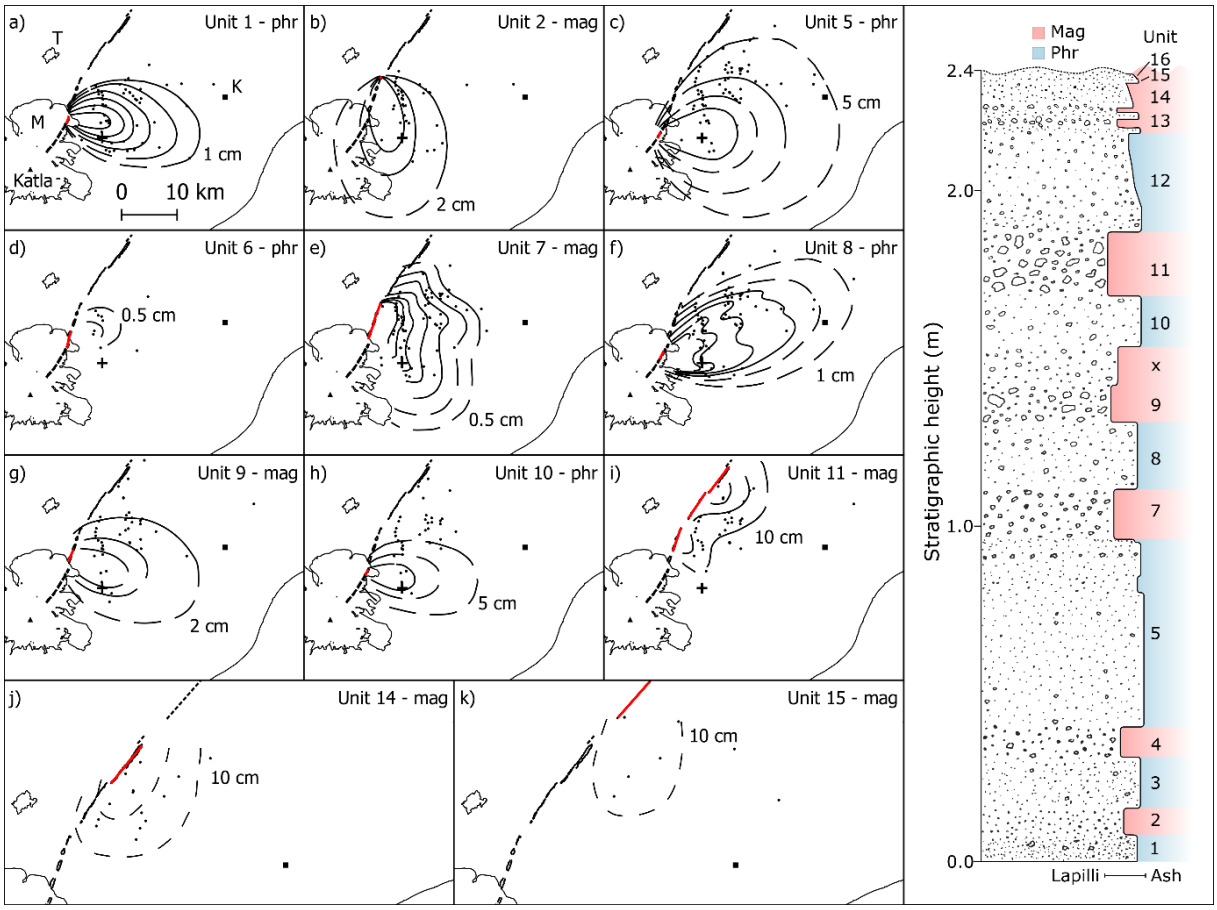

Figure 5.1 The sequence of explosive events as revealed by the Eldgjá tephra stratigraphy and shown using isopach maps. For the names of active vents (red lines) refer to Figure 1.6. The location of the example stratigraphic section, Stóragil, is shown by a cross. The abbreviations in a) are: M, Mýrdalsjökull; K, Kirkjubæjarklaustur; T, Torfajökull. Dashed isopach lines indicate areas of inadequate data. Isopach maps with thickness labels are available in the supplementary material

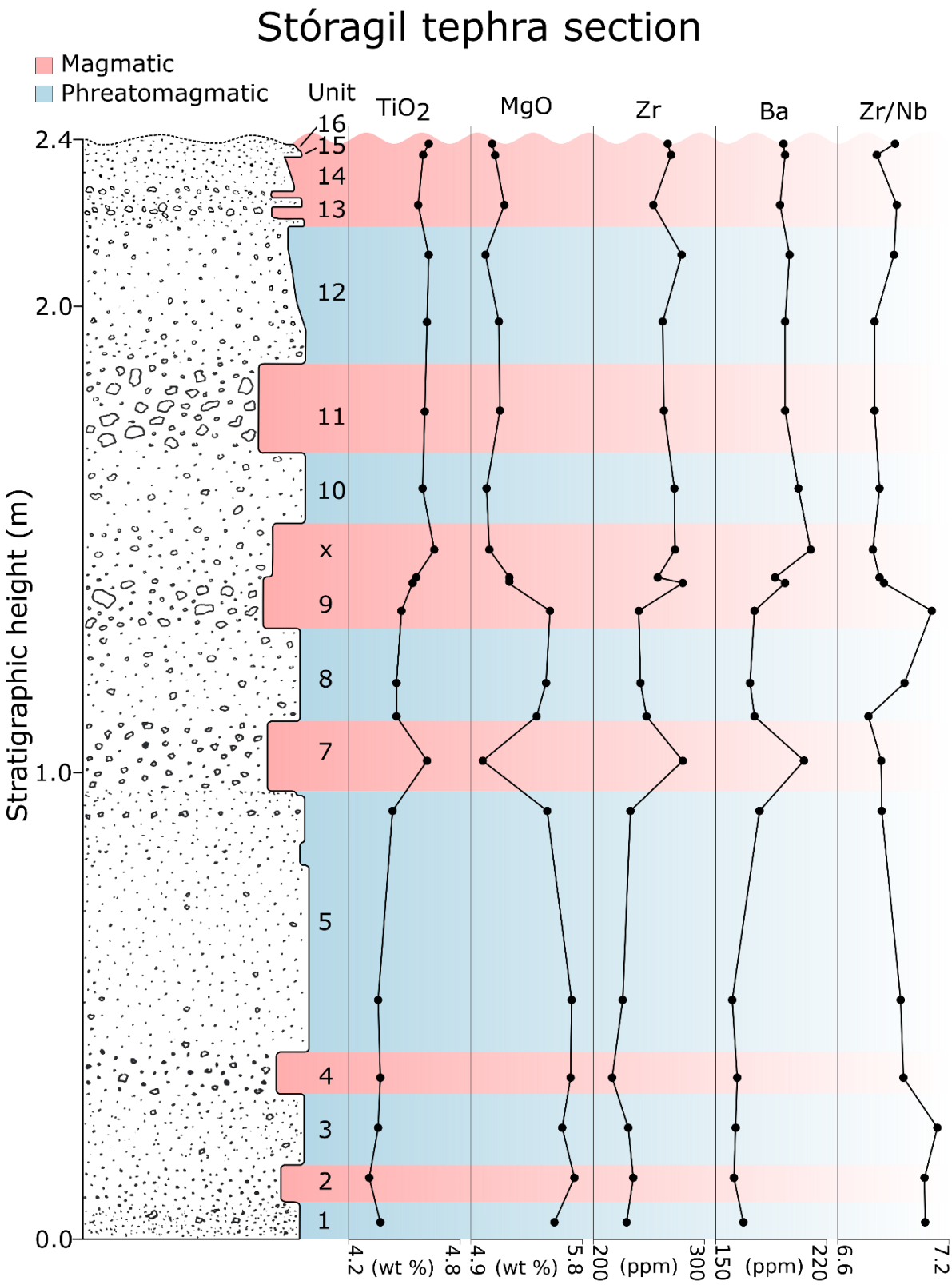

Figure 5.2 Element – profile plots for selected elements measured in tephra from the Stóragil section. Every plot demonstrates the magma composition evolving with time; incompatible elements increase and compatible elements decreases with stratigraphic height/time

6 General Conclusions

The explosive episodes of the 10th century fissure eruption of Eldgjá have been analysed for a range of measurements including grain-size, density, vesicle-size, and major and trace element chemistry. Because explosive activity took place at only relatively short lengths of the fissure at any one time, data gathered from a range of points in the Eldgjá tephra stratigraphy reveal both temporal and spatial characteristics. In addition to this, the combination of subaerial and subglacial explosive activity means that there is a wealth of data describing a range of processes. Eldgjá is an excellent analogue for the much larger flood lava eruptions which formed the likes of the Deccan and Siberian Traps or Columbia River Basalts. By studying Eldgjá we have a better understanding of the processes which govern these Earth-altering events.

The following conclusions will be discussed in the order in which the analysed samples acquired their characteristics. For example, the chemistry will be first as this was quality was imparted upon the magma prior to any surface processes.

The chemistry of Eldgjá is typical for the propagating-rift setting in which it was found. It is high in iron and titanium, as are most magmas associated with the Katla volcanic system. It is a transitional alkaline basalt which is a trait of the Eastern Volcanic Zone in which the Katla system is situated. That being said, the Eldgjá magma is on the primitive end of the Katla products whilst also being highly evolved with respect to other EVZ basalts. Analyses of a detailed stratigraphic section have revealed that the composition of the Eldgjá magma became slightly more evolved with time going from a MgO concentration of 5.6 to 5.0 wt.%. This trend, while small, is steady and seen in both major and trace, and compatible and incompatible elements. It is important to bear in mind that activity not only propagated along the length of the fissure with time but also made several recursions to previously active segments, so the fact that there is a relatively constant trend is remarkable.

This raises questions about the origin of the magma. The Eldgjá flood lava eruption is the most voluminous eruption on Earth in the last 1100 years, erupting nearly 20 km^3 of magma. The 1875 Askja eruption removed 0.3 km^3 of magma from a shallow storage zone beneath the volcano and resulted in the formation of Öskjuvatn (Hartley and Thordarson 2012). Nearly 100 meters of subsidence was associated with the 2014-15 Bárðarbunga–Holuhraun eruption which emplaced between 1 and 2 km^3 of lava (Gudmundsson et al. 2016). If 20 km^3 of magma was removed from the shall crust, there should certainly be some visible evidence for it.

Microlite-rich domains within tephra clasts point to a velocity gradient in the upper conduit. The conduit geometry is a factor in the proportion of microlite-rich to microlite-poor domains and as such the quantification of these kinds of microtextural observations may provide insights into the subsurface pathways of erupting magma.

Vesicle-size analysis has revealed that the nucleation histories beneath subaerial and subglacial fissure segments are essentially identical. Vesicle volume distributions exhibit a unimodal distribution, indicating a single burst of nucleation forming most of the bubbles. Bubble coalescence appears to have played an insignificant role although due to the short relaxation times of basaltic melts perhaps a record of this process is not fully preserved.

Strings of bubbles are occasionally preserved and may record a mesh-like network of bubbles throughout the foam which form rapidly enough to preclude high permeability and pressure loss. When this meshed foam reaches its point of fragmentation the first planes of

weakness are the bubble strings. Hence, the cell-size of the bubble string mesh dictates the coarse peak in magmatic TGSD.

Vesicle number densities of Eldgjá tephra are very high, similar to values measured from basaltic Plinian eruptions such as the 122 CE Etna eruption and higher than values measured from Hawaiian fire-fountains or Strombolian explosions at Stromboli. Vesicle number densities seem to correlate with ascent rates based upon previous studies, providing an independent appraisal of this otherwise unmeasurable parameter in old eruptions.

Density and vesicularity measurements show a difference between magmatic and phreatomagmatic tephra. The magmatic samples feature a narrow range of vesicularities whereas the phreatomagmatic samples are wider. Given that the bubble nucleation histories are identical between the two tephra types, the difference in vesicularity must be a result of processes occurring once the magma has reached the uppermost part of conduit. It is suggested that external water was able to access the magma ascending at subglacial vents and quench it, preventing further bubble nucleation or growth. The range in vesicularities would then be a result of water encountering magma at various stages of vesiculation.

The most striking difference between the magmatic and phreatomagmatic tephra units in the Eldgjá deposit is their grain-size distribution. In the proximal to medial area (5 to 20 km from source) the magmatic tephra typically consists of lapilli to coarse ash whereas the phreatomagmatic is a poorly sorted mix of very fine to fine ash with a small amount of coarse ash or lapilli. The magmatic tephra have unimodal, positively-skewed distributions with a mode at around -2 Φ whereas the phreatomagmatic tephra are bimodal with one peak at 0 Φ and another at 5 Φ. The coarse peak in the phreatomagmatic distribution is 2 Φ finer-grained than the magmatic.

It has already been shown that the magma beneath subglacial and subaerial fissure segments was physically identical so it can be assumed that the grain-size distribution of the magmatic tephra is the unmodified distribution with respect to external water – the only difference between the two tephra types. It is suggested that thermal granulation of the hot magma upon contact with cold external water is the primary process of fragmentation in the phreatomagmatic tephra. If this is the case, then only about half of the erupting magma came into contact with external water at the subglacial fissure segments based upon the difference between the total grain-size distributions. This half was thermally-granulated with about 30 wt.% being reduced from lapilli to very fine or finer ash and the remainder to between fine and coarse ash. It may be that only the outer margin of individual lapilli clasts was fully granulated to very fine ash leaving a core of coarser ash.

There remain countless avenues of investigation left open with respect to the Eldgjá eruption, explosive basaltic eruptions, and flood lava eruptions in general. A particularly interesting research theme which Eldgjá could help explore is the nature of conduit geometries, particularly in fissure eruptions. The mixed-cone row nature of Eldgjá and its great length provide many variations of vent style and context onto which methods such as vesicle-size analysis or microlite-content variation analysis could be applied. The Earth is an open book; we just need to read it.

References

Baillie MGL, McAneney J (2015) Tree ring effects and ice core acidities clarify the volcanic record of the first millennium. Clim Past 11:105–114. doi: 10.5194/cp-11-105-2015

Biass S, Bonadonna C (2014) TOTGS: Total grainsize distribution of tephra fallout.

Bjarnason IT (2008) An Iceland hotspot saga. Jökull 58:3–16.

Björnsson H, Pálsson F, Guðmundsson MT (2000) Surface and bedrock topography of the Mýrdalsjökull ice cap. Jökull 49:29–46.

Bonadonna C, Costa A (2013) Plume height, volume, and classification of explosive volcanic eruptions based on the Weibull function. Bull Volcanol 75:1–19. doi: 10.1007/s00445-013-0742-1

Bonadonna C, Houghton BF (2005) Total grain-size distribution and volume of tephra-fall deposits. Bull Volcanol 67:441–456. doi: 10.1007/s00445-004-0386-2

Borselli L, Sarocchi D (2016) DECOLOG.

Brown RJ, Blake S, Thordarson T, Self S (2014) Pyroclastic edifices record vigorous lava fountains during the emplacement of a flood basalt flow field, Roza Member, Columbia River Basalt Province, USA. Geol Soc Am Bull 126:875–891. doi: 10.1130/B30857.1

Carey S, Sparks RSJ (1986) Quantitative models of the fallout and dispersal of tephra from volcanic eruption columns. Bull Volcanol 48:109–125. doi: 10.1007/BF01046546

Carlson RW (1991) Physical and chemical evidence on the cause and source characteristics of flood basalt volcanism. Aust J Earth Sci 38:525–544. doi: 10.1080/08120099108727989

Cioni R, Pistolesi M, Rosi M (2015) Plinian and Subplinian Eruptions. In: Sigurdsson H (ed) The Encyclopedia of Volcanoes, 2nd edn. Academic Press, Amsterdam, pp 519–535

Coltelli M, Carlo PD, Vezzoli L (1998) Discovery of a Plinian basaltic eruption of Roman age at Etna volcano, Italy. Geology 26:1095–1098.

Costantini L, Houghton BF, Bonadonna C (2010) Constraints on eruption dynamics of basaltic explosive activity derived from chemical and microtextural study: The example of the Fontana Lapilli Plinian eruption, Nicaragua. J Volcanol Geotherm Res 189:207–224. doi: 10.1016/j.jvolgeores.2009.11.008

Daggitt ML, Mather TA, Pyle DM, Page S (2014) AshCalc–a new tool for the comparison of the exponential, power-law and Weibull models of tephra deposition. J Appl Volcanol 3:1. doi: 10.1186/2191-5040-3-7

Dellino P, Gudmundsson MT, Larsen G, et al (2012) Ash from the Eyjafjallajökull eruption (Iceland): Fragmentation processes and aerodynamic behavior. J Geophys Res Solid Earth 117:B00C04. doi: 10.1029/2011JB008726

Fei J, Zhou J (2006) The Possible Climatic Impact in China of Iceland's Eldgjá Eruption Inferred from Historical Sources. Clim Change 76:443–457. doi: 10.1007/s10584-005-9012-3

Fierstein J, Nathenson M (1992) Another look at the calculation of fallout tephra volumes. Bull Volcanol 54:156–167. doi: 10.1007/BF00278005

Froggatt PC (1982) Review of methods of estimating rhyolitic tephra volumes; applications to the Taupo volcanic zone, New Zealand. J Volcanol Geotherm Res 14:301–318. doi: 10.1016/0377-0273(82)90067-1

Gonnermann HM (2015) Magma Fragmentation. Annu Rev Earth Planet Sci 43:431–458. doi: 10.1146/annurev-earth-060614-105206
Grattan J (2005) Pollution and paradigms: lessons from Icelandic volcanism for continental flood basalt studies. Lithos 79:343–353. doi: 10.1016/j.lithos.2004.09.006
Gudmundsson A (1995) Infrastructure and mechanics of volcanic systems in Iceland. J Volcanol Geotherm Res 64:1–22. doi: 10.1016/0377-0273(95)92782-Q
Gudmundsson MT (2003) Melting of Ice by Magma-Ice-Water Interactions During Subglacial Eruptions as an Indicator of Heat Transfer in Subaqueous Eruptions. In: White JDL, Smellie JL, Clague DA (eds) Explosive Subaqueous Volcanism. American Geophysical Union, pp 61–72
Gudmundsson MT, Thordarson T, Höskuldsson Á, et al (2012) Ash generation and distribution from the April-May 2010 eruption of Eyjafjallajökull, Iceland. Sci Rep 2:572.
Gudmundsson MT, Jónsdóttir K, Hooper A, et al (2016) Gradual caldera collapse at Bárdarbunga volcano, Iceland, regulated by lateral magma outflow. Science 353:aaf8988. doi: 10.1126/science.aaf8988
Hartley ME, Thordarson T (2012) Formation of Öskjuvatn caldera at Askja, North Iceland: Mechanism of caldera collapse and implications for the lateral flow hypothesis. Journal of Volcanology and Geothermal Research 227–228:85–101. doi: 10.1016/j.jvolgeores.2012.02.009
Hammer CU (1984) Traces of icelandic eruptions in the Greeland ice sheet. Jökull 51–65.
Hon K, Kauahikaua J, Denlinger R, Mackay K (1994) Emplacement and inflation of pahoehoe sheet flows: observations and measurements of active lava flows on Kilauea Volcano, Hawaii. Geol Soc Am Bull 106:351–370.
Houghton BF, Gonnermann HM (2008) Basaltic explosive volcanism: Constraints from deposits and models. Chem Erde - Geochem 68:117–140. doi: 10.1016/j.chemer.2008.04.002
Houghton BF, Wilson CJN (1989) A vesicularity index for pyroclastic deposits. Bull Volcanol 51:451–462.
Houghton BF, Wilson CJN, Del Carlo P, et al (2004) The influence of conduit processes on changes in style of basaltic Plinian eruptions: Tarawera 1886 and Etna 122 BC. J Volcanol Geotherm Res 137:1–14. doi: 10.1016/j.jvolgeores.2004.05.009
Jakobsson SP (1979) Petrology of recent basalts of the Eastern Volcanic Zone, Iceland. Icelandic Museum of Natural History
Jóhannesson H, Sæmundsson K (1998) Geological Map of Iceland. Icelandic Insitute of Natural History and Iceland Geodetic Survey, Reykjavík.
Keszthelyi L, Self S (1998) Some physical requirements for the emplacement of long basaltic lava flows. J Geophys Res 103:27447–27464. doi: 10.1029/98JB00606
Kokelaar P (1986) Magma-water interactions in subaqueous and emergent basaltic volcanism. Bull Volcanol 48:275–289. doi: 10.1007/BF01081756
Larsen G (1984) Recent volcanic history of the Veidivötn fissure swarm, southern Iceland — an approach to volcanic risk assessment. J Volcanol Geotherm Res 22:33–58. doi: 10.1016/0377-0273(84)90034-9
Larsen G (2000) Holocene eruptions within the Katla volcanic system, south Iceland: characteristics and environmental impact. Jökull 49:1–28.
Larsen G (2010) Katla: tephrochronology and eruption history. Dev Quat Sci 13:23–49.
Lautze NC, Houghton BF (2007) Linking variable explosion style and magma textures during 2002 at Stromboli volcano, Italy. Bull Volcanol 69:445–460. doi: 10.1007/s00445-006-0086-1

Lautze NC, Houghton BF (2005) Physical mingling of magma and complex eruption dynamics in the shallow conduit at Stromboli volcano, Italy. Geology 33:425–428. doi: 10.1130/G21325.1

Lautze NC, Houghton BF (2008) Single explosions at Stromboli in 2002: Use of clast microtextures to map physical diversity across a fragmentation zone. J Volcanol Geotherm Res 170:262–268. doi: 10.1016/j.jvolgeores.2007.10.011

Lawver LA, Müller RD (1994) Iceland hotspot track. Geology 22:311–314. doi: 10.1130/0091-7613(1994)022<0311:IHT>2.3.CO;2

Lesher CE, Spera FJ (2015) Thermodynamic and transport properties of silicate melts and magma. In: Sigurdsson H (ed) Encyclopedia of Volcanoes, 2nd edn. Elsevier, Amsterdam, pp 113–141

Loughlin SC, Aspinall WP, Vye-Brown C, et al (2012) Large-magnitude fissure eruptions in Iceland: source characterisation. British Geological Survey

Mahoney JJ, Coffin MF (1997) Large Igneous Provinces: Continental, Oceanic, and Planetary Flood Volcanism. American Geophysical Union

Malinverno A (1990) A quantitative study of the axial topography of the Mid-Atlantic Ridge. J Geophys Res Solid Earth 95:2645–2660. doi: 10.1029/JB095iB03p02645

Mangan MT, Cashman KV, Newman S (1993) Vesiculation of basaltic magma during eruption. Geology 21:157–160. doi: 10.1130/0091-7613(1993)021<0157:VOBMDE>2.3.CO;2

Mastin LG, Guffanti M, Servranckx R, et al (2009) A multidisciplinary effort to assign realistic source parameters to models of volcanic ash-cloud transport and dispersion during eruptions. J Volcanol Geotherm Res 186:10–21. doi: 10.1016/j.jvolgeores.2009.01.008

McCarthy D, Breen A (1997) An evaluation of astronomical observations in the Irish annals. Vistas Astron 41:117–138. doi: 10.1016/S0083-6656(96)00052-9

McClintock M, White JDL (2006) Large phreatomagmatic vent complex at Coombs Hills, Antarctica: Wet, explosive initiation of flood basalt volcanism in the Ferrar-Karoo LIP. Bull Volcanol 68:215–239. doi: 10.1007/s00445-005-0001-1

Namiki A, Manga M (2008) Transition between fragmentation and permeable outgassing of low viscosity magmas. J Volcanol Geotherm Res 169:48–60. doi: 10.1016/j.jvolgeores.2007.07.020

Németh K, Suwesi SK, Peregi Z, et al (2003) Plio/Pleistocene flood basalt related scoria and spatter cones, rootless lava flows, and pit craters, Al Haruj Al Abiyad, Libya. GeoLines 15:98–103.

Oman L, Robock A, Stenchikov GL, Thordarson T (2006) High-latitude eruptions cast shadow over the African monsoon and the flow of the Nile. Geophys Res Lett 33:L18711. doi: 10.1029/2006GL027665

Óskarsson BV, Andersen CB, Riishuus MS, et al (2017) The mode of emplacement of Neogene flood basalts in Eastern Iceland: The plagioclase ultraphyric basalts in the Grænavatn group. J Volcanol Geotherm Res 332:26–50. doi: 10.1016/j.jvolgeores.2017.01.006

Óskarsson BV, Riishuus MS (2013) The mode of emplacement of Neogene flood basalts in Eastern Iceland: Facies architecture and structure of the Hólmar and Grjótá olivine basalt groups. J Volcanol Geotherm Res 267:92–118. doi: 10.1016/j.jvolgeores.2013.09.010

Óskarsson BV, Riishuus MS (2014) The mode of emplacement of Neogene flood basalts in eastern Iceland: Facies architecture and structure of simple aphyric basalt groups. J Volcanol Geotherm Res 289:170–192. doi: 10.1016/j.jvolgeores.2014.11.009

Papale P (1999) Strain-induced magma fragmentation in explosive eruptions. Nature 397:425–428. doi: 10.1038/17109

Parfitt EA, Wilson L (1999) A Plinian treatment of fallout from Hawaiian lava fountains. J Volcanol Geotherm Res 88:67–75. doi: 10.1016/S0377-0273(98)00103-6

Pedersen GBM, Höskuldsson A, Dürig T, et al (2017) Lava field evolution and emplacement dynamics of the 2014–2015 basaltic fissure eruption at Holuhraun, Iceland. J Volcanol Geotherm Res. doi: 10.1016/j.jvolgeores.2017.02.027

Polacci M, Corsaro RA, Andronico D (2006) Coupled textural and compositional characterization of basaltic scoria: Insights into the transition from Strombolian to fire fountain activity at Mount Etna, Italy. Geology 34:201–204. doi: 10.1130/G22318.1

Pyle DM (1989) The thickness, volume and grainsize of tephra fall deposits. Bull Volcanol 51:1–15.

Pyle DM (1995) Assessment of the minimum volume of tephra fall deposits. J Volcanol Geotherm Res 69:379–382. doi: 10.1016/0377-0273(95)00038-0

Rampino MR, Stothers RB (1988) Flood Basalt Volcanism during the Past 250 Million Years. Sci Wash 241:663.

Robson GR (1956) The volcanic geology of Vestur – Skaftarfellssysla Iceland. Doctoral, Durham University

Sable JE, Houghton BF, Del Carlo P, Coltelli M (2006) Changing conditions of magma ascent and fragmentation during the Etna 122 BC basaltic Plinian eruption: Evidence from clast microtextures. J Volcanol Geotherm Res 158:333–354. doi: 10.1016/j.jvolgeores.2006.07.006

Sable JE, Houghton BF, Wilson CJN, Carey RJ (2009) Eruption mechanisms during the climax of the Tarawera 1886 basaltic Plinian eruption inferred from microtextural characteristics of the deposits. Stud Volcanol Leg George Walk Geol Soc Lond 129–154.

Sahagian DL, Proussevitch AA (1998) 3D particle size distributions from 2D observations: stereology for natural applications. J Volcanol Geotherm Res 84:173–196. doi: 10.1016/S0377-0273(98)00043-2

Saunders AD, Fitton JG, Kerr AC, et al (1997) The North Atlantic Igneous Province. In: J.honey J, Coffin MF (eds) Large Igneous Provinces: Continental, Oceanic, and Planetary Flood Volcanism. American Geophysical Union, pp 45–93

Schmidt A, Ostro B, Carslaw KS, et al (2011) Excess mortality in Europe following a future Laki-style Icelandic eruption. Proc Natl Acad Sci 108:15710–15715.

Schneider CA, Rasband WS, Eliceiri KW (2012) NIH Image to ImageJ: 25 years of image analysis. Nat Methods 9:671–675. doi: 10.1038/nmeth.2089

Self S, Thordarson T, Widdowson M (2005) Gas Fluxes from Flood Basalt Eruptions. Elements 1:283–287. doi: 10.2113/gselements.1.5.283

Self S, Thordarson T, Keszthelyi L, et al (1996a) A new model for the emplacement of Columbia River basalts as large, inflated Pahoehoe Lava Flow Fields. Geophys Res Lett 23:2689–2692. doi: 10.1029/96GL02450

Self S, Zhao J-X, Holasek RE, et al (1996b) The atmospheric impact of the 1991 Mount Pinatubo eruption. In: Newhall CG, Punongbayan RS (eds) Fire and Mud: The eruptions and Lahars of Mount Pinatubo, Phillippines. University of Washington Press, Seattle, pp 1089–1116

Self S, Thordarson T, Keszthelyi L (1997) Emplacement of Continental Flood Basalt Lava Flows. In: Large Igneous Provinces: Continental, Oceanic, and Planetary Flood Volcanism. American Geophysical Union, pp 381–410

Sharma K, Self S, Blake S, et al (2008) The AD 1362 Öræfajökull eruption, S.E. Iceland: Physical volcanology and volatile release. J Volcanol Geotherm Res 178:719–739. doi: 10.1016/j.jvolgeores.2008.08.003

Shea T, Houghton BF, Gurioli L, et al (2010) Textural studies of vesicles in volcanic rocks: An integrated methodology. J Volcanol Geotherm Res 190:271–289. doi: 10.1016/j.jvolgeores.2009.12.003

Sigurðardóttir SS, Gudmundsson MT, Hreinsdóttir S (2015) Mapping of the Eldgjá lava flow on Mýrdalssandur with magnetic surveying. Jökull 65:61–71.

Sparks RSJ (1986) The dimensions and dynamics of volcanic eruption columns. Bull Volcanol 48:3–15. doi: 10.1007/BF01073509

Stothers RB (1998) Far reach of the tenth century Eldgjá eruption, Iceland. Clim Change 39:715–726.

Stothers RB, Wolff JA, Self S, Rampino MR (1986) Basaltic fissure eruptions, plume heights, and atmospheric aerosols. Geophys Res Lett 13:725–728. doi: 10.1029/GL013i008p00725

Stovall WK, Houghton BF, Gonnermann H, et al (2011) Eruption dynamics of Hawaiian-style fountains: the case study of episode 1 of the Kīlauea Iki 1959 eruption. Bull Volcanol 73:511–529. doi: 10.1007/s00445-010-0426-z

Stovall WK, Houghton BF, Hammer JE, et al (2012) Vesiculation of high fountaining Hawaiian eruptions: episodes 15 and 16 of 1959 Kīlauea Iki. Bull Volcanol 74:441–455. doi: 10.1007/s00445-011-0531-7

Thordarson T, Höskuldsson Á (2008) Postglacial volcanism in Iceland. Jökull 58:197–228.

Thordarson T, Larsen G (2007) Volcanism in Iceland in historical time: Volcano types, eruption styles and eruptive history. J Geodyn 43:118–152. doi: 10.1016/j.jog.2006.09.005

Thordarson T, Miller DJ, Larsen G, et al (2001) New estimates of sulfur degassing and atmospheric mass-loading by the 934 AD Eldgjá eruption, Iceland. J Volcanol Geotherm Res 108:33–54. doi: 10.1016/S0377-0273(00)00277-8

Thordarson T, Self S (1993) The Laki (Skaftár Fires) and Grímsvötn eruptions in 1783–1785. Bull Volcanol 55:233–263.

Thordarson T, Self S (1998) The Roza Member, Columbia River Basalt Group: A gigantic pahoehoe lava flow field formed by endogenous processes? J Geophys Res 103:27411–27445. doi: 10.1029/98JB01355

Thordarson T, Self S, Miller DJ, et al (2003) Sulphur release from flood lava eruptions in the Veidivotn, Grimsvotn and Katla volcanic systems, Iceland. Geol Soc Lond Spec Publ 213:103–121. doi: 10.1144/GSL.SP.2003.213.01.07

Thordarson T, Self S, Oskarsson N, Hulsebosch T (1996) Sulfur, chlorine, and fluorine degassing and atmospheric loading by the 1783–1784 AD Laki (Skaftár Fires) eruption in Iceland. Bull Volcanol 58:205–225.

Thordarson T, Self S (1996) Sulfur, chlorine and fluorine degassing and atmospheric loading by the Roza eruption, Columbia River Basalt Group, Washington, USA. Journal of Volcanology and Geothermal Research 74:49–73. doi: 10.1016/S0377-0273(96)00054-6

UK Cabinet Office (2012) National Risk Register of Civil Emergencies - 2012 edition.

Vye-Brown C, Self S, Barry TL (2013) Architecture and emplacement of flood basalt flow fields: case studies from the Columbia River Basalt Group, NW USA. Bull Volcanol. doi: 10.1007/s00445-013-0697-2

Walker GPL (1973) Explosive volcanic eruptions — a new classification scheme. Geol Rundsch 62:431–446. doi: 10.1007/BF01840108

Walker GPL, Self S, Wilson L (1984) Tarawera 1886, New Zealand — A basaltic plinian fissure eruption. J Volcanol Geotherm Res 21:61–78. doi: 10.1016/0377-0273(84)90016-7

Williams SN (1983) Plinian airfall deposits of basaltic composition. Geology 11:211–214. doi: 10.1130/0091-7613(1983)11<211:PADOBC>2.0.CO;2

Wilson L, Sparks RSJ, Huang TC, Watkins ND (1978) The control of volcanic column heights by eruption energetics and dynamics. J Geophys Res Solid Earth 83:1829–1836. doi: 10.1029/JB083iB04p01829

Wohletz KH (1986) Explosive magma-water interactions: Thermodynamics, explosion mechanisms, and field studies. Bull Volcanol 48:245–264. doi: 10.1007/BF01081754

Wohletz KH, Zimanowski B, Büttner R (2013) Magma-water interactions. In: Fagents SA, Gregg TKP, Lopes RMC (eds) Modelling volcanic processes: the physics and mathematics of volcanism, 1st edn. Cambridge University Press, Cambridge, p 421

Wolfe EW, Neal CA, Banks NG, Duggan TJ (1988) Geologic observations and chronology of eruptive events. In: Wolfe EW (ed) The Puu Oo eruption of Kilauea Volcano, Hawaii; episodes 1 through 20, January 3, 1983, through June 8, 1984. U. S. Geological Survey, pp 1–97

Wolfe CJ, Th Bjarnason I, VanDecar JC, Solomon SC (1997) Seismic structure of the Iceland mantle plume. Nature; London 385:245–247. doi: http://dx.doi.org/10.1038/385245a0

Woods AW (1993) Moist convection and the injection of volcanic ash into the atmosphere. J Geophys Res Solid Earth 98:17627–17636. doi: 10.1029/93JB00718

Zielinski GA, Germani MS, Larsen G, et al (1995) Evidence of the Eldgjá (Iceland) eruption in the GISP2 Greenland ice core: relationship to eruption processes and climatic conditions in the tenth century. The Holocene 5:129–140. doi: 10.1177/095968369500500201

Zielinski GA, Mayewski PA, Meeker LD, et al (1994) Record of Volcanism Since 7000 B.C. from the GISP2 Greenland Ice Core and Implications for the Volcano-Climate System. Science 264:948–952. doi: 10.1126/science.264.5161.948

Zimanowski B, Büttner R, Dellino P, et al (2015) Magma-water interaction and phreatomagmatic fragmentation. In: Sigurdsson H (ed) The Encyclopedia of Volcanoes, 2nd edn. Academic Press, Amsterdam, pp 473–484

Paper I

Contrasting explosive products of the 10th century Eldgjá fissure eruption, southern Iceland

William M. Moreland[1, 2, *], Thorvaldur Thordarson[2], Bruce F. Houghton[3], Gudrun Larsen[1]
* wmm2@hi.is
[1] Institute of Earth Sciences, University of Iceland, Askja, Sturlugata 7, 101 Reykjavík, Iceland
[2] Faculty of Earth Sciences, University of Iceland, Askja, Sturlugata 7, 101 Reykjavík, Iceland
[3] Department of Geology and Geophysics, SOEST, University of Hawai'i at Mānoa, Honolulu, HI 96822, USA

Abstract

The 10th century eruption of the Icelandic basaltic fissure volcano, Eldgjá, produced at least sixteen explosive phases and deposited 1.3 km^3 (dense rock equivalent, DRE) of tephra in addition to 19.7 km^3 of lava. The explosive phases took place successively along the 70-km-long vent system, starting beneath the glacier Mýrdalsjökull and progressively moving northeast with time, and featured both magmatic and phreatomagmatic activity as a result. The internal stratigraphy of Eldgjá tephra is composed of alternating magmatic and phreatomagmatic tephra units which, together with dispersal patterns, indicates activity alternated between subaerial and subglacial vents. In order to compare the two styles of activity, units 7 and 8 of the Eldgjá tephra deposit were mapped in detail and sampled. These units were selected because they appear immediately above a very identifiable horizon in the deposit and so were easy to trace in the field. Unit 7 is a magmatic deposit originating from a subaerial fissure segment. It has a positively-skewed, unimodal total deposit grain-size distribution (TGSD) and a mode of -2.2 Φ. Unit 8 originates from beneath the glacier and is phreatomagmatic with a bimodal TGSD with modes at 0.0 and 5.0 Φ. The volume of units 7 and 8 are 0.024 and 0.028 km^3 (DRE) respectively. The height of the plumes during these phases is estimated to have been between 11 and 18 km, higher than the tropopause above Iceland.

Introduction

Because of the Eyjafjallajökull eruption in 2010, many European governments have realized that they must consider the impact of distant volcanic eruptions on aviation and society. For example, from 2012 the UK government have included both explosive and effusive volcanic eruptions on the National Risk Register of Civil Emergencies (UK Cabinet Office 2012). Particular emphasis was placed on the risk from Icelandic fissure eruptions due to their long-lifespan and varied eruption styles (Loughlin et al. 2012).

An example is the 10th century Eldgjá eruption which is the most voluminous basaltic flood lava eruption to have occurred on Earth in the last 11 centuries. Although the eruption was dominantly effusive there was a total of 1.3 km^3 (dense rock equivalent, DRE) of tephra produced. In this paper, we describe examples of two end-member styles of explosive activity which took place during the Eldgjá eruption and produced two distinct tephra deposits. One is a magmatic sub-aerial event occurring on the Southwestern fissure segment, the other is a

phreatomagmatic event from the sub-glacial segment beneath Mýrdalsjökull. These events occurred in close succession demonstrating the need to understand the controls on all styles of activity during an Icelandic eruption and be prepared for a variety of hazards.

The Eldgjá eruption

The Eldgjá vents belong to the Katla volcanic system in the Eastern Volcanic Zone of Iceland (Jakobsson 1979). The southwestern end of the vent system is inferred to be beneath Mýrdalsjökull, where radio-echo soundings have revealed the subglacial topography (Björnsson et al. 2000). Isopachs of the Eldgjá tephra layers (Larsen 2000) indicate a major source area west of Öldufellsjökull where a depression flanked by a steep ridge striking N33°E is the most prominent feature (Figure 1). The vent system continues subaerially in the form of a mixed cone row on a bearing of between N15°E and N45°E for ~70 km until it terminates 6 km short of Vatnajökull (Figure 1; e.g. Larsen 2000; Thordarson et al. 2001). The Eldgjá fissure system is one of the largest fissure systems in the world; in Iceland, it is only matched by the Vatnaöldur (60 km) and Veiðivötn (67 km) (Larsen 1984, 2005) cone rows of the Bárðarbunga-Veiðivötn volcanic system and it is three times longer than the Laki vent system (27 km) of Grímsvötn volcanic system (Larsen 1984; Thordarson and Self 1993).

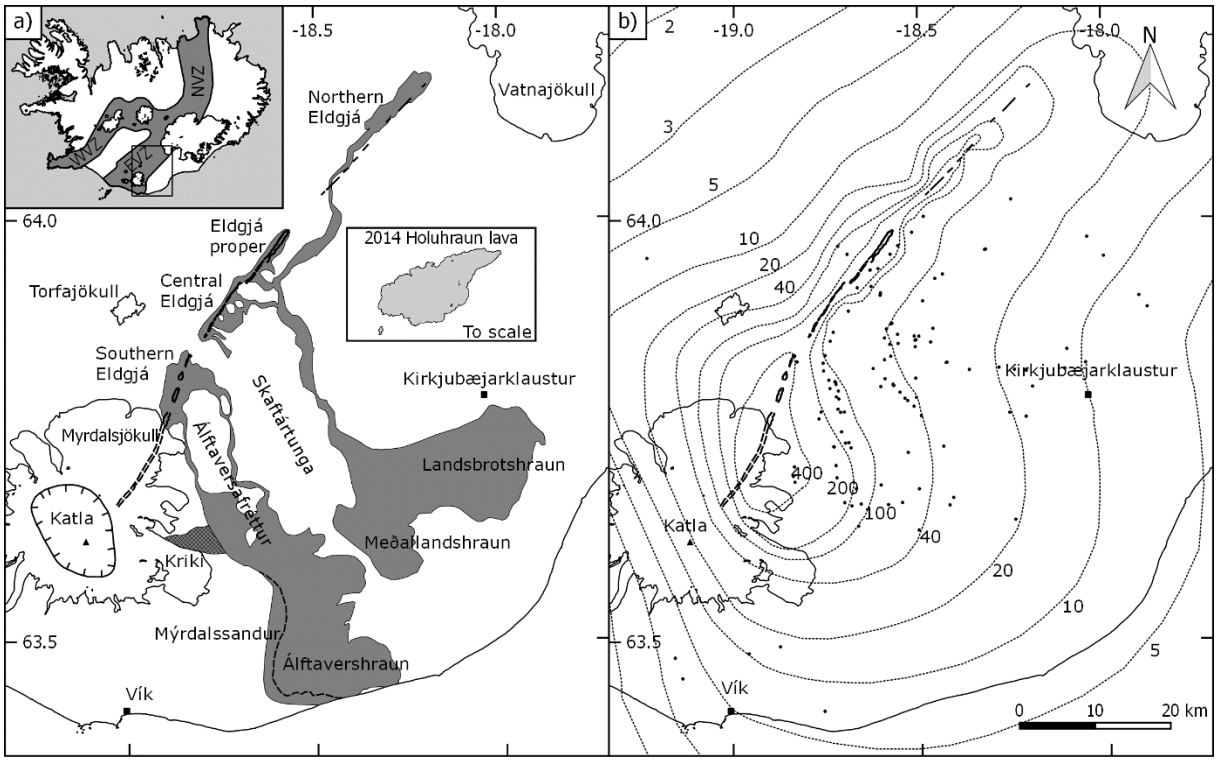

Figure 1 ***a)*** *Map of study area with labeled key localities. Shaded area to the west of the dashed line on Álftavershraun lava field indicates the suspected buried margin of the lava beneath Mýrdalssandur (Modified from Sigurðardóttir et al. 2015). The outline of the 2014-15 Holuhraun lava, erupted in the north of Iceland, has been overlain for comparison of size. Its volume is 1.44 km^3 (Pedersen et al. 2017) compared to 1.3 km^3 DRE for the Eldgjá tephra alone.* ***b)*** *Isopach map for the entire tephra deposit of Eldgjá (Larsen 2000). Dots indicate tephra sections from the current work*

The Eldgjá flood lava eruption took place during the first half of the 10th century, shortly after the Katla 920 CE event but before the Hekla 1104 CE (H1) layer (Larsen 2000, 2010). The eruption has been dated to 939 CE based upon Greenland ice core records (Sigl et al. 2015), historical accounts of meteorological and astronomical phenomena (McCarthy and Breen 1997; Stothers 1998; Fei and Zhou 2006), and environmental records (Oman et al. 2006; Baillie and McAneney 2015). Unlike the 1783 CE Laki flood lava eruption, (Thordarson and Self 1993; Thordarson et al. 1996), a similar but 25% smaller event), there is very little contemporary information on Eldgjá. It is briefly mentioned in The Book of Settlement (Landnáma) which describes lava flows forcing newly-arrived Norse settlers off their lands.

Eldgjá produced up to 19.7 km^3 of lava (Sigurðardóttir et al. 2015) including at least 0.5 km^3 of hyaloclastite flow at Kriki (Figure 1; Larsen 2000). About 1.3 km^3 (DRE) of tephra (Larsen 2000) was produced by vents along the full length of the fissure in at least 16 explosive phases. This volume of tephra is almost an order of magnitude larger than Laki (0.4 km^3; Thordarson and Self 1993), not much less than the total volume that Hekla has produced in subplinian-Plinian eruptions in historical times (2.2 km^3; Thordarson and Larsen 2007), and on a par with the 1362 CE Plinian eruption of Öræfajökull (1.2 km^3; Sharma et al. 2008). This tephra volume is also larger than the total bulk volume of the lava flow field produced by the 2014-15 effusive eruption at Holuhraun (1.44 km^3; Pedersen et al. 2017).

The first sign of activity was an explosive eruption beneath the northeast margin of Mýrdalsjökull. Successive explosive phases occurred from ever more north-easterly sites although activity continued at the subglacial fissure segments after subaerial activity commenced. This mixture of subglacial and subaerial activity resulted in a tephra stratigraphy composed of alternating phreatomagmatic and magmatic units. Interspersed between explosive phases were periods of lava effusion from subaerial and subglacial fissure segments and jökulhlaups from beneath the glacier which produced extensive and thick (up to 2 m) deposits.

The exact duration of the event is not known however several sources provide suggestions. An absolute minimum duration of 6 months was estimated by Thordarson et al. (2001) by measuring the pahoehoe lava crust thickness at several localities and applying the method of Hon et al. (1994). The acidity peaks found in Greenland ice-cores dated to this time period indicate elevated atmospheric sulfate levels for between 3 to 6 years (Zielinski et al. 1994, 1995).

Methods

Two explosive phases, one magmatic and one phreatomagmatic, were chosen based upon the ease of identifying them in the field and the fact that the two units generally thickened and thinned together at a similar rate allowing fieldwork to be focussed on a smaller area. Units 7 and 8 were chosen as the magmatic and phreatomagmatic phases respectively. The unit immediately below these two units contains a distinct train of lapilli and served as a marker layer to identify these units. Thickness measurements and bulk samples were taken at a total of 141 locations.

The grain-size distribution for tephra coarser than 4 φ (63 μm) was determined by dry sieving samples at 0.5 φ intervals. The samples were generally split at 3 φ (125 μm) and half was then analysed in a Micromeritics Sedigraph® III Plus Particle Size Analyzer down to 10 φ (1 μm) using a density of 2600 kg.m-3 obtained using a glass pycnometer. This gave four bins of overlap with which to manually splice the data from the two methods. Total grain-size distributions for the two phases were calculated using the Voronoi tessellation method of Bonadonna and Houghton (2005) with the TOTGS Matlab® script of Biass and Bonadonna

(2014). The bimodal distribution of Unit 8 was deconvolved into two probability density functions using the program Decolog (Borselli and Sarocchi 2016).

The volume of units 7 and 8 have been calculated using the trapezoidal (e.g. Froggatt 1982; Fierstein and Nathenson 1992), exponential (Pyle 1995), power-law (Bonadonna and Houghton 2005), and Weibull methods (Bonadonna and Costa 2013). The latter three methods were calculated using the AshCalc python script (Daggitt et al. 2014) which allows the easy comparison of the exponential, power-law, and Weibull models of volume estimation. The proximal integration limits used in the power-law method were as calculated by AshCalc using equation 7 in Bonadonna and Houghton (2005): unit 7, 2.79 km and unit 8, 3.75 km. The distal limit was set at 1000 km for both deposits. Bulk volumes were converted to dense rock equivalent values by multiplying by (1-φ) where φ is the average vesicle fraction of the tephra in question (0.70 and 0.76 for unit 7 and 8 respectively). The quality of the fit of each method to the data was measured using the mean relative squared error (MRSE) and a summary of this is presented in Table 1.

The column height for the phases producing units 7 and 8 was calculated using the methods of Carey and Sparks (1986), Mastin et al. (2009) and Wilson et al. (1978). The empirical method of Mastin et al. (2009) uses the following formula to calculate column height (H) from erupted volume (V):

$$H = 25.9 + 6.64 \log_{10}(V) \quad (1)$$

The formula of Wilson et al. (1978) calculates column height from the rate of release of thermal energy at the vent (Q):

$$H = 8.2Q^{\frac{1}{4}} \quad (2)$$

where Q can be calculated as shown by Stothers et al. (1986):

$$Q = \sigma(1 - x - y)vs_m\Delta T_f + \sigma xvs_m\Delta T_a + \sigma yvs_w\Delta T_a \quad (3)$$

where σ = magma density (2850 kg.m^{-3}), x = weight fraction of tephra < 1 mm in diameter (see results), y = weight fraction of volatiles (0.005), v = volumetric eruption rate (m s^{-1}, see below), s_m = specific heat of basaltic magma (1100 J kg^{-1} K^{-1}), s_w = specific heat of steam (2000 J.kg^{-1}.K^{-1}), ΔT_f = change in temperature of tephra in the fountain (50 °C), and ΔT_a = change in temperature of tephra < 1 mm in diameter and volatiles in the plume (1150 °C). Stothers et al. (1986) use a variation of equation 2 to find the column height above a linear vent. This method is appropriate if the length of the fissure is significantly longer than the plume is high:

$$H = 9.1q^{\frac{1}{3}} \quad (4)$$

where q is Q from equation 3 divided by the length of the fissure in question.

Results

Description of the deposits

The Eldgjá tephra deposit consists of alternating units which can be placed into two broad categories: magmatic and phreatomagmatic units. The two end-members are easily

distinguished from each other in the field based on their colour and physical appearance (Figure 2a).
The magmatic tephra units are generally darker in colour, ranging from black to metallic blue whereas the phreatomagmatic units are usually dull brown. The submetallic lustre of the magmatic tephra is due to the high abundance of achneliths which have a thin (<0.01 mm), reflective, smooth-surfaced skin (Figure 2b). This skin is a product of fluidal moulding induced by streaming of hot magmatic gasses around foamy melt fragments upon eruption (Thordarson et al 1996). The lack of achneliths and abundance of fines in the phreatomagmatic units causes these units to have a duller appearance (Figure 2c).

The magmatic and phreatomagmatic units are eroded from exposed sections at different rates as a result of their grain-size distributions. The magmatic units are generally better sorted and coarser grained and thus more easily eroded than the phreatomagmatic units.

Unit 7

Unit 7 consists of black to metallic blue coloured tephra which in the proximal to medial regions (< 10 km from vent) consists of very well to poorly sorted (graphic standard deviation, σ_{Φ}, between 0.81 and 2.45 Φ) lapilli-sized achneliths (2-64 mm; Figure 3). The deposit is dominantly juvenile tephra comprised of basaltic pumice clasts and achneliths. Pele's tears and hair are present in minor amounts. The unit 7 tephra contains less than 5% wall-rock lithics which, when present, are red or yellow fragments of lava and scoria fragments.

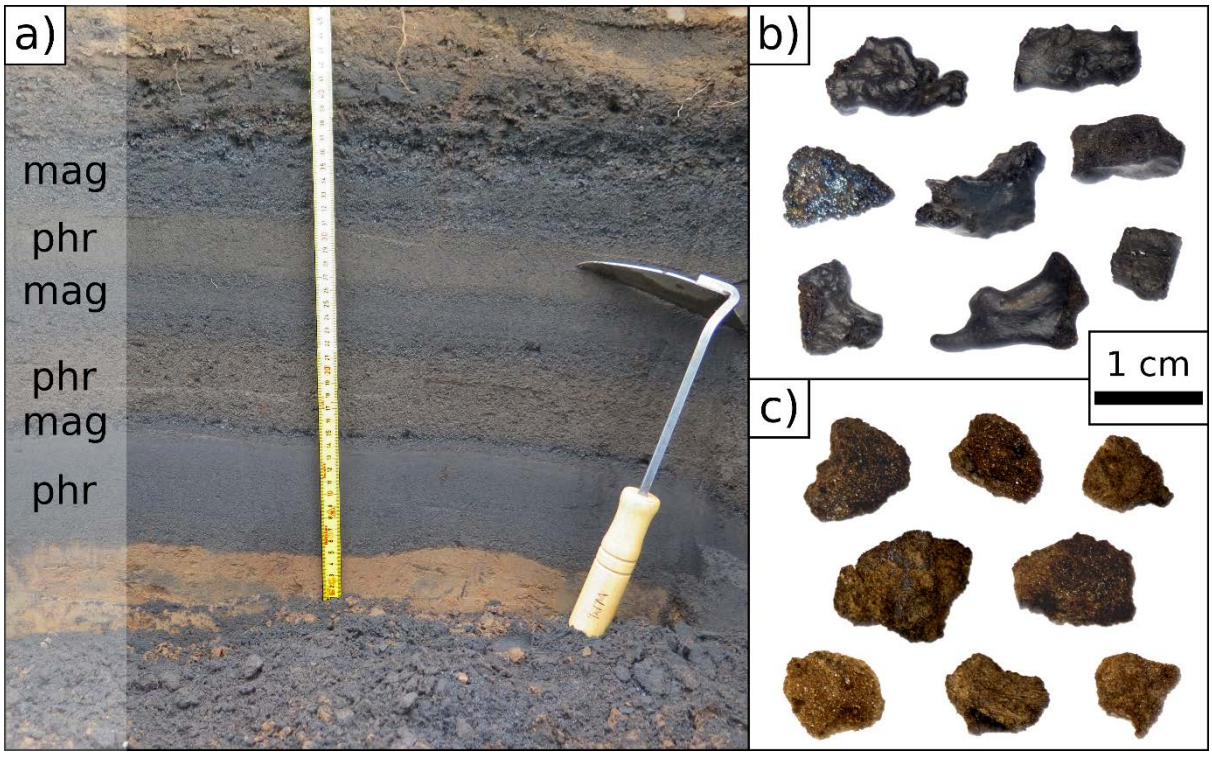

Figure 2 Comparison of Eldgjá magmatic and phreatomagmatic tephras. ***a)*** *Typical Eldgjá tephra section E15-016 (63.82514°N, -18.28625°E) 30 cm thick and showing up to 15 units of alternating magmatic (mag) and phreatomagmatic (phr) origin. Brown colouring of some phreatomagmatic units is due to presence of very fine ash.* ***b)*** *Magmatic and* ***c)*** *phreatomagmatic lapilli morphology. Achneliths are absent from the phreatomagmatic tephra. Note the similarly vesicular appearance of magmatic and phreatomagmatic clasts but the more rugged outline of the latter*

Unit 7 was erupted during a magmatic explosive phase from the subaerial Southwestern Fissure located immediately northeast of Mýrdalsjökull (Figure 1). The tephra was dispersed over a wide area (1 cm isopach covers 770 km^2) towards the south-east and its deposit features three lobes each with different dispersal axes (Figure 4).

The median grainsize changes with distance from vent from -2 Φ to more than 1 Φ and the sorting of the deposit shows no correlation with distance (Figure 3). The thickness half-distance (Pyle 1989) of unit 7 is 5.7 km. Preservation of the deposit closest to the glacier is sparse due to the combined erosive action of the glacier itself and jökulhlaups originating from beneath the glacier.

Unit 8

The unit 8 tephra is generally brown in colour and the clasts are typified by dull surfaces. Clasts with smooth shiny outer surfaces are absent indicating that the temperature of the plume was not hot enough for the fusing and fluidal moulding of foamy melt fragments. In the proximal to medial regions unit 8 contains a high concentration of very fine ash (<3 φ, 125 μm) and is well to poorly sorted (σ_Φ between 1.62 and 3.59 Φ).

Unit 8 originates from part of the subglacial fissure beneath Mýrdalsjökull. The median grain-size diameter decreases from -1 Φ to 2 Φ with distance from vent and the sorting of the deposit exhibits a strong negative correlation with distance demonstrating an improvement in sorting with distance from source (Fig. 3). The thickness half-distance of unit 8 is similar to that of unit 7 at 5.6 km. The very proximal portion of the deposit is inaccessible or absent due to glacial cover or later erosion by the glacier and related runoff.

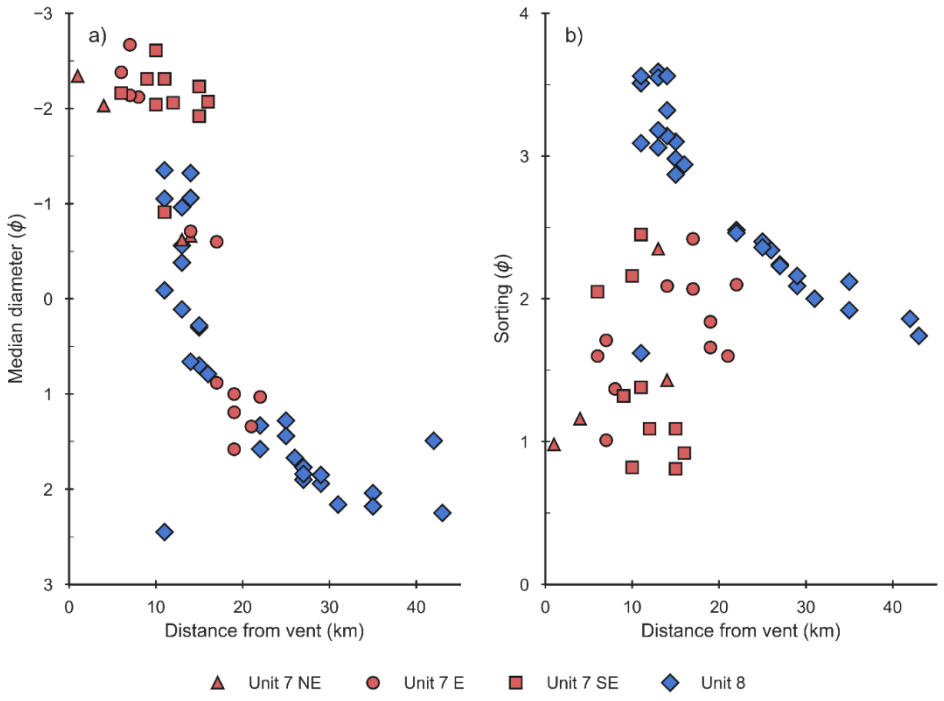

Figure 3 ***a)*** *Median diameter versus distance from vent for tephra grain-size samples from units 8 (blue diamonds) and 7 (red symbols). The unit 7 samples have been divided up by lobe (Fig. 4a): north-eastern (triangles), eastern (circles), and south-eastern (squares). Both deposits clearly show a decrease in median grain-size away from the vent.* ***b)*** *Sorting versus distance from vent for the same grain-size samples. Unit 7 shows no correlation whereas unit 8 shows a strong negative correlation. Symbols are as in a)*

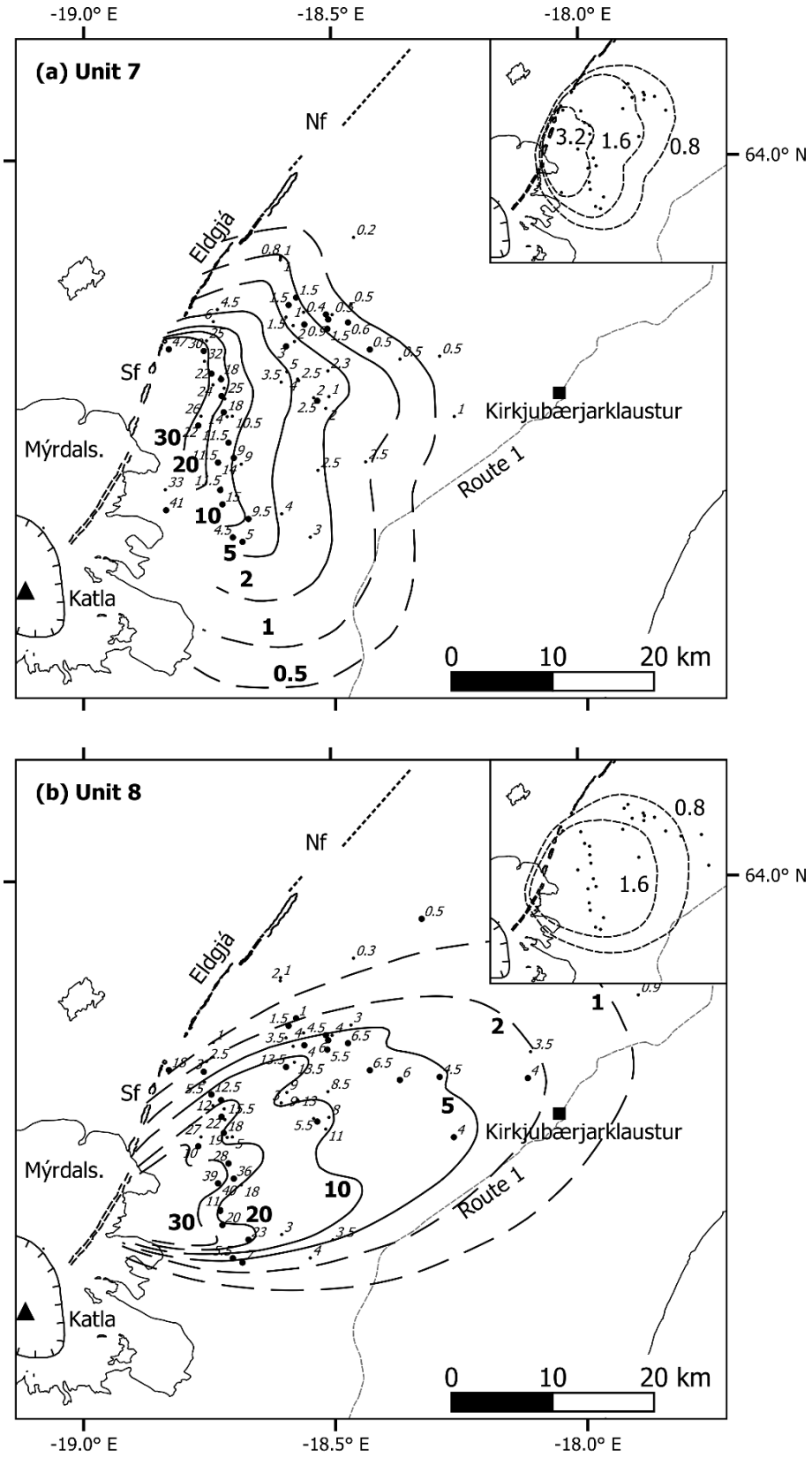

Figure 4 Isopach maps of units 7 and 8. The points are tephra sections with larger points indicating grain-size locations. Values in bold are isopach thicknesses in centimetres and dashed isopach lines represent regions unconstrained by sufficient data. All abbreviations are as in figure 1. Inset are isopleth maps for units 7 and 8 with maximum pumice size in centimetres

Volumes of the deposits

The volumes of units 7 and 8 were calculated using the trapezoidal, exponential, power-law, and Weibull methods. The calculated volume of these deposits depends strongly on the method used. For unit 7 the trapezoidal method returns a volume of 0.018 km^3 (all volumes are DRE). A two-segment exponential curve gives a volume of 0.024 km^3 and produces the best fit in terms of MRSE (0.0011; Figure 5; Table 1). The Weibull method gives a volume of 0.056 km^3 with only a slightly larger error (0.0027). The power-law curve does not fit well in either the proximal (< 9 km) or distal regions (> 30 km) where it tends to be thicker than the data and this method produces a volume more than three times that of the exponential (0.075 km^3).

Unit 8 is well modelled both by a single-segment exponential curve or a Weibull curve (Figure 5). Both methods produce similar volume estimates (0.028 and 0.029 km^3 respectively), also similar to that of the trapezoidal method (0.025 km^3), and identical MRSE (Table 1). The power-law method produces a volume nearly twice that of the other two methods (0.058 km^3) but does not fit the data well and has a larger error associated with it (0.072).

Table 1 Comparison of DRE volumes (km^3) and mean relative squared error (MRSE) in the fit of the model to the data calculated by various methods

	Unit 7		Unit 8	
	Volume (km^3)	**MRSE**	**Volume (km^3)**	**MRSE**
Trapezoidal	0.018	-	0.025	-
Exponential	0.024[a]	0.001	0.028[b]	0.007
Power-law	0.075[c]	0.015	0.058[d]	0.072
Weibull	0.056	0.003	0.029	0.007

[a] two-segment curve
[b] single-segment curve
[c] 2.79 km proximal and 1000 km distal integration limits
[d] 3.75 km proximal and 1000 km distal integration limits

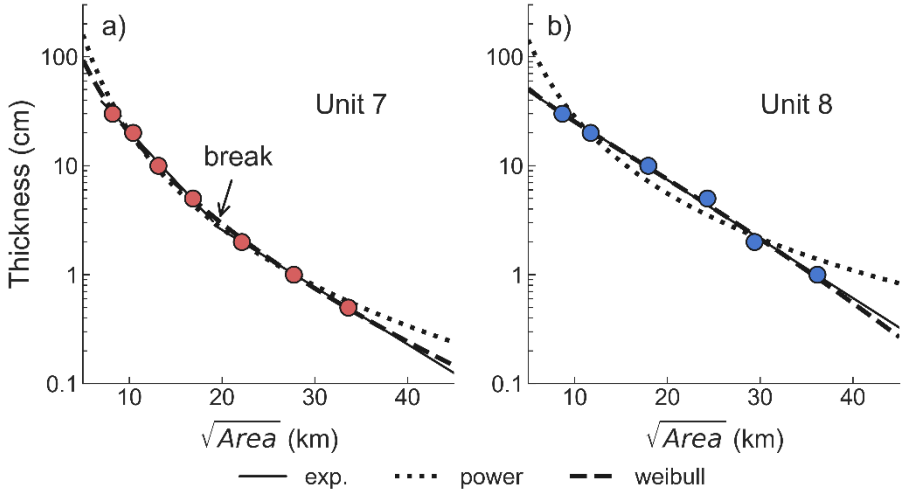

Figure 5 Semi-log plots of thickness versus square root of isopach area showing exponential, power-law, and Weibull functions fitted to field data. The exponential function for unit 7 uses two segments (break in slope labelled) whilst for unit 8 a single segment is used

Total grain-size distributions

Unit 7 has a positively-skewed, unimodal TGSD with a median grain-size diameter (Md_Φ) of -2.2 Φ and a sorting value (inclusive graphic standard deviation) of 1.6 Φ (Figure 6). Unit 8 is bimodal with a broad peak about 0.0 and a narrower peak at 5.0 Φ. The unit 8 TGSD was deconvolved using the software DECOLOG (Borselli and Sarocchi 2016) to produce two unimodal peaks with Md_Φ of -0.1 and 4.5 Φ and sorting values of 2.0 and 0.9 Φ. The coarse peak of the deconvolved distribution is positively skewed but generally finer grained than thepeak of the magmatic unit 7.

There is a lack of samples of either unit in the very proximal (< 5 km) and distal (30 km for unit 7, 50 km for unit 8) sectors. This will affect the TGSD by underestimating the very coarse and very fine fractions, although the latter will be less of an issue in the unit 7 TGSD where over 90% of the mass is coarser than 1 mm.

Eruption parameters

The eruption column heights for the explosive phases that produced units 7 and 8 were calculated using the isopleth method of Carey and Sparks (1986). The isopleths (Figure 4)

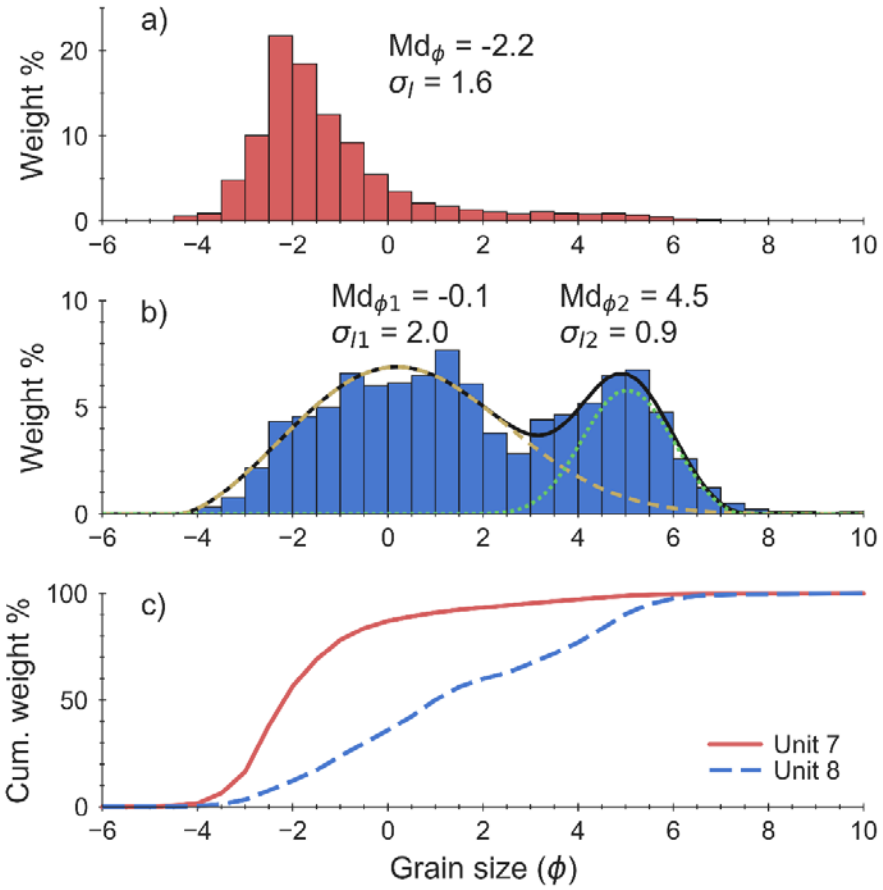

Figure 6 ***a)*** *Total grain-size distribution for Unit 7 with median grain size (Md_Φ) and sorting (σ_I, inclusive graphic standard deviation);* ***b)*** *TGSD for Unit 8, yellow dashed and green dotted curves are deconvolved distributions of TGSD for Unit 8 with median grain size and sorting;* ***c)*** *cumulative grain-size distributions for Units 7 (solid red line) and 8 (dashed blue line)*

return a range of column heights for both units: for unit 7 it is 14 to 17 km and for unit 8 it is 17 to 18 km.

The Mastin et al. (2009) empirical formula gives column heights of 15.1 and 15.7 km for units 7 and 8 using volumes of 0.02 and 0.03 km^3 DRE, respectively.

By assuming that the volumetric eruption rate was similar to that of the 1783 Laki eruption (maximum 8500 m^3 s^{-1}; after Thordarson and Self, 1993) for both phases, the Wilson at al. (1978) formula, a column height of 11.0 is obtained for unit 7 and 14.7 km for unit 8 (Figure 7). Equation 2 was used rather than the equation as the length of the fissure was not found to be significant in comparison to the height of the plume. If the equation 4 had been used the resulting column heights would have been 62.1 and 115.8 km for units 7 and 8 respectively.

That the two column height methods produce similar results suggests that the input parameters for the Wilson et al. (1978) model are reasonable. Specifically, it suggests that the volumetric eruption rate may have been similar to that of Laki. Using a magma density of 2850 kg m^{-3} (calculated from an equation of state using the Eldgjá melt composition) to convert the volumetric eruption rate of 8500 m^3 s^{-1} gives a mass eruption rate of 2.4 $\times 10^7$ kg s^{-1}.

The magnitude and intensity of unit 7 and 8 can be calculated from the estimated mass eruption rate and erupted mass (Pyle 2015; Table 2). The magnitudes are 3.8 and 3.9 respectively; and the intensity is 10.4 using the single value for mass eruption rate. The volcanic explosivity index (VEI Newhall and Self 1982) for unit 7 is 3 and for unit 8 it is 4.

The dispersal index and degree of fragmentation (Walker 1973) for units 7 and 8 are 420 and 1350 km^2 and 38 and 95%, respectively. Using the classification of Walker (1973) unit 7 can be classified as a strong subplinian or weak Plinian eruption whilst unit 8 is phreatoplinian (Figure 8).

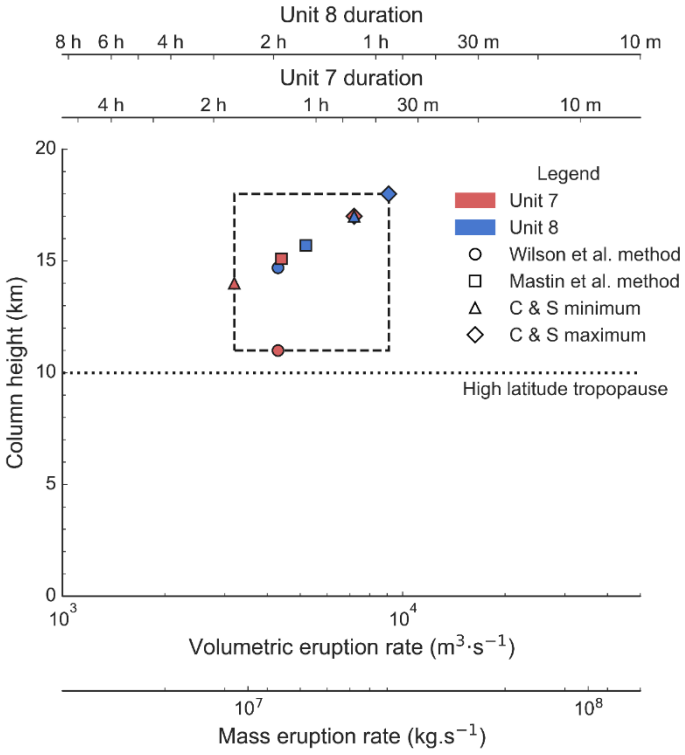

Figure 7 Summary of column height results using the Wilson et al. (1978), Carey and Sparks (1986), and Mastin et al. (2009) methods. MER calculated from VER by multiplying by the melt density 2850 kg.m^{-3}. Duration for each episode calculated by dividing the DRE volume by VER

Discussion

Tephra dispersal

Unit 7 exhibits a lobate tephra dispersal pattern with three dispersal axes (Figure 4a). This change in dispersal axis indicates that the wind field must have changed during the deposition of this unit, either from a north-westerly wind to a south-westerly, or vice versa. The dispersal pattern of unit 7 suggests that nearly 10 km of the Southern fissure segment was active during that phase; from near the margins of Mýrdalsjökull to the crater of Rauðibotn (63.83993°N, -18.83743°E).

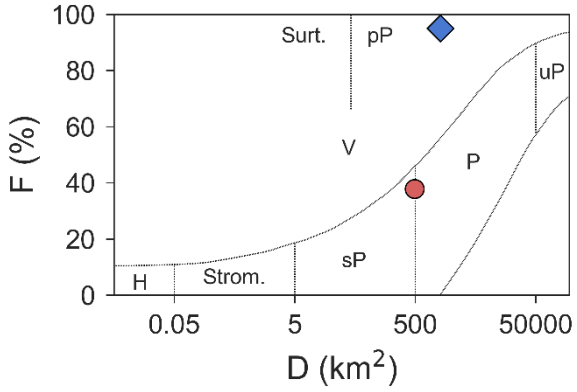

Figure 8 Classification of units 7 (red circle) and 8 (blue diamond) using the method of Walker (1973). Abbreviations are: F, degree of fragmentation; D, dispersal index; H, Hawaiian; Strom, Strombolian; sP, subplinian; P, Plinian; uP, ultra-plinian; Surt, Surtseyan; pP, phreatoplinian; V, Vulcanian

Table 2 Summary of physical parameters of Eldgjá units 7 and 8

Episode	Unit 7	Unit 8	Methods
Column height (km)	11.0 15.1 14-17	14.7 15.7 17-18	Wilson et al. (1978) Carey and Sparks (1986) Mastin et al. (2009)
Erupted volume (DRE, km^3)	0.024	0.029	Integration of isopach areas, exponential method (Pyle 1995)
Erupted mass (kg)	7×1010	8×1010	Converted from bulk volume using deposit density (840 and 690 kg m^{-3} for unit 7 and 8 respectively)
Mass eruption rate (kg s^{-1})	9×106 to 2×107	1×107 to 3×107	Taken from Figure 7
Volcanic explosivity index	3	4	Newhall and Self (1982)

There are many combinations of location of activity and wind direction which could have occurred to produce the pattern of dispersal shown by unit 7 but one likely scenario is outlined in Figure 9. Activity on this fissure segment may have begun with a continuous curtain of ejecta which then quickly (hours to a day) focused upon several discrete vents as seen during in 2014-15 at Holuhraun (Pedersen et al. 2017). The wind changed while explosive activity was still ongoing at the separate vents which combined to produce a composite, poly-lobate tephra deposit lacking any internal stratigraphy that would indicate its multi-vent origins. Since the vents were first thoroughly mapped by Robson (1956) another vent has been exposed from beneath Mýrdalsjökull. This vent may have been active during unit 7 but it is not possible to prove due to the lack of tephra preservation immediately east of Mýrdalsjökull.

Unit 8 was, as indicated by converging isopach lines, erupted from a more limited stretch of fissure, entirely beneath Mýrdalsjökull – around 4-5 km long. It too has a poly-lobate pattern but, given the limited lateral spread, was likely caused by simultaneous eruption from three main sources as opposed to a variation in wind direction. The dispersal pattern of unit 8, deposited after unit 7, supports a progressive change from a north-westerly wind to south-westerly during the eruption of these units.

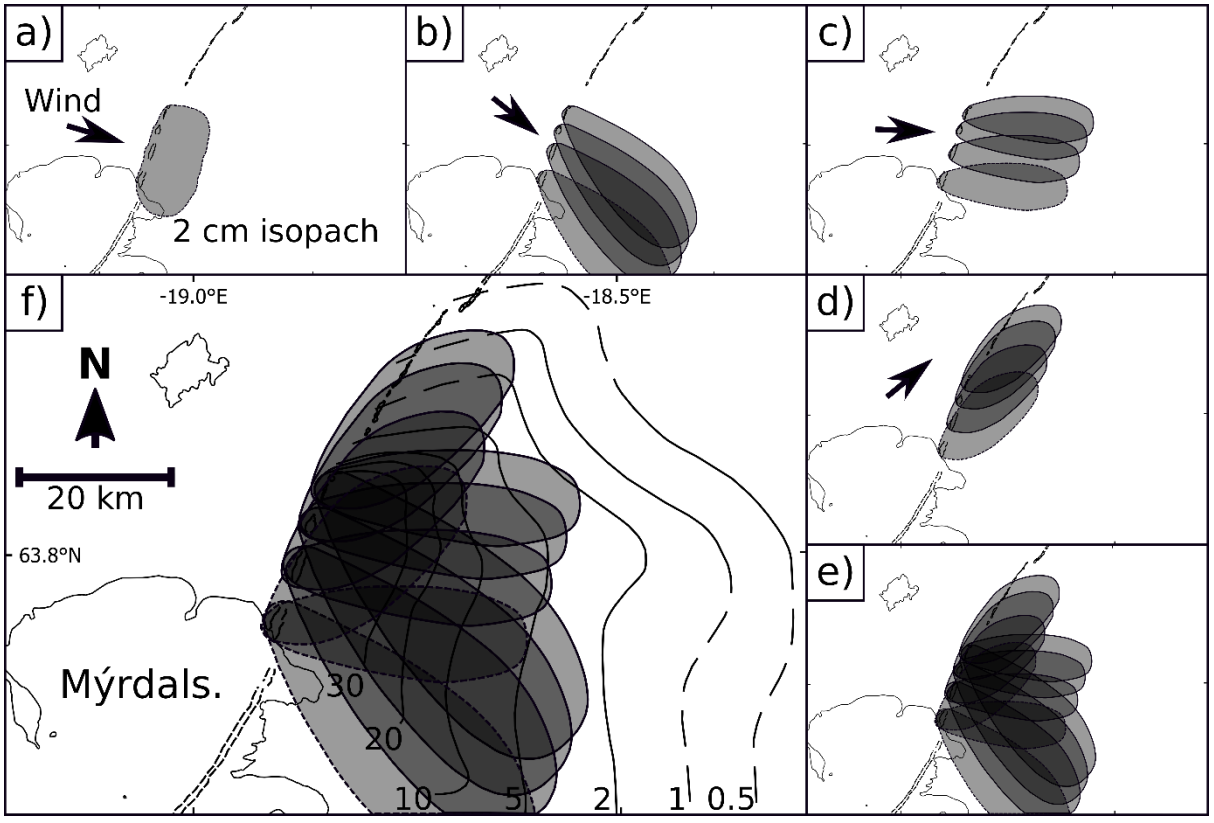

Figure 9 Diagram demonstrating one possible scenario to form the unit 7 dispersal pattern. Shaded polygons represent the 2 cm isopach and with dashed lines indicating deposition from a hypothetical vent beside Mýrdalsjökull. Clockwise from top left: a) a continuous ejecta curtain during the activation of the new Southwestern fissure segment; b) activity quickly (within hours to a day) focuses upon several discrete vents; c) and d) the wind changes direction while explosive activity continues; and e) the result is an irregularly-shaped deposit featuring several lobes from a continuous deposition of tephra. f) comparison of the shape of the model to the isopachs drawn from field data

The thinning relationships of units 7 and 8 are compared with other eruptions of various types in Figure 10. The Eldgjá units 7 and 8 are more extensive deposits when compared to cone-forming eruptions such as Kilauea Iki 1959 (Richter et al. 1970) and Keanakako'i unit 6 (McPhie et al. 1990). The Eldgjá explosive phases present higher rates of thinning than does the 1875 Askja unit C deposit, a phreatoplinian eruption (Carey et al. 2009) but lower than the 122 BC basaltic Plinian eruption of Etna (Coltelli et al. 1998). When compared to the medial to distal deposits of the 1886 basaltic Plinian fissure eruption of Tarawera the Eldgjá episodes show a similar thinning rate although it should be noted that the Tarawera measurements are whole-deposit (Walker et al. 1984; Sable et al. 2006).

Deposit volume

For both unit 7 and 8 the trapezoidal method of calculating the deposit volume gives a value close to or the same as the method with the lowest error as calculated by AshCalc (Daggitt et al. 2014). In the case of unit 7 the trapezoidal method produced a tephra volume of 0.018 km^3, close to the 0.024 km^3 calculated using the two-segment exponential method, which had a lower error than both the power-law and Weibull methods. In the case of unit 8 the trapezoidal method found a volume of 0.025 km^3, - the same value as the single-segment exponential and Weibull methods, both of which had much lower error values than the power-law method. The power-law method found a volume much higher than the other methods. Figure 5 shows that in both cases the power-law model overestimates the deposits in the proximal and distal regions. The volumes calculated by the exponential method are considered the most reliable for both episodes due to the low error associated with each.

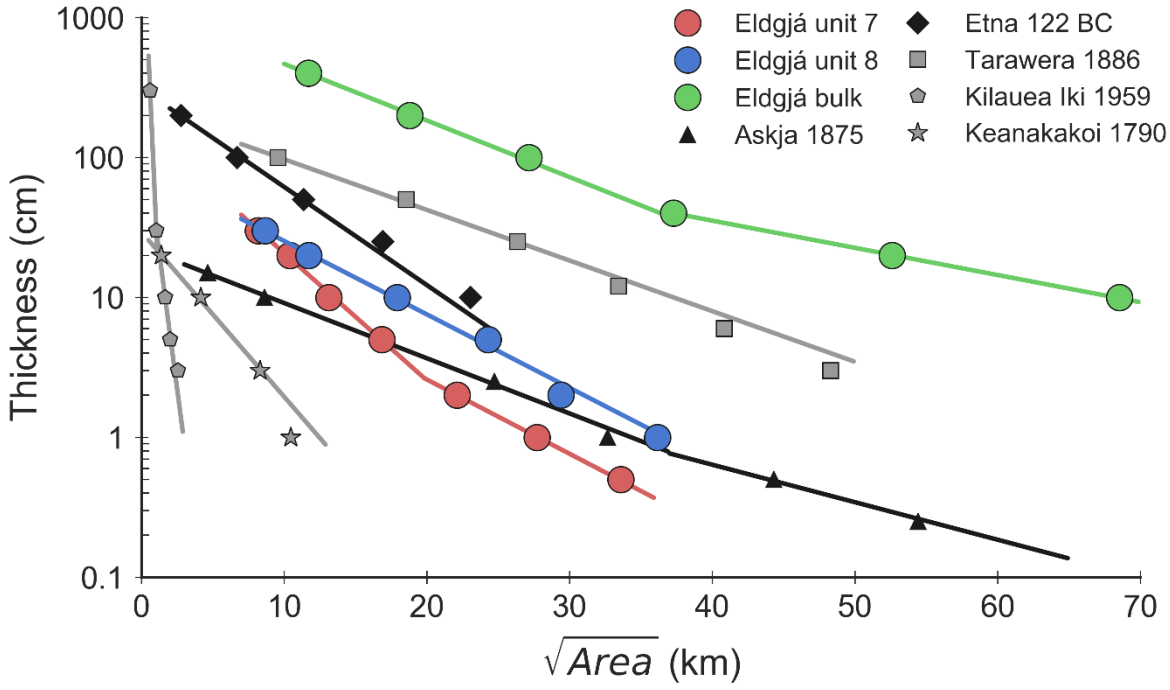

Figure 10 Comparison of thickness-area plots for Eldgjá units 7 and 8, and Eldgjá whole-deposit (Larsen 2000) with various other explosive eruptions: Askja 1875 unit C (Carey et al. 2009), Etna 122 BC (Coltelli et al. 1998), Tarawera 1886 (Sable et al. 2006), Kīlauea Iki 1959 (Richter et al. 1970), and Keanakako'i 1790 unit 6 (McPhie et al. 1990)

Total grain-size distribution

Unit 7

The TGSD for unit 7 (Figure 6) reveals that this magmatic deposit is dominated by lapilli with a median grain-size (Md_{Φ}) of -2 Φ (4 mm). The high vesicularity of lapilli clasts in magmatic tephra from Eldgjá (Moreland et al. in prep.) indicates that the lapilli mode in the TGSD is a product of fragmentation driven by the expansion of exsolved magmatic gases, similar to the products of Hawaiian-style eruptions such as Kilauea Iki 1959 (Stovall et al. 2011, 2012). Results of vesicle-size analysis of Eldgjá pumice clasts are consistent with the notion that the intensity of explosive activity was on a par with Plinian basaltic eruptions such as the Etna 122 CE and Tarawera 1886 (Moreland et al. in prep.) and this is supported by the dispersal and grain size data presented here (Figure 8, Figure 10).

This raises the question: why does foam formed by the volatile exsolution and expansion upon decompression to ~ 1 atmosphere form a lapilli-dominated deposit? In other words, what is the process which fragments the magma into fine lapilli but no further?

The high vesicularity of the Eldgjá tephra is evidence of the coupled rise of melt and bubbles which allows for the accumulation of overpressure within bubbles which ultimately rupture and disintegrate the magma. Examination of vesiculation patterns and structures within Eldgjá tephra clasts has revealed the presence of strings of bubbles that have length scales comparable to the lapilli (Moreland et al. in prep.). These bubble strings are envisaged to be the remnants of a lattice of planes of weakness that formed throughout the foaming magma and along which fractures would preferentially propagate resulting in the lapilli seen in the Eldgjá tephra. As these bubble strings begin to form and coalesce the permeability of the magma would rapidly increase to the point that the system moves from a closed- to an open-state with respect to volatile flux. Once the system is fully open, overpressure is lost, and fragmentation of the foam due to magmatic decompression would cease.

Unit 8

The TGSD for unit 8 (Figure 6) contains two subpopulations: a broad mode between -4 Φ and 3 Φ (16 to 0.13 mm), and a narrower peak centred on 4.5 Φ (0.044 mm). Eldgjá phreatomagmatic lapilli have similarly high vesicularities and bubble number densities as the magmatic clasts which has been interpreted as demonstrating that in the phreatomagmatic phases the ascending magma was able to reach the same level of vesiculation and expansion as in the magmatic episodes (Moreland et al. in prep.). This constrains the timing, and hence depth, of magma-water interaction to relatively late and near the surface (i.e. approximately 1 atmosphere of pressure). This is supported by the low concentration of volatiles found in highly vesicular phreatomagmatic clasts (Thordarson et al. 2001).

The magma-water interaction will result in cooling of the system if the volume of the incoming water is large enough: the foamy lapilli clasts will be quenched and the temperature of the gas phase will be significantly lowered. Evidence for the latter can be seen in the unit 8 tephra which lacks clasts with smooth shiny outer surfaces (e.g. achneliths) which require a high temperature gas phase during formation.

Vesiculated foam has much higher yield strength than non-vesicular magma and so processes such as fuel-coolant interaction are less likely to have taken place during the magma-water interaction. A more likely scenario is thermal granulation of the foam via quenching, forming fine-scale hydrofractures within the pumices, which eventually partly or wholly disintegrated to form the ash. This process does not add any explosivity to the system (Kokelaar 1986) but simply changes the grain-size distribution of the resulting tephra deposit.

It is evident that thermal granulation was not able to reduce all lapilli to ash as unit 8 still contains 24 wt.% lapilli. However, the coarse peak of unit 8 is finer than the coarse peak of unit 7 (a Md_{Φ} of -0.1 versus -2.2 Φ respectively) demonstrating that much of the lapilli fraction has been reduced in size. In fact, the lapilli fraction (< -1 Φ; Figure 11) is 78.2 wt.% in the magmatic unit 7 but only 23.7 wt.% in the phreatomagmatic unit 8; a decrease of 54.4 wt.%. Of this 54.4 wt.% of lapilli, 31.5% was fully disintegrated into very fine to extremely fine ash. This left 22.9 wt.% which was reduced from lapilli size to very coarse to fine ash fractions (Figure 11).

So, from this one can deduce that whilst two thirds of the lapilli tephra was affected by the interaction with external water, only 30% went to producing very fine ash. The remaining 20% was reduced in size, presumably consisting of the cores of clasts which have lost their outer rind by thermal granulation. This leaves about one third of the original lapilli relatively unaffected by external water (Figure 12).

Column height and mass eruption rate

The methods used for calculating column heights for the two explosive phases are in good agreement for all three methods. Given that there are some caveats to each method this agreement might not be expected. All of the point source models assume a sustained, steady-state eruption; it is likely that the Eldgjá explosive phases were unsteady and changing. With the exception of the Wilson et al. (1978) model, the models were established for cooler silica-rich magmas and plumes. Another potential issue is that, given that there is no data on duration of any of the Eldgjá events, it is impossible to calculate an exact eruption rate. Given the many similarities between the Eldgjá and Laki events it seems reasonable to use the volumetric eruption rates of Laki as at least a minimum for Eldgjá.

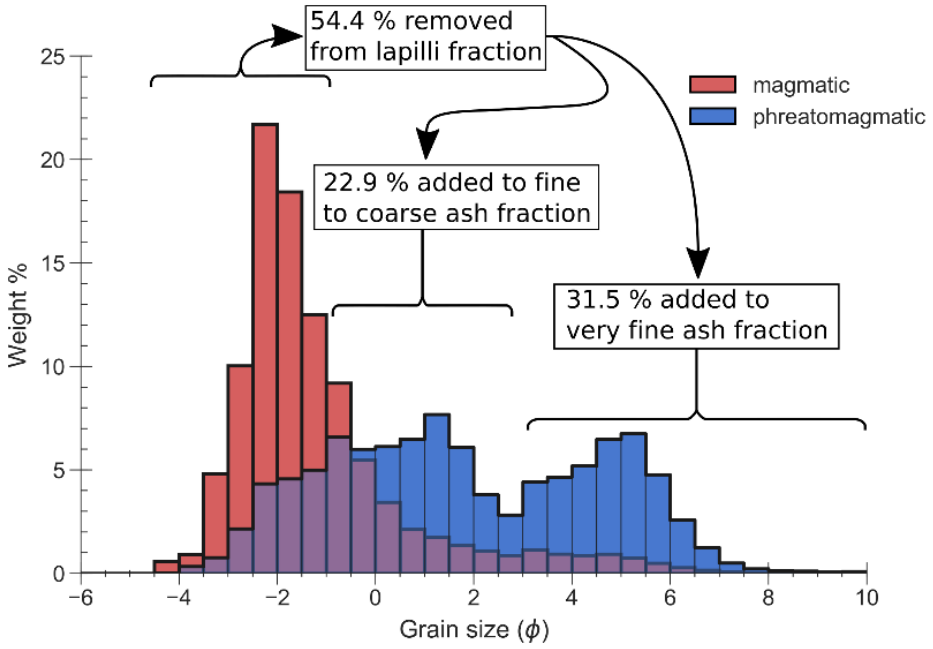

Figure 11 Assuming the grain-size distribution of the magma prior to interacting with water is similar to the distribution of magmatic unit 7 (red distribution) about 50% of total erupted material is reduced from lapilli-sized clasts into fine to coarse ash (~20%) and very fine ash or finer (~30%). This results in the phreatomagmatic distribution exhibited by unit 8 (blue distribution partially overlying the red)

Column height during phreatomagmatic eruptions

The finer grained nature of the phreatomagmatic ejecta is clear from the total deposit grain-size distribution (Figure 6). Air which is entrained in the rising plume will be heated more efficiently by the finer grained tephra potentially allowing the plume to rise to higher levels of the atmosphere. However, heat which would otherwise have been available to heat entrained air is used to heat and vaporize the external water fraction. The eruption columns produced by the magmatic unit 7 and phreatomagmatic unit 8 have been shown to have reached similar heights. This suggests these two processes may have offset one another. The net result, at least as far as Eldgjá is concerned, is that the column height is relatively unchanged from what it would have been had the vent been subaerial despite the additional fragmentation of the tephra.

Conclusions

The unusual subaerial/subglacial setting of the Eldgjá fissure system permitted us to contrast fragmentation processes during two magmatic and phreatomagmatic eruption phases of comparable intensity, where many parameters are held unchanged. Total deposit grain-size data suggests that magma-water interaction was late in the phreatomagmatic phase, following primary fragmentation during vesiculation. Interaction of the clast assemblage with external water was, at best, partial, affecting approximately two thirds of the lapilli-sized population, approximately half of which was reduced to very fine ash and the remainder only partially comminuted. This partial interaction probably reflects heterogeneity in the conduit and initial plume where the interior of the pyroclast-gas mixture is effectively shielded from contact with the external water.

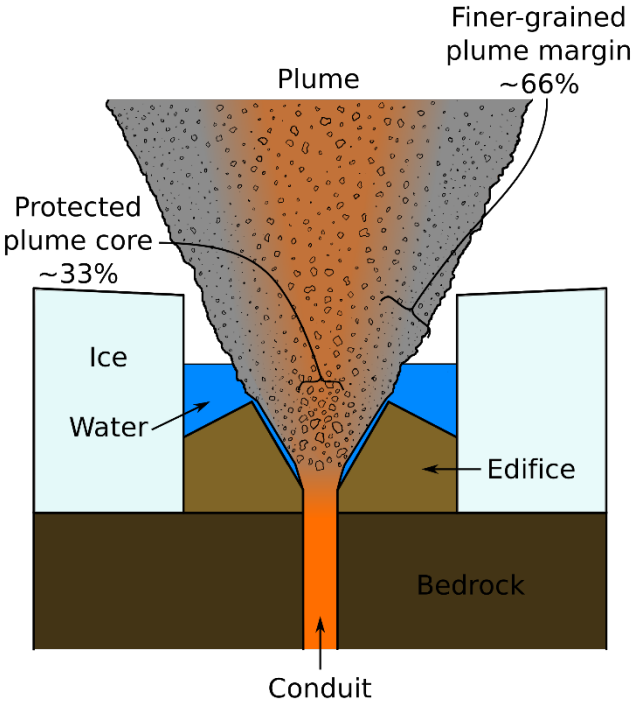

Figure 12 Schematic illustration demonstrating the partial interaction of the erupting magma with external water from the glacier. About two thirds of the erupting magma undergoes full or partial thermal granulation to ash but the remaining third is essentially unaffected by water-related fragmentation

Although this example is in the context of a basaltic eruption of strong subplinian to weak Plinian intensity, we suggest broadly similar processes prevail in mixed Plinian/phreatoplinian eruptions of all compositions where the magma in both dry and wet phases is fragmented at the peak of its vesiculation and degassing.

The threat from Icelandic fissure eruptions stems from their longevity; a long-lasting eruption increases the chances of an explosive episode occurring whilst the wind is blowing towards Europe. We have shown here that the Eldgjá fissure eruption was capable of producing volcanic plumes more than 15 km high, easily capable of reaching Europe in the right wind conditions. We also show that, despite the preconception that subglacial eruptions are more explosive, the magmatic episodes in a fissure eruption like Eldgjá can produce plumes as high as phreatomagmatic episodes.

References

Baillie MGL, McAneney J (2015) Tree ring effects and ice core acidities clarify the volcanic record of the first millennium. Clim Past 11:105–114. doi: 10.5194/cp-11-105-2015

Biass S, Bonadonna C (2014) TOTGS: Total grainsize distribution of tephra fallout.

Björnsson H, Pálsson F, Guðmundsson MT (2000) Surface and bedrock topography of the Mýrdalsjökull ice cap. Jökull 49:29–46.

Bonadonna C, Costa A (2013) Plume height, volume, and classification of explosive volcanic eruptions based on the Weibull function. Bull Volcanol 75:1–19. doi: 10.1007/s00445-013-0742-1

Bonadonna C, Houghton BF (2005) Total grain-size distribution and volume of tephra-fall deposits. Bull Volcanol 67:441–456. doi: 10.1007/s00445-004-0386-2

Borselli L, Sarocchi D (2016) DECOLOG.

Carey RJ, Houghton BF, Thordarson T (2009) Tephra dispersal and eruption dynamics of wet and dry phases of the 1875 eruption of Askja Volcano, Iceland. Bull Volcanol 72:259–278. doi: 10.1007/s00445-009-0317-3

Carey S, Sparks RSJ (1986) Quantitative models of the fallout and dispersal of tephra from volcanic eruption columns. Bull Volcanol 48:109–125. doi: 10.1007/BF01046546

Coltelli M, Carlo PD, Vezzoli L (1998) Discovery of a Plinian basaltic eruption of Roman age at Etna volcano, Italy. Geology 26:1095–1098.

Daggitt ML, Mather TA, Pyle DM, Page S (2014) AshCalc–a new tool for the comparison of the exponential, power-law and Weibull models of tephra deposition. J Appl Volcanol 3:1. doi: 10.1186/2191-5040-3-7

Fei J, Zhou J (2006) The Possible Climatic Impact in China of Iceland's Eldgjá Eruption Inferred from Historical Sources. Clim Change 76:443–457. doi: 10.1007/s10584-005-9012-3

Fierstein J, Nathenson M (1992) Another look at the calculation of fallout tephra volumes. Bull Volcanol 54:156–167. doi: 10.1007/BF00278005

Froggatt PC (1982) Review of methods of estimating rhyolitic tephra volumes; applications to the Taupo volcanic zone, New Zealand. J Volcanol Geotherm Res 14:301–318. doi: 10.1016/0377-0273(82)90067-1

Hammer CU (1984) Traces of icelandic eruptions in the Greeland ice sheet. Jökull 51–65.

Hon K, Kauahikaua J, Denlinger R, Mackay K (1994) Emplacement and inflation of pahoehoe sheet flows: observations and measurements of active lava flows on Kilauea Volcano, Hawaii. Geol Soc Am Bull 106:351–370.

Jakobsson SP (1979) Petrology of recent basalts of the Eastern Volcanic Zone, Iceland. Icelandic Museum of Natural History
Kokelaar P (1986) Magma-water interactions in subaqueous and emergent basaltic volcanism. Bull Volcanol 48:275–289. doi: 10.1007/BF01081756
Larsen G (1984) Recent volcanic history of the Veidivötn fissure swarm, southern Iceland — an approach to volcanic risk assessment. J Volcanol Geotherm Res 22:33–58. doi: 10.1016/0377-0273(84)90034-9
Larsen G (2005) Explosive volcanism in Iceland: three examples of hydromagmatic basaltic eruptions on long volcanic fissures within the past 1200 years. In: Geophysical Research Abstracts. Vienna, p 2005
Larsen G (2000) Holocene eruptions within the Katla volcanic system, south Iceland: characteristics and environmental impact. Jökull 49:1–28.
Larsen G (2010) 3 Katla: tephrochronology and eruption history. Dev Quat Sci 13:23–49.
Loughlin SC, Aspinall WP, Vye-Brown C, et al (2012) Large-magnitude fissure eruptions in Iceland: source characterisation. British Geological Survey
Mastin LG, Guffanti M, Servranckx R, et al (2009) A multidisciplinary effort to assign realistic source parameters to models of volcanic ash-cloud transport and dispersion during eruptions. J Volcanol Geotherm Res 186:10–21. doi: 10.1016/j.jvolgeores.2009.01.008
McCarthy D, Breen A (1997) An evaluation of astronomical observations in the Irish annals. Vistas Astron 41:117–138. doi: 10.1016/S0083-6656(96)00052-9
McPhie J, Walker GPL, Christiansen RL (1990) Phreatomagmatic and phreatic fall and surge deposits from explosions at Kilauea volcano, Hawaii, 1790 a.d.: Keanakakoi Ash Member. Bull Volcanol 52:334–354. doi: 10.1007/BF00302047
Newhall CG, Self S (1982) The volcanic explosivity index (VEI) an estimate of explosive magnitude for historical volcanism. J Geophys Res Oceans 87:1231–1238. doi: 10.1029/JC087iC02p01231
Oman L, Robock A, Stenchikov GL, Thordarson T (2006) High-latitude eruptions cast shadow over the African monsoon and the flow of the Nile. Geophys Res Lett 33:L18711. doi: 10.1029/2006GL027665
Parfitt EA (1998) A study of clast size distribution, ash deposition and fragmentation in a Hawaiian-style volcanic eruption. J Volcanol Geotherm Res 84:197–208. doi: 10.1016/S0377-0273(98)00042-0
Pedersen GBM, Höskuldsson A, Dürig T, et al Lava field evolution and emplacement dynamics of the 2014–2015 basaltic fissure eruption at Holuhraun, Iceland. J Volcanol Geotherm Res. doi: 10.1016/j.jvolgeores.2017.02.027
Pyle DM (1995) Assessment of the minimum volume of tephra fall deposits. J Volcanol Geotherm Res 69:379–382. doi: 10.1016/0377-0273(95)00038-0
Pyle DM (1989) The thickness, volume and grainsize of tephra fall deposits. Bull Volcanol 51:1–15.
Pyle DM (2015) Chapter 13 - Sizes of Volcanic Eruptions. In: Sigurdsson H (ed) The Encyclopedia of Volcanoes (Second Edition). Academic Press, Amsterdam, pp 257–264
Richter DH, Eaton JP, Murata KJ, et al (1970) Chronological narrative of the 1959-1960 eruption of Kilauea volcano, Hawaii. United States Geological Survey
Robson GR (1956) The volcanic geology of Vestur – Skaftarfellssysla Iceland. Doctoral, Durham University
Sable JE, Houghton BF, Wilson CJN, Carey RJ (2006) Complex proximal sedimentation from Plinian plumes: the example of Tarawera 1886. Bull Volcanol 69:89–103. doi: 10.1007/s00445-006-0057-6

Sharma K, Self S, Blake S, et al (2008) The AD 1362 Öræfajökull eruption, S.E. Iceland: Physical volcanology and volatile release. J Volcanol Geotherm Res 178:719–739. doi: 10.1016/j.jvolgeores.2008.08.003

Sigurðardóttir SS, Gudmundsson MT, Hreinsdóttir S (2015) Mapping of the Eldgjá lava flow on Mýrdalssandur with magnetic surveying. Jökull 65:61–71.

Stothers RB (1998) Far reach of the tenth century Eldgjá eruption, Iceland. Clim Change 39:715–726.

Stothers RB, Wolff JA, Self S, Rampino MR (1986) Basaltic fissure eruptions, plume heights, and atmospheric aerosols. Geophys Res Lett 13:725–728. doi: 10.1029/GL013i008p00725

Thordarson T, Larsen G (2007) Volcanism in Iceland in historical time: Volcano types, eruption styles and eruptive history. J Geodyn 43:118–152. doi: 10.1016/j.jog.2006.09.005

Thordarson T, Miller DJ, Larsen G, et al (2001) New estimates of sulfur degassing and atmospheric mass-loading by the 934 AD Eldgjá eruption, Iceland. J Volcanol Geotherm Res 108:33–54. doi: 10.1016/S0377-0273(00)00277-8

Thordarson T, Self S (1993) The Laki (Skaftár Fires) and Grímsvötn eruptions in 1783–1785. Bull Volcanol 55:233–263.

Thordarson T, Self S, Oskarsson N, Hulsebosch T (1996) Sulfur, chlorine, and fluorine degassing and atmospheric loading by the 1783–1784 AD Laki (Skaftár Fires) eruption in Iceland. Bull Volcanol 58:205–225.

UK Cabinet Office (2012) National Risk Register of Civil Emergencies - 2012 edition.

Walker GPL (1973) Explosive volcanic eruptions — a new classification scheme. Geol Rundsch 62:431–446. doi: 10.1007/BF01840108

Walker GPL, Self S, Wilson L (1984) Tarawera 1886, New Zealand — A basaltic plinian fissure eruption. J Volcanol Geotherm Res 21:61–78. doi: 10.1016/0377-0273(84)90016-7

Wilson L, Sparks RSJ, Huang TC, Watkins ND (1978) The control of volcanic column heights by eruption energetics and dynamics. J Geophys Res Solid Earth 83:1829–1836. doi: 10.1029/JB083iB04p01829

Zielinski GA, Germani MS, Larsen G, et al (1995) Evidence of the Eldgjá (Iceland) eruption in the GISP2 Greenland ice core: relationship to eruption processes and climatic conditions in the tenth century. The Holocene 5:129–140. doi: 10.1177/095968369500500201

Zielinski GA, Mayewski PA, Meeker LD, et al (1994) Record of Volcanism Since 7000 B.C. from the GISP2 Greenland Ice Core and Implications for the Volcano-Climate System. Science 264:948–952. doi: 10.1126/science.264.5161.948

Paper II

Driving mechanism of explosive activity during the 10th century Eldgjá fissure eruption, southern Iceland

William M. Moreland[1, 2, *], Thorvaldur Thordarson[2], Bruce F. Houghton[3], Gudrun Larsen[1]
* wmm2@hi.is
[1] Institute of Earth Sciences, University of Iceland, Askja, Sturlugata 7, 101 Reykjavík, Iceland
[2] Faculty of Earth Sciences, University of Iceland, Askja, Sturlugata 7, 101 Reykjavík, Iceland
[3] Department of Geology and Geophysics, SOEST, University of Hawai'i at Mānoa, Honolulu, HI 96822, USA

Abstract

The 10th century Eldgjá eruption is the largest in Iceland in historical time (i.e. the last 1140 years). Whilst it was dominantly effusive, producing 19.7 km^3 of lava, a significant amount of tephra was also formed in at least 13 separate explosive episodes from both subaerial and subglacial fissure segments along the 70-km-long vent system. These produced magmatic and phreatomagmatic tephra deposits respectively. The grain-size of these two end-members reveals distinct distributions: a coarse, unimodal, positively-skewed distribution (magmatic deposits) and a bimodal distribution rich in fine particles for the phreatomagmatic phases. At first examination, these distributions seem to record different fragmentation histories. However, the vesicle-size distributions of pyroclasts from each type of deposit show the pyroclasts underwent similar vesicle nucleation and growth prior to fragmentation. We feel this is compelling evidence that the role of external water from the glacier was at a comparatively late-stage, to fragment further an already disrupting magma by quench granulation.

Introduction

Icelandic eruptions can produce significant large impacts on the atmosphere and hence on aviation and the global economy, as demonstrated by the 2010 eruption of Eyjafjallajökull (Gudmundsson et al. 2012; Dellino et al. 2012). This is primarily due to the widespread ash plumes produced by these events. Plume dispersal is strongly influenced by the discharge rate and grain size of the tephra (Mastin et al. 2009) and so it is essential to understand the fragmentation mechanism for such eruptions, and to constrain accurately eruptive volumes, particularly for the very fine ash fraction (< 63 μm) as it has the greatest potential to produce widespread impacts and disruption.

'Dry' or magmatic fragmentation is driven by the explosive release and expansion of magmatic volatiles (e.g. Mangan and Cashman 1996; Sparks 2003; Gonnermann 2015) and so to understand fragmentation it is necessary to understand processes of vesiculation. When external water has access to the ascending magma during an eruption, as was the case for the subglacial eruptions of Eyjafjallajökull 2010 or Grímsvötn 2011 (Stevenson et al. 2013), it is thought that thermally efficient magma-water interaction (phreatomagmatism) will increase

thermal efficiency and the abundance of fine ash particles present in the tephra (Kokelaar 1986; Wohletz 1986; Wohletz et al. 2013). Given the importance of fine-ash to aviation hazards and national power grids (Wilson et al. 2012) it is important to assess the role of external water in 'wet' tephra-producing eruptions.

The 10th century Eldgjá fissure eruption presents an excellent natural laboratory in which to study both magmatic vesiculation and the impact of external water for several reasons: 1) Eldgjá produced > 16 voluminous and widespread tephra units which are preserved such that many can be mapped accurately and sampled with fine temporal resolution, for lab-based analyses and measurements. 2) Eldgjá produced tephra units which are the products of alternating magmatic (dry) as well as phreatomagmatic (wet, subglacial) explosive phases (Larsen 2000). 3) The Eldgjá magma has a very narrow compositional range and so the magma was essentially uniform in terms of bulk physical properties. These characteristics make Eldgjá an ideal case study for comparing the processes during magmatic versus phreatomagmatic

Figure 1 Map of study area with labelled for key localities. Skælingar and Stóragil tephra sections are indicated by white circles. Shaded area to the west of the dashed line on Álftavershraun lava field indicates the suspected buried margin of the lava beneath Mýrdalssandur (modified from Sigurðardóttir et al. 2015)

explosive phases because complications which arise when comparing products of different events or magmas of different composition can be eliminated.

The aim of this paper is to explore and quantify shallow conduit and vent processes which influenced the nature of the explosive phases of Eldgjá. This was achieved by a combination of acquiring both field-based observations and measuring clast density and vesicle-size distributions in magmatic and phreatomagmatic tephra. In addition, microtextural observations of the tephra allow the relative timing of shallow-conduit processes to be established.

The 939 CE Eldgjá eruption

The ~70 km long Eldgjá fissure is part of the Katla volcanic system in Iceland's Eastern Volcanic Zone. It extends from the Katla caldera below the Mýrdalsjökull in the southwest, intermittently through the mountainous terrain northeast of the glacier to Eldgjá proper and almost to the edge of Vatnajökull (Figure 1). Eldgjá is the longest known fissure in historical time in Iceland. The vent structures on the subaerial fissure segments are ramparts and occasional cones of scoria and spatter. Unlike the 1783 CE Laki eruption (Thordarson and Self 1993; Thordarson et al. 1996; Thordarson and Self 2003) there are no contemporary descriptions available of the eruption despite occurring almost a generation after Iceland was first settled (the Landnámabók descriptions are written about 200 years later). Initially, the Eldgjá eruption was dated via the Greenland ice core record to 934 CE (Hammer et al. 1980; Hammer 1984; Zielinski et al. 1994, 1995); more recent studies have dated the Eldgjá eruption at 939 CE (Oman et al. 2006; Baillie and McAneney 2015; Sigl et al. 2015). The duration of the event is unknown but is likely between 6 months (Thordarson et al. 2001) and 3 to 6 years (Zielinski et al. 1994, 1995).

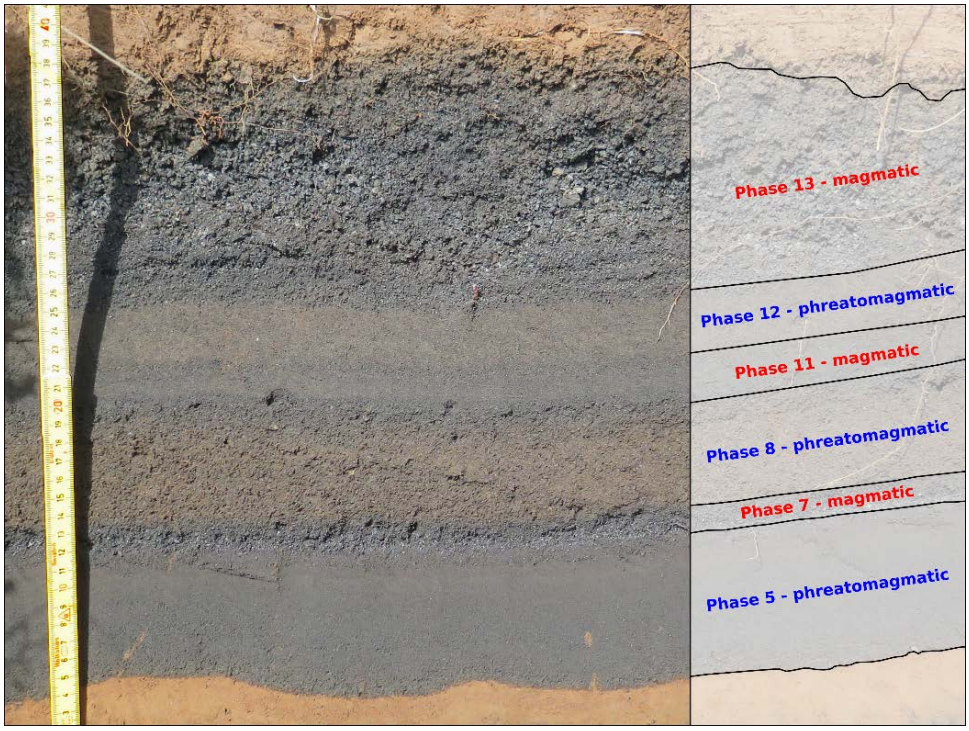

Figure 2 Typical photograph of the Eldgjá tephra deposit showing alternating magmatic and phreatomagmatic tephra units. Brown colouring of some phreatomagmatic units is due to presence of very fine ash. Sample location E15-022, 63.85028°N, -18.51112°E, 13 km from fissure, 37 cm thick

There were at least 16 explosive episodes originating from either subglacial or subaerial fissure segments. In addition to the two large lava fields from the fissure, a lava flow emanated from the Katla caldera creating the Kriki lava and jökulhlaup deposit intercalation (Figure 1; Larsen 2000). Explosive activity began beneath Mýrdalsjökull and activity generally propagated to the northeast with time although there were at least four more subglacial episodes after subaerial activity commenced.

Eldgjá tephra

Although Eldgjá was dominantly an effusive eruption, producing a minimum of 19.7 km^3 of lava (Sigurðardóttir et al. 2015), a significant volume of tephra was produced: about 1.3 km^3 (dense rock equivalent; Larsen 2000). The Eldgjá tephra deposit consists of alternating units which can be placed into two broad categories: magmatic and phreatomagmatic. The two end-members easily distinguished from each other in the field (Figure 2).

The magmatic tephra deposits form loose, very well- to poorly-sorted, unconsolidated layers which are rich in black to shiny blue-black achneliths (Walker and Croasdale 1971). The clasts are variable in shape, ranging from equant to elongate and near-spherical to ragged and very angular. Wall rock lithics are absent from most units but when present are red or yellow basalt and hyaloclastite and form < 5% of the deposit. Pele's hair and tears are present in minor amounts in a few of the fall units and distinctly less abundant than in the 1783-4 Laki tephra (Thordarson and Self 1993).

The phreatomagmatic tephra deposits are brownish in colour and well- to poorly-sorted, making the layers much more consolidated than the magmatic equivalents. The layers are rich in fine ash and achneliths are conspicuously absent whilst accretionary lapilli are present. The clasts are equant and have distinctly dull surfaces. The lithic content is identical to that in the magmatic deposits.

As well as being easily distinguished in the field, the magmatic and phreatomagmatic tephra deposits of Eldgjá exhibit distinctive, characteristic total grain-size distributions (Moreland et al. in prep.). The magmatic units have a narrow, coarse unimodal and positively skewed distribution with a single mode in the lapilli size range whilst the phreatomagmatic units are bimodal with peaks in the coarse and very fine ash ranges, suggesting that more than one fragmentation process was at work.

The two sections used in this study, Stóragil and Skælingar, are chosen to represent the diversity of magmatic and phreatomagmatic tephra. The section at Stóragil is about 10 km east of the subglacial fissure segment beneath Mýrdalsjökull (Figure 1) and is over 2 m thick with nearly half being comprised of phreatomagmatic units (Figure 3). Closer to the glacier undisturbed tephra sections are scarce due to erosion by advancement of the glacier and by jökulhlaups since the Eldgjá eruption (Larsen 2000). Thirteen units in this section can be broadly split into a phreatomagmatic-rich lower half and a dominantly magmatic upper half. This illustrates how activity began beneath the glacier, producing wet explosive deposits, before moving to adjacent subaerial fissure segments and becoming essentially dry.

The section at Skælingar is less than 1 km south of the fissure at Eldgjá proper (Figure 1). It is nearly 4 metres thick consisting almost entirely of magmatic tephra (Figure 3), except for the lowermost 4 cm, which contain three phreatomagmatic units. Despite being almost twice the thickness of the Stóragil section, Skælingar contains just nine units with the lowermost magmatic unit (samples 9 to 20 in Figure 3) accounting for 65% of the tephra thickness at this site. An abrupt shift in grain-size occurs 2.5 metres from the base of the Skælingar section (sample 22 and up in Figure 3) with a thin coarse ash to fine lapilli fall immediately overlying a thicker bomb layer.

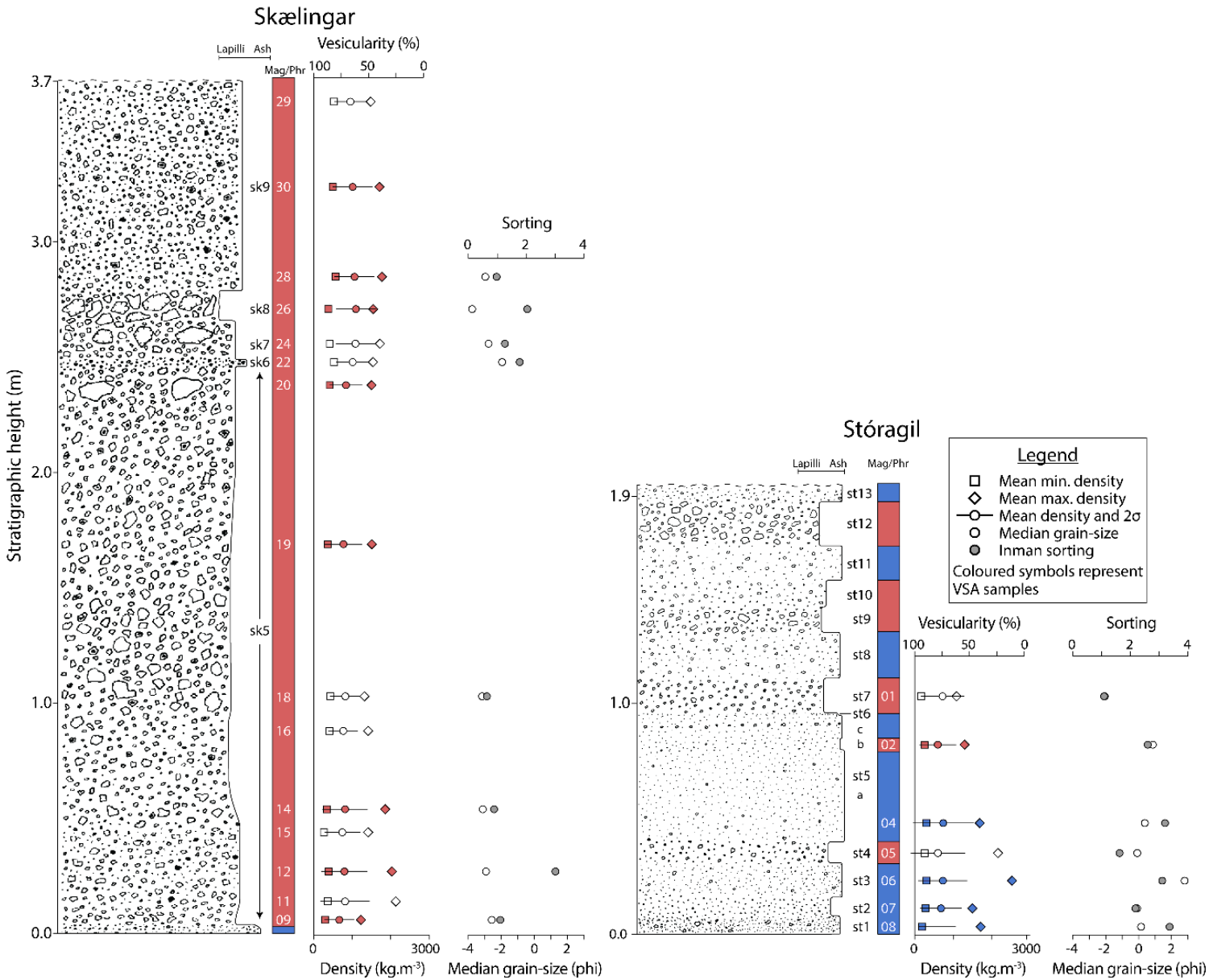

Figure 3
Stratigraphic logs of the key localities Skælingar and Stóragil. Red and blue shapes represent magmatic and phreatomagmatic samples respectively which were analysed for vesicles-size, white shapes are all magmatic. Unit labels begin with sk or st for Skælingar and Stóragil respectively and sample numbers are alongside each density measurement set. The minimum and maximum densities for each sample were calculated from the mean of the lowest and highest three pyroclasts in each sample respectively

Methods

Sampling

The tephra sections at Skælingar and Stóragil were logged, individual units described in detail, and sampled for both density and grain-size analysis. The density technique follows Houghton and Wilson (1989). Each sample consists of 100 pyroclasts between 8 and 32 millimetres in diameter collected from a horizon not more than 3 clasts thick. This size range ensures a large enough surface area in subsequent thin-sections for image analysis whilst attempting to exclude any significant post-fragmentation expansion of vesicles. The small sampling interval is used to justify the assumption that the clasts in each sample represent magma ejected from the vent during very narrow time windows.

Density and bulk vesicularity

The samples were cleaned in a sonic bath to remove any fine particles, and dried in an oven at 40°C. The pyroclasts were weighed, wrapped in Parafilm M® to waterproof them, and weighed again, this time suspended in deionised water by a wire cage. The density of the pyroclast was then calculated using Archimedes' principle. Vesicularity is calculated from density using a value for melt density, 2850 $kg.m^{-3}$, which was in this case calculated from Eldgjá glass major element concentrations.

Textural analysis

Polished thin-sections were made from pyroclasts selected from the central (mean ± 0.5 × s.d.) portion of representative density distributions. Nested sets of images of the thin-sections were acquired over four magnifications following the method outlined in Shea et al. (2010). The first level of magnification (c. 4.5 x) was collected on a desktop scanner. Backscattered electron images at 50x, 100x, and 250x magnification were collected on a Hitachi TM3000 SEM. The images were processed, bubbles decoalesced, and made binary in the free and open-source raster graphics editor GNU Image Manipulation Program (GIMP - http://www.gimp.org/). The binary images are analysed using the free and open-source image processing software ImageJ (Schneider et al. 2012). Each vesicle in the reference area is counted and measured for area.

ImageJ results for each magnification level were collated in a spreadsheet to give the total bubble count and the reference area in each image. The area of each vesicle was then converted to a diameter of an equivalent circle. A minimum vesicle size was imposed based on the error associated with measuring circular objects represented by square pixels (Shea et al. 2010), here a 11-pixel limit was set corresponding to an equivalent diameter of 7 μm at the 250 x magnification level. The data was binned using a geometric bin size (equivalent diameter multiplied by $10^{0.1}$). The number of vesicles per unit area, N_A, was calculated for each bin in each magnification level and the results plotted against the equivalent diameter. Using this plot transitions between magnifications were selected, ensuring a smooth transition where possible. The method of Sahagian and Proussevitch (1998) was used to convert from number of vesicles per unit area, N_A, to number per unit volume, N_V. This method relies upon the assumption that the vesicles are spherical which is generally true in these samples. The number per unit volume can then be corrected for vesicularity to give the number of vesicles per unit volume of melt, N_V^m (Table 1).

Upon first inspection, the clasts of the Eldgjá tephra seem to have very little variability in morphology within each sample and so standard component analysis was omitted. However, once thin-sections were made for the vesicle-size analysis it became clear that the clasts were composed of glass +/- varying quantities of microlites. For this reason, a form of componentry based on microlite abundance was carried out on only the 117 thin-sections which had already been acquired.

Results

Density and bulk vesicularity

The Eldgjá tephra is highly vesicular with mean vesicularity values between 61.2 and 80.4%. This is equivalent to a clast density of 560 to 1100 $kg.m^{-3}$ (Figure 3 and 4, Table 1). Magmatic tephra exhibit the largest range in mean vesicularity, ranging from 61 to 80% whilst the phreatomagmatic tephra cover a narrower range of mean vesicularities: 75 to 79%.

Skælingar: After a sudden decrease in vesicularity from 77 to 73% at the beginning, unit 5 has a constant vesicularity of around 74% (Figure 3 and 4). There is a significant decrease in vesicularity to 65% in unit 6, which is a coarse ash to fine lapilli unit and followed immediately by two units containing many dense bombs. Kernel density estimates (KDE; Figure 4) show that the magmatic density measurements are generally unimodal, Gaussian distributions; any skewness tends to be positive.

Stóragil: The phreatomagmatic units exhibit both the minimum and maximum ranges found in the Eldgjá tephra (E13-060-08, 60 – 94%; E13-060-06, 14 – 92%; Figure 3 and 4). The phreatomagmatic density measurements have either broad plateau or extreme fine-skewed distributions in the KDE plots (Figure 4) with one sample (E13-060-08) appearing to be weakly bimodal. The magmatic units present in Stóragil are similar to those found in Skælingar insofar as they have lower standard deviations and higher kurtoses than the phreatomagmatic tephra. However, two of the three magmatic units do have higher modal vesicularities than any of those found at Skælingar.

Qualitative vesicle and microlite observations

In thin-section, regardless of whether the sample is magmatic or phreatomagmatic, the smallest vesicles (3–16 μm) appear perfectly round, gradually becoming elliptical as they grow. Also, the largest vesicles (> 250 μm) are generally, but not always, the product of coalescence (Figure 5, 6, 8). The median vesicle size across all thin-sections ranges from 192 to 340 μm. The walls between vesicles are generally between 10 to 40 μm thick.

In many of the samples strings of vesicles stretch across the thin-section at various scales from several centimetres to microns (Figure 5). The vesicles making up these strings are generally small (30 to 100 μm) although rarely the strings feature smaller vesicles coalescing to form larger vesicles. It is uncommon to find more than one string in a single thin-section. The strings are up to 30 mm in length and between 0.2 and 1 mm wide.

Thin-sections also reveal that the pyroclasts feature two distinct types of domains; one characterised by golden-coloured sideromelane and the other by black tachylite. The colouring derives from the microlite content of each domain with the sideromelane being microlite poor (~3% by area excluding vesicles) and the tachylite being microlite rich (30–50%). Therefore, the terms microlite-poor (MPD) and microlite-rich domains (MRD) will be used hereafter (after

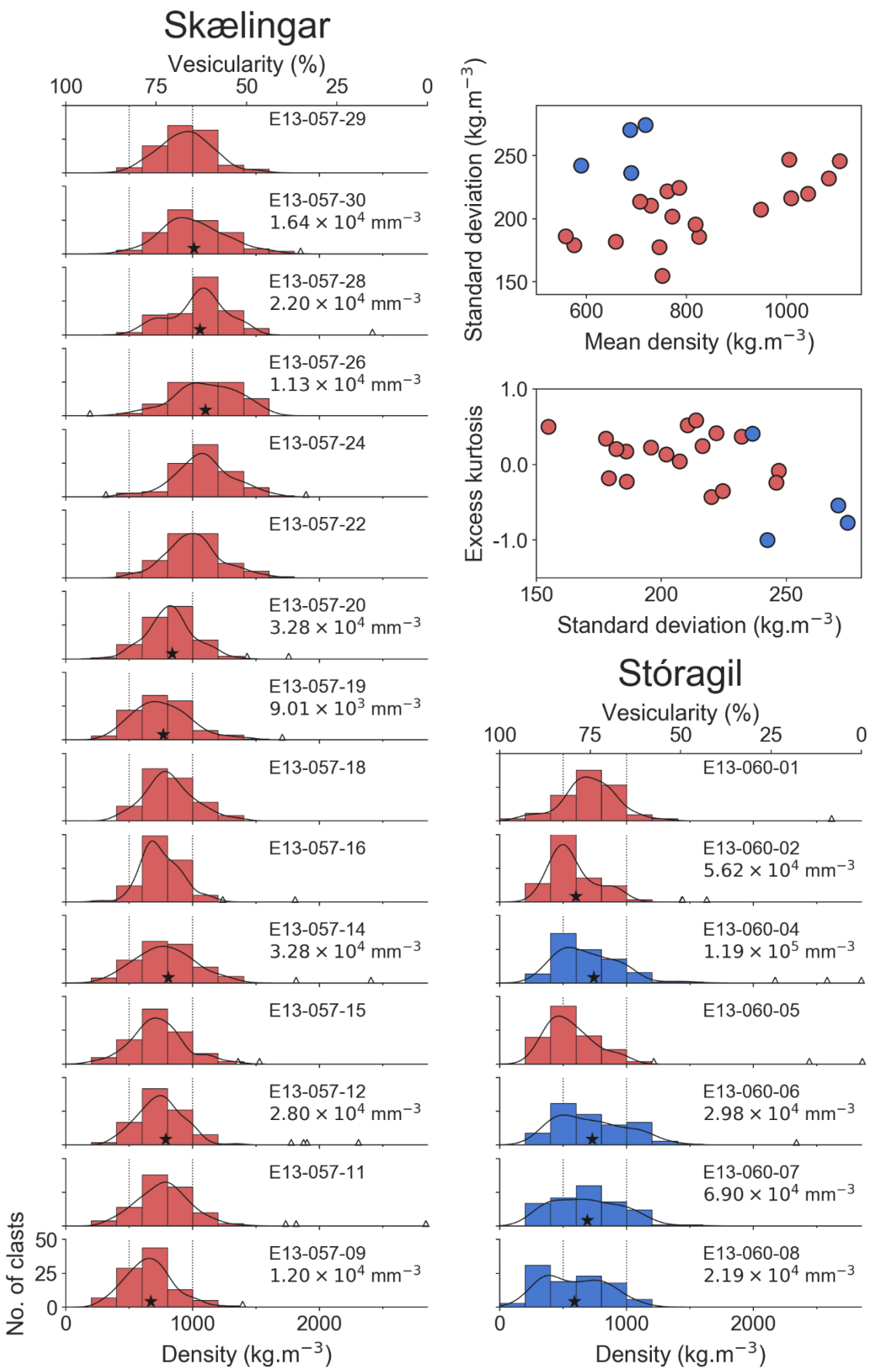
Skælingar
Vesicularity (%)
100
75
50
25
0
E13-057-29
E13-057-30
1.64 × 10^4 mm^-3
E13-057-28
2.20 × 10^4 mm^-3
E13-057-26
1.13 × 10^4 mm^-3
E13-057-24
E13-057-22
E13-057-20
3.28 × 10^4 mm^-3
E13-057-19
9.01 × 10^3 mm^-3
E13-057-18
E13-057-16
E13-057-14
3.28 × 10^4 mm^-3
E13-057-15
E13-057-12
2.80 × 10^4 mm^-3
E13-057-11
E13-057-09
1.20 × 10^4 mm^-3
No. of clasts
50
25
0
0
1000
2000
Density (kg.m^-3)
Standard deviation (kg.m^-3)
250
200
150
600
800
1000
Mean density (kg.m^-3)
Excess kurtosis
1.0
0.0
-1.0
150
200
250
Standard deviation (kg.m^-3)
Stóragil
Vesicularity (%)
100
75
50
25
0
E13-060-01
E13-060-02
5.62 × 10^4 mm^-3
E13-060-04
1.19 × 10^5 mm^-3
E13-060-05
E13-060-06
2.98 × 10^4 mm^-3
E13-060-07
6.90 × 10^4 mm^-3
E13-060-08
2.19 × 10^4 mm^-3
0
1000
2000
Density (kg.m^-3)

Figure 4 (overleaf) Density distributions of the Eldgjá tephra samples. Red histograms: magmatic samples; blue histograms: phreatomagmatic samples. The black curves are kernel density estimates for the density measurements. Black stars indicate the density of the pyroclasts which were used for vesicle size analysis and triangles along x-axis indicate outliers which were excluded from the statistical analyses. The vesicle number density of analysed clasts is included below the sample numbers. Vertical dotted lines are to facilitate comparisons between samples

Cimarelli et al. 2010). These domains occur in varying proportions in each thin-section but both domains are present in the magmatic and the phreatomagmatic tephra (Figure 6).

In general, the denser (i.e. less vesicular) clasts tend to be either entirely microlite-rich or contain MRDs whilst the less dense (i.e. more vesicular) clasts are generally microlite-poor (Figure 7). An example of this is seen in unit 5 in Skælingar; as density increases with stratigraphic height (Figure 3 and 4) so does the proportion of microlite-rich clasts (Figure 7).

Figure 8 highlights the two types of domain and the boundaries between them which, whilst sharp and distinct, are fluidal with complex embayments and enclaves. The microlites within the MPDs are sparse plagioclase laths with an average length of 20 µm. The MRDs also contain some large plagioclase microlites but in higher abundance whilst most microlites are smaller, at around 6 µm average length. Within the MRDs microlites commonly appear aligned with the edge of vesicles (Figure 8, red arrows).

The MRDs vesicles tend to have more ragged outlines. Vesicles which straddle the border between two contrasting domains have ragged outlines on edges within the MRD and smooth outlines on edges within the MPD. However, in both domains the larger vesicles are of overall similar morphology and as is shown in Figure 10 it is impossible to distinguish between clasts which are entirely microlite-poor and those which are microlite-rich based on vesicle populations alone. Although the MRDs and MPDs have very similar vesicle size populations, it is noteworthy that the MRDs contain significantly lesser abundance of small (i.e. <16 µm) vesicles than the MPDs.

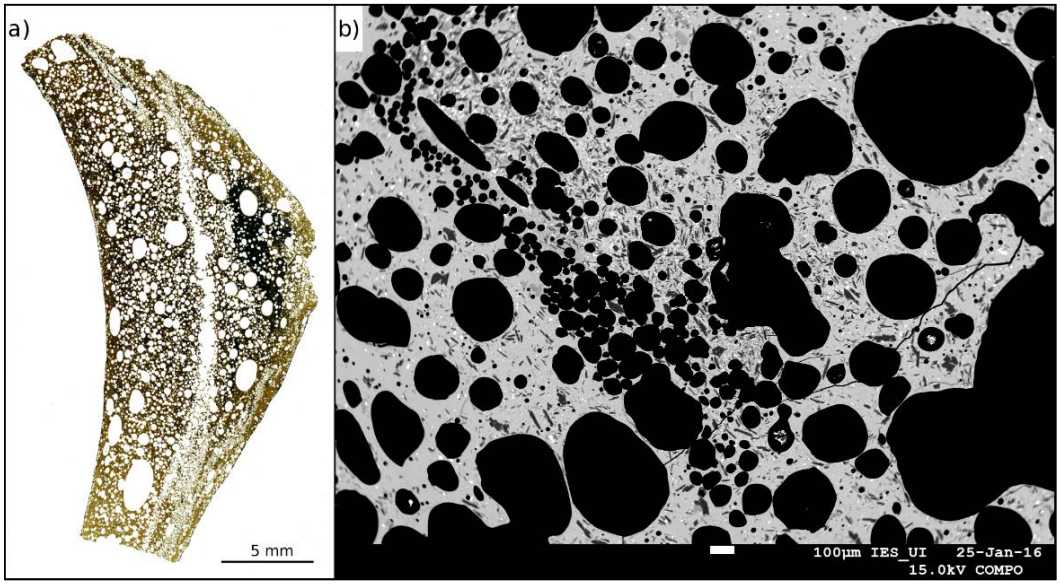

Figure 5 Two examples of vesicle strings at two different scales: a) scanned image of thin-section E13-057-26-097 showing a coalesced vesicle string along the length of the pyroclast of width 1 mm and length > 29 mm; b) Electron microprobe image showing fine-scale vesicle string of width 0.23 mm and length > 2.33 mm consisting of vesicles between 30 and 100 µm

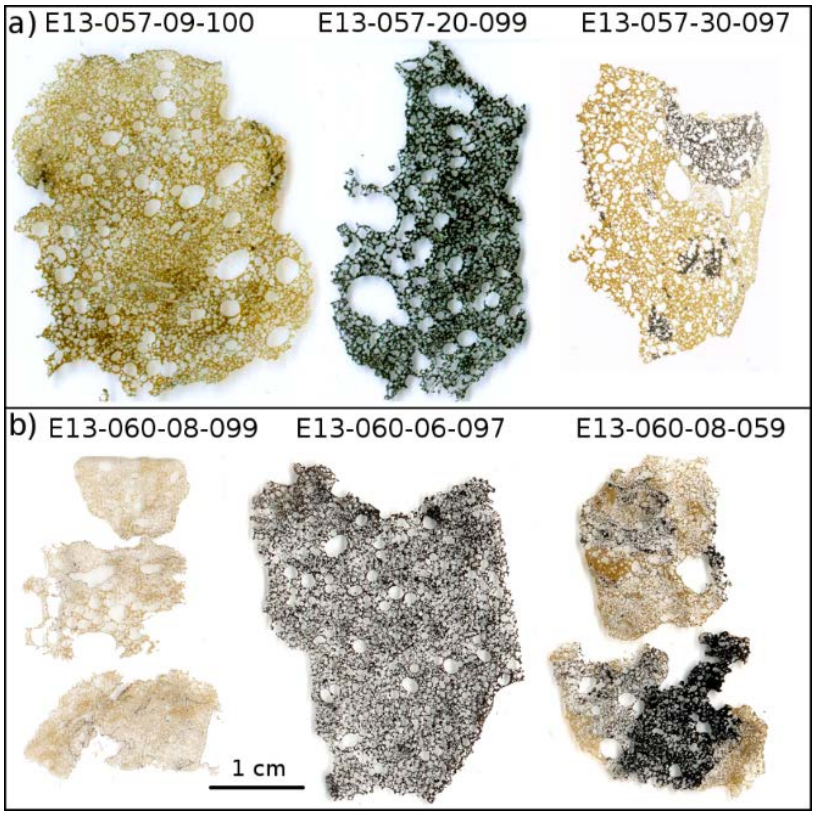

Figure 6 Example images of Eldgjá pyroclast thin-sections. a) magmatic b) phreatomagmatic. Both eruption style endmembers exhibit both microlite-free (golden) and microlite-rich (black) domains. With the exception of E13-060-08-059, all of these clasts have undergone vesicle-size analysis (Figure 11)

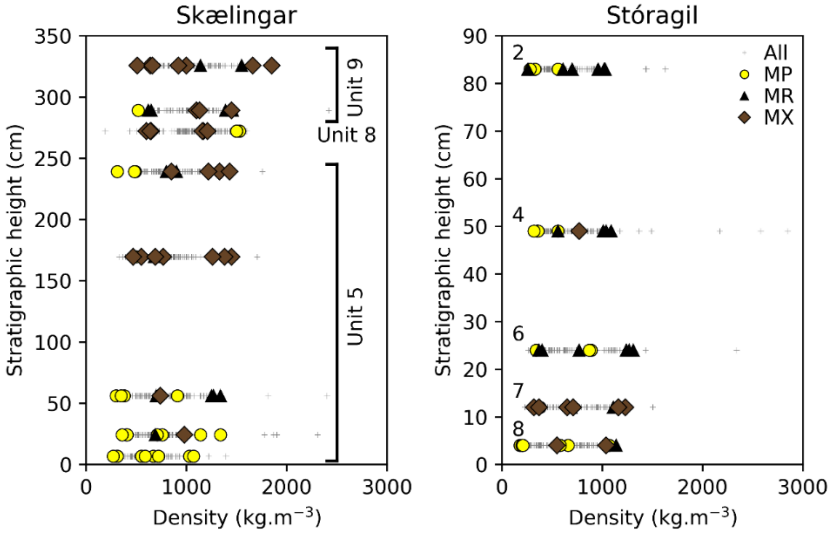

Figure 8 Plots of density against stratigraphic height for the two key tephra sections. Grey crosses indicate density measurements of individual clasts from each sampled horizon whilst MP, MR, and MX refer to microlite-poor, microlite-rich, and clasts containing both domains respectively. Numbers to the left of Stóragil data points indicate unit numbers

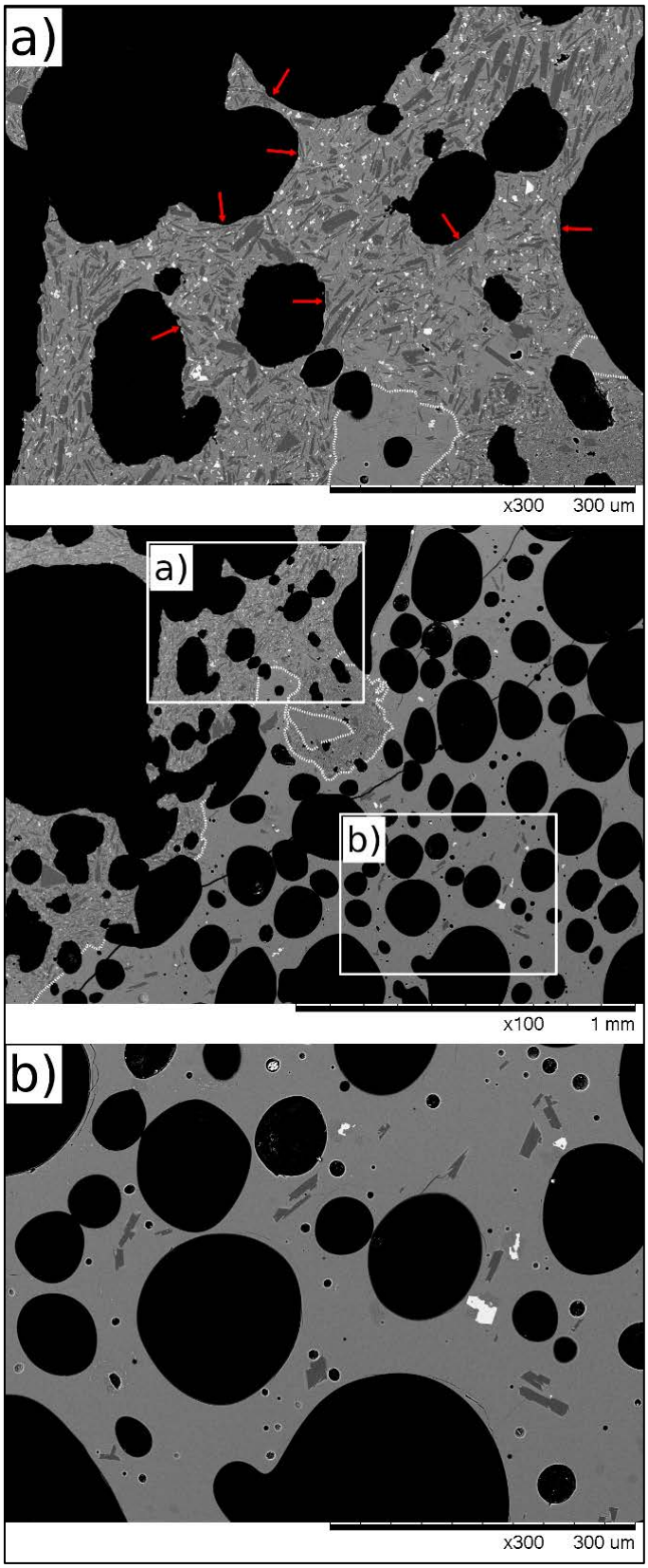

Figure 9 Microlite-rich versus poor domains within a single pyroclast (E13-057-30-097). The microlite-rich domains (a) contain over 30% microlites by area but have similar vesicle size distributions to the microlite-poor domains (b). Red arrows in a) point to microlites which appear to have aligned with the bubble edges during bubble growth

Quantification of Vesicle Textures

Vesicle number densities

Vesicle number densities (VND; N_V) for magmatic and phreatomagmatic tephra clasts are similar, both are in the range 3.1×10^3 to 2.3×10^4 mm^{-3} and when corrected for melt abundance (N_V^m) the corresponding values are 9.0×10^3 to 1.2×10^5 mm^{-3} (Figure 9, Table 1). The phreatomagmatic samples exhibit a greater range in terms of N_V^m values than the magmatic samples; 9.3×10^4 versus 4.6×10^4 mm^{-3}; and have a higher average N_V^m or 5.7×10^4 versus 2.3×10^4 mm^{-3}.

Vesicle volume distributions

Vesicle volume distributions, VVDs, (Figure 10) show the volume fraction within a given vesicle size range. These plots can be used to identify nucleation events, represented by modes; intervals of free growth of bubbles, represented by a Gaussian distribution; coalescence events, represented by positive skew; and bubble collapse, represented by decreased volume fractions.

There is essentially no difference between the magmatic and phreatomagmatic samples with both types having broadly unimodal distributions. The modes of all but one of the samples are between 0.16 and 0.41 mm (Figure 10); E13-060-08, has a lower mode between 0.13 and 0.16 mm. The median vesicle size remains relatively uniform throughout all samples; between 0.19 and 0.34 mm for magmatic and 0.20 and 0.24 mm for phreatomagmatic. It is important to note that the presence of MRD make no difference to the VVDs.

Interpretation and discussion

Density and bulk vesicularity

The magmatic tephra have tight, unimodal vesicularity/density distribution compared to the phreatomagmatic tephra (Figure 3 and 4). The Skælingar tephra also have slightly lower average vesicularities than Stóragil irrespective of whether the latter are magmatic or

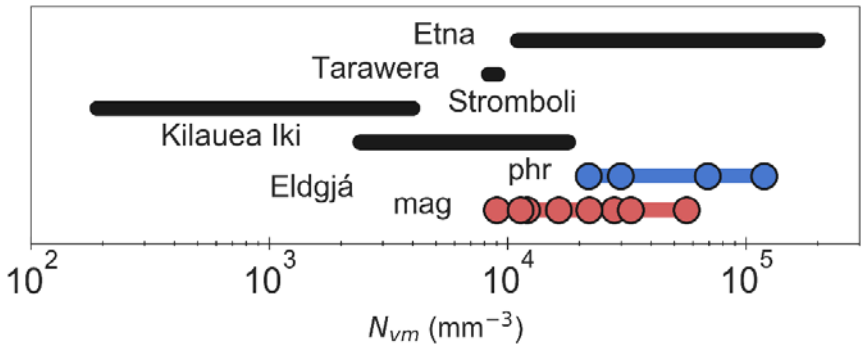

Figure 10 Eldgjá magmatic and phreatomagmatic vesicle number densities compared with those of other basaltic eruptions determined by the same methods (Etna 122 CE, Sable et al. (2006); Tarawera 1886, Sable et al. (2009); Stromboli 2002, Lautze and Houghton (2005, 2007, 2008); Kilauea Iki 1959, Stovall et al. (2011, 2012)

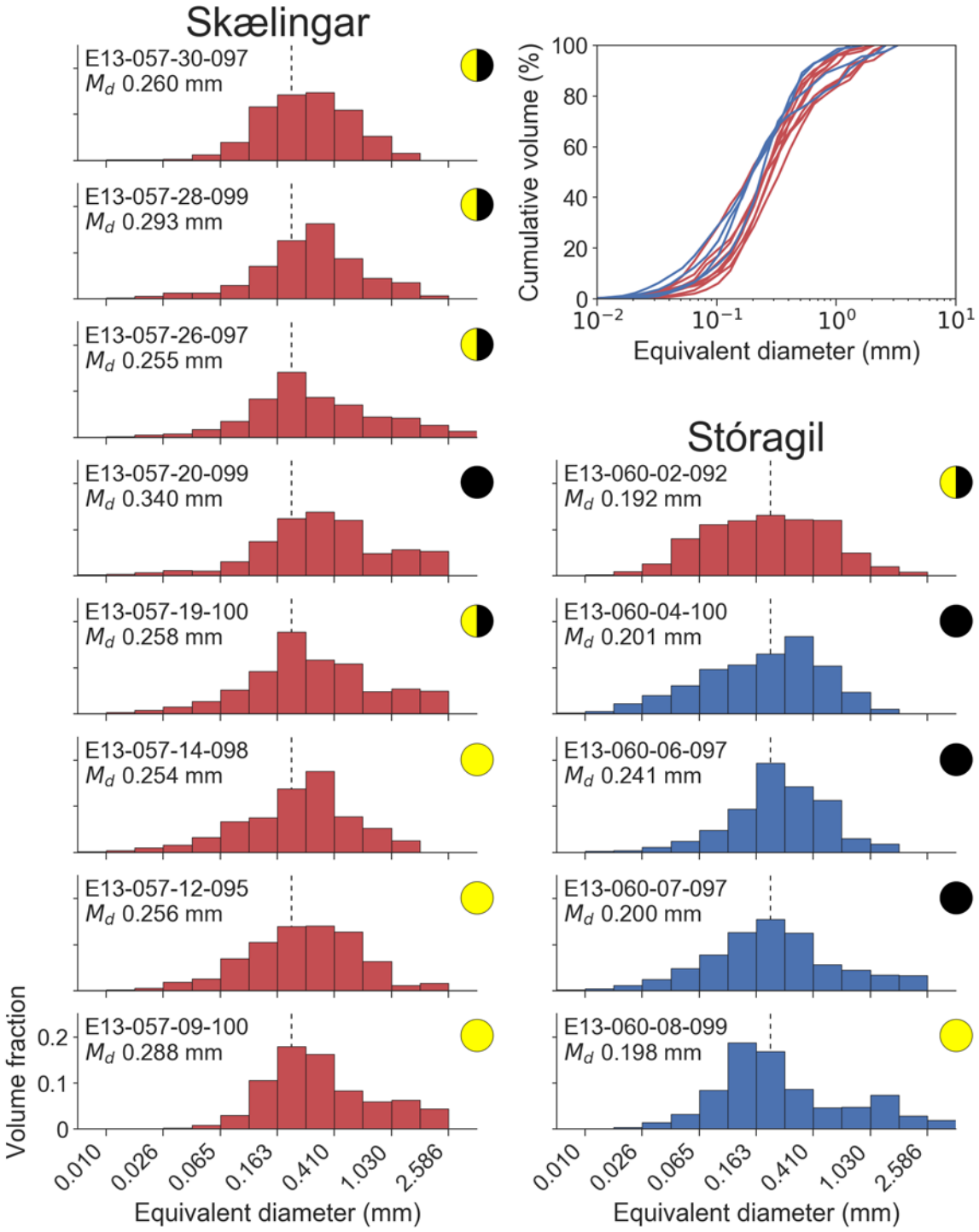

Figure 11 Vesicle volume distributions for the Skælingar and Stóragil tephra sections. Red plots are magmatic samples and blue phreatomagmatic. Each plot is labelled with the sample number and median vesicle diameter (M_d). The black dotted line is to aid comparison between distributions and is located at 0.2 mm equivalent diameter. Yellow or black circles indicate pyroclasts with only microlite-poor or -rich domains respectively, with yellow and black circles representing clasts containing both domain types. Inset is a cumulative vesicle volume plot summarising all sample data and highlights how similar each sample's nucleation history is

phreatomagmatic. Skælingar is also much closer (1 km) to its source vent than Stóragil is to its source vents (10 km) and since dense clast fall out faster and earlier than highly vesicular clasts it is possible that this difference is just a function of distance to site of deposition. Both the Skælingar and Stóragil tephra sections contain several dense outlier clasts although they are more common at Stóragil.

The tight vesicularity distributions (Figure 4) are to be expected for the magmatic tephra if the controlling factor in driving the magma to fragmentation at some critical threshold (and therefore cessation of bubble nucleation and growth) is the expansion of exsolved magmatic gases (Houghton and Wilson 1989).

The phreatomagmatic tephra have relatively broad, plateau-like vesicularity distributions (Figure 3 and 4, Table 1). It is suggested that external water was able to access the magma ascending at subglacial vents and quench it, preventing further bubble nucleation or growth. The range in vesicularities would then be a result of water encountering magma at various stages of vesiculation.

Qualitative microtextural observations

Vesicle strings

The strings of smaller vesicles as shown on Figure 5, are common in the Eldgjá tephra clasts and may be the prequel to the formation of permeable pathways which allow the efficient outgassing that typifies basaltic fissure eruptions (e.g. Thordarson et al. 2003). As such, the

Table 1 Summary of vesicle-size analysis results. Column headings are explained in the footnotes below the table

Sample[a]	Location	Type	Density × 1,000 (kg m^{-3})	Ves.[b] (%)	V_G/V_L[c]	N_A[d] (mm^{-2})	N_V[e] (mm^{-3})	N_V^m[f] (mm^{-3})
09-100	Sk	M	0.72	74.6	3.27	5.81E+01	3.06E+03	1.20E+04
12-095	Sk	M	0.76	73.3	2.58	1.32E+02	7.48E+03	2.80E+04
14-098	Sk	M	0.91	68.0	2.51	1.63E+02	1.05E+04	3.28E+04
19-100	Sk	M	0.69	75.9	2.69	1.51E+02	8.94E+03	9.01E+03
20-100	Sk	M	0.90	68.3	2.39	1.28E+02	1.04E+04	3.28E+04
26-097	Sk	M	1.21	57.6	1.60	9.92E+01	4.80E+03	1.13E+04
28-099	Sk	M	1.12	60.6	1.70	1.27E+02	8.66E+03	2.20E+04
30-097	Sk	M	1.00	64.9	1.81	7.85E+01	5.75E+03	1.64E+04
02-092	St	M	0.56	80.3	3.74	2.55E+02	1.11E+04	5.62E+04
04-100	St	P	0.56	80.4	2.83	8.85E+02	2.33E+04	1.19E+05
06-097	St	P	0.89	68.9	2.88	1.47E+02	9.27E+03	2.98E+04
07-097	St	P	0.71	75.1	3.15	2.77E+02	1.72E+04	6.90E+04
08-099	St	P	0.58	79.7	3.83	1.16E+02	4.44E+03	2.19E+04

[a] Sample numbers for Skælingar prefixed with E13-057 and Stóragil by E13-060

[b] Vesicularity calculated from density using a melt density of 2850 kg m^{-3}

[c] Vesicle-to-melt ratio (Gardner et al. 1996)

[d] N_A is number of vesicles per unit area, excluding phenocrysts

[e] N_V is number of vesicles per unit of volume and is calculated from N_A using the method of Sahagian and Proussevitch (1998)

[f] N_V^m is N_V corrected for vesicularity and is calculated by (N_V × 100) / (100 - vesicularity)

strings may represent the stage immediately prior to long pathways forming via the coalescence of these smaller vesicles that become planes of weakness along which any shearing would fragment the foam. If these are planes of disintegration, it explains why the fully-developed strings are not common in the lapilli clasts; the strings would be lost through coalescence to permeable pathways and/or occur along the edges of the soon-to-be clasts much like the perforations in a book of stamps. These irregular surface textures are commonly healed/sealed in the case of the magmatic tephra via fusion of the outer surface by the high-velocity hot gas that streams around the particles upon eruption to form the black shiny surfaces that typify many of the magmatic tephra clasts (Thordarson et al. 1996). Although a margin of smaller vesicles around a clast may indicate that the larger vesicles in the core of the clast are the product of post- fragmentation growth and coalescence, it may be that this rim of smaller vesicles represents the boundaries along which the clast fractured in the foam.

Microlite textures

The two domains of contrasting microlite crystallinity are interpreted as once having been texturally identical. Both domains contain a coarser microlite fraction which is considered to have been present prior to this divergence and formed predominantly by degassing-induced crystallization in the magma upon venting (Metrich and Rutherford 1998). We interpret this contrast in further microlite crystallization to have taken place along the margins versus the axis of the conduit. Along the margins slower moving magma could form the smaller microlite population that dominates the MRDs through cooling-induced crystallization. The smaller microlite population is two orders of magnitude smaller than the median vesicle size whilst the larger microlite population is only one order of magnitude smaller. The fluidal contact between the two domains seen in the mixed type clasts and the fact that growing bubbles cross the contact (Figure 6 and 8) indicates that the domains were both molten at the time of mingling. The vesicles which appear to straddle the contact between domains suggest that the bubbles nucleated after the mingling of the domains. The VVDs (Figure 10) also support bubble nucleation after mingling because both the MRDs and MPDs exhibit similar VVDs. The main difference, in terms of vesicles, between the two domains is that the MPDs contain more of the smallest vesicles (Figure 8). This can be explained either by lower supersaturation of volatiles in the marginal magma (perhaps lost through the conduit walls) or that the newly formed smaller microlite populations inhibited ongoing nucleation of new bubbles. The presence of microlites within the MRDs which seem to align with the vesicle edges suggests that the growing bubbles were capable of pushing the microlites out of their way. However, the ragged appearance of many of the vesicles indicates that this was not always successful and that the bubbles were forced to grow up into and somewhat around the jagged microlites.

Quantitative vesicle data

Vesicle number densities

In Figure 9 we compare the VNDs with other known basaltic explosive eruptions or eruption phases, quantified by the same methods, namely: Stromboli 2002 (Lautze and Houghton 2007, 2008), Kilauea Iki 1959 (Stovall et al. 2011, 2012), Tarawera 1886, (Sable et al. 2009), and Etna 122 CE (Sable et al. 2006). These comparisons show that the Eldgjá VNDs fall on the higher end of the intensity spectrum and are comparable with those of the 122 CE Plinian event at Etna.

High VND values have been associated with rapid magma ascent rates (Houghton and Gonnermann 2008) which are to be expected with any powerful explosive basaltic eruption

where high ascent rates are required to keep the volatile and melt phases coupled. Many studies have demonstrated that VND is proportional to eruption intensity (Polacci et al. 2006; Sable et al. 2006; Stovall et al. 2012). Our results imply that individual explosive episodes during the Eldgjá flood lava eruption had similar or greater intensities than some of the most powerful basaltic explosive eruptions known.

Vesicle volume distributions

Both magmatic and phreatomagmatic samples present unimodal vesicle volume distributions (Figure 10) with the mode indicating a single significant nucleation event.

Two possible exceptions to the unimodal pattern are samples E13-057-20 and E13-060-02 which have broader, more plateau-like distributions. Both samples are from the upper parts of particularly thick units and so may have experienced a more prolonged bubble nucleation process as magma ascent rates waned during that particular episode.

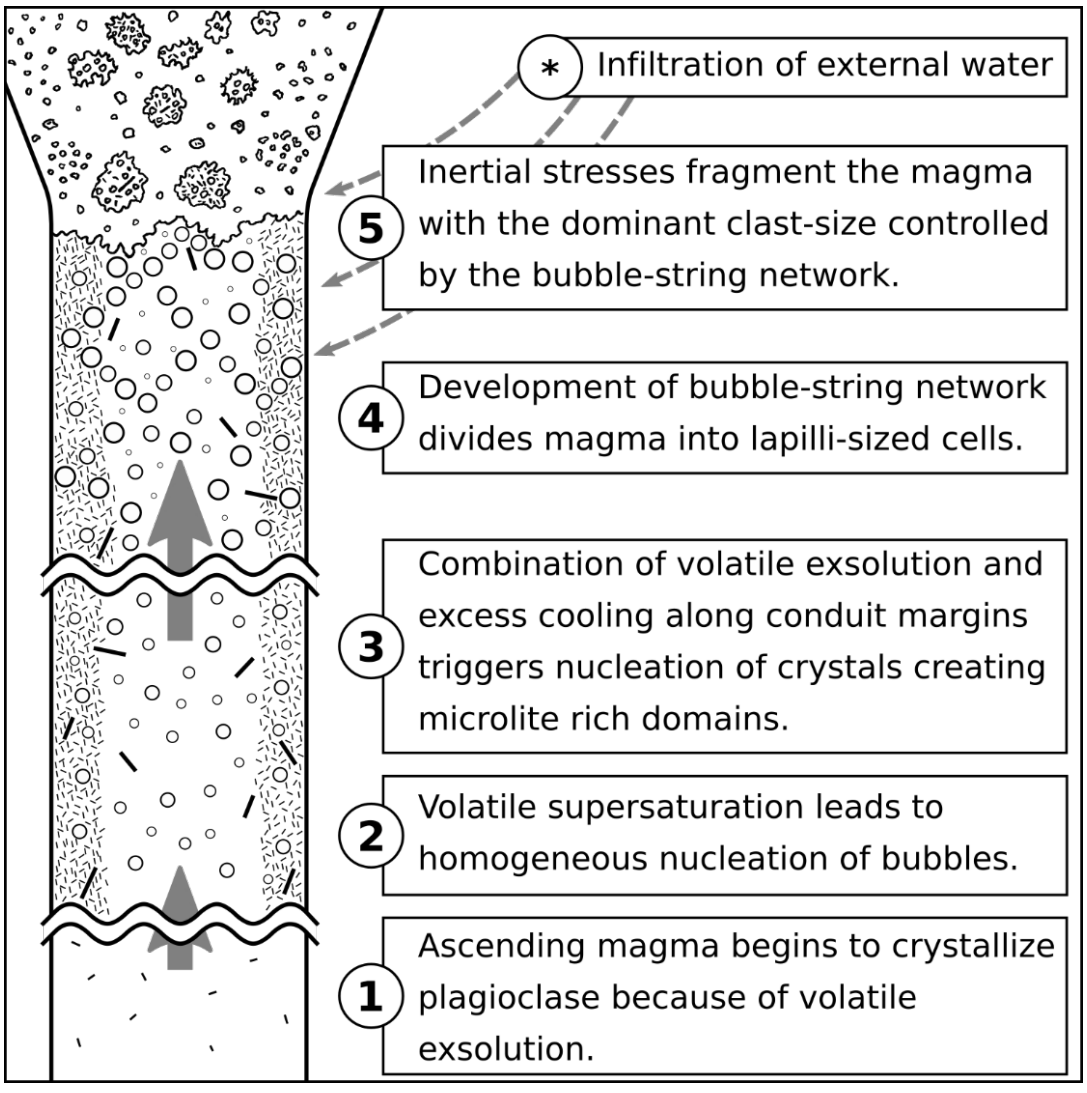

Figure 11 Schematic diagram outlining the conditions and processes which formed the Eldgjá tephra deposit. Large grey arrows within the conduit indicate acceleration of the magma whilst thin dashed arrows above and right of the conduit indicate a scenario wherein external water makes contact with magma at variable depths resulting in the range in vesicularity seen in figure 5

Conditions of ascent in the shallow conduit

Figure 11 outlines the conduit conditions and processes we interpret as having formed the Eldgjá tephra products. The magma ascending beneath subglacial and subaerial fissure segments of Eldgjá was initially physically identical. Rising magma began to crystallize the larger plagioclase laths, which are present in both domains, in response to initial volatile exsolution. The rapid ascent of the magma led to volatile supersaturation and the homogeneous nucleation of bubbles. The combination of volatile exsolution and excess heat-loss along the conduit margins resulted in undercooling and the formation of the microlite-rich domains. The contact between this microlite-rich periphery and the microlite-poor core must have been sharp given the lack of samples recording textures transitional between the two domain types. The development of bubble strings formed a mesh-like network throughout the magmatic foam but without significant outgassing and loss of pressure. The cell size within this bubble string network was lapilli-sized and, once fragmentation commenced due to inertial stresses from the rapid ascent, determined the size of the resultant pyroclasts.

Comparison with other explosive basaltic eruptions

Many other studies have proposed similar conditions for the formation of microlite-rich domains in basaltic melts (e.g. Taddeucci et al. 2004; Lautze and Houghton 2005, 2008; Costantini et al. 2010; Cimarelli et al. 2010; Stovall et al. 2012; Murtagh and White 2013) although it should be noted that in some cases vesicle-size distributions are similar across domains (Murtagh and White 2013) and in others are different (Costantini et al. 2010; Cimarelli et al. 2010). This may be due to the timing of the formation of this outer annular margin of slower, cooler magma in the conduit.

The ratio of microlite-poor to microlite-rich domains has been suggested as a possible monitoring parameter, able to detect increasing eruption intensity ahead of time (Cimarelli et al. 2010). It has already been suggested that conduit geometry may control the ratio of the domains (Cimarelli et al. 2010) and this is supported by the large proportion of microlite-rich clasts and domains in the Eldgjá tephra (Figure 8): for the same cross-sectional area, magma rising through a circular conduit would have less contact with the cooler conduit walls than in a linear conduit. It may therefore be expected to have an increased ratio of microlite-rich to microlite-poor material in a linear conduit such as those feeding fissure eruptions.

An additional note is that the apparent lack of wall-rock lithics suggests wall-rock erosion was not a dominant process during the Eldgjá eruption and that the width of the dyke(s) feeding the vents must have been established primarily by tectonic forces (Wilson and Head 1981).

Conclusions

Explosive episodes during the 10th century Eldgjá fissure eruption were driven by late-stage, rapid nucleation of bubbles regardless of whether the fissure segment in question was subglacial or subaerial. Microlite textures within the tephra suggest a zoned conduit with a high-velocity, hotter core generating microlite-poor material and a lower-velocity, cooler margin producing microlite-rich material. This division occurred at a late stage with the marginal microlites forming only slightly before onset of rapid bubble nucleation. The range in microlite textures is found in most Eldgjá tephra and so this conduit model is likely common to every part of the fissure.

References

Baillie MGL, McAneney J (2015) Tree ring effects and ice core acidities clarify the volcanic record of the first millennium. Clim Past 11:105–114. doi: 10.5194/cp-11-105-2015

Cimarelli C, Traglia FD, Taddeucci J (2010) Basaltic scoria textures from a zoned conduit as precursors to violent Strombolian activity. Geology 38:439–442. doi: 10.1130/G30720.1

Costantini L, Houghton BF, Bonadonna C (2010) Constraints on eruption dynamics of basaltic explosive activity derived from chemical and microtextural study: The example of the Fontana Lapilli Plinian eruption, Nicaragua. J Volcanol Geotherm Res 189:207–224. doi: 10.1016/j.jvolgeores.2009.11.008

Dellino P, Gudmundsson MT, Larsen G, et al (2012) Ash from the Eyjafjallajökull eruption (Iceland): Fragmentation processes and aerodynamic behavior. J Geophys Res Solid Earth 117:B00C04. doi: 10.1029/2011JB008726

Gonnermann HM (2015) Magma Fragmentation. Annu Rev Earth Planet Sci 43:431–458. doi: 10.1146/annurev-earth-060614-105206

Gudmundsson MT, Thordarson T, Höskuldsson Á, et al (2012) Ash generation and distribution from the April-May 2010 eruption of Eyjafjallajökull, Iceland. Sci Rep 2:572.

Hammer CU (1984) Traces of icelandic eruptions in the Greeland ice sheet. Jökull 51–65.

Hammer CU, Clausen HB, Dansgaard W (1980) Greenland ice sheet evidence of post-glacial volcanism and its climatic impact. Nature 288:230–235. doi: 10.1038/288230a0

Houghton BF, Gonnermann HM (2008) Basaltic explosive volcanism: Constraints from deposits and models. Chem Erde - Geochem 68:117–140. doi: 10.1016/j.chemer.2008.04.002

Houghton BF, Wilson CJN (1989) A vesicularity index for pyroclastic deposits. Bull Volcanol 51:451–462.

Kokelaar P (1986) Magma-water interactions in subaqueous and emergent basaltic volcanism. Bull Volcanol 48:275–289. doi: 10.1007/BF01081756

Larsen G (2000) Holocene eruptions within the Katla volcanic system, south Iceland: characteristics and environmental impact. Jökull 49:1–28.

Lautze NC, Houghton BF (2007) Linking variable explosion style and magma textures during 2002 at Stromboli volcano, Italy. Bull Volcanol 69:445–460. doi: 10.1007/s00445-006-0086-1

Lautze NC, Houghton BF (2008) Single explosions at Stromboli in 2002: Use of clast microtextures to map physical diversity across a fragmentation zone. J Volcanol Geotherm Res 170:262–268. doi: 10.1016/j.jvolgeores.2007.10.011

Lautze NC, Houghton BF (2005) Physical mingling of magma and complex eruption dynamics in the shallow conduit at Stromboli volcano, Italy. Geology 33:425–428. doi: 10.1130/G21325.1

Mangan MT, Cashman KV (1996) The structure of basaltic scoria and reticulite and inferences for vesiculation, foam formation, and fragmentation in lava fountains. J Volcanol Geotherm Res 73:1–18. doi: 10.1016/0377-0273(96)00018-2

Mastin LG, Guffanti M, Servranckx R, et al (2009) A multidisciplinary effort to assign realistic source parameters to models of volcanic ash-cloud transport and dispersion during eruptions. J Volcanol Geotherm Res 186:10–21. doi: 10.1016/j.jvolgeores.2009.01.008

Metrich N, Rutherford MJ (1998) Low Pressure Crystallization Paths of H2O-Saturated Basaltic-Hawaiitic Melts from Mt Etna: Implications for Open-System Degassing of Basaltic Volcanoes. Geochim Cosmochim Acta 62:1195–1205. doi: 10.1016/S0016-7037(98)00048-9

Murtagh RM, White JDL (2013) Pyroclast characteristics of a subaqueous to emergent Surtseyan eruption, Black Point volcano, California. J Volcanol Geotherm Res 267:75–91. doi: 10.1016/j.jvolgeores.2013.08.015

Oman L, Robock A, Stenchikov GL, Thordarson T (2006) High-latitude eruptions cast shadow over the African monsoon and the flow of the Nile. Geophys Res Lett 33:L18711. doi: 10.1029/2006GL027665

Pedersen GBM, Höskuldsson A, Dürig T, et al (2017) Lava field evolution and emplacement dynamics of the 2014–2015 basaltic fissure eruption at Holuhraun, Iceland. J Volcanol Geotherm Res. doi: 10.1016/j.jvolgeores.2017.02.027

Polacci M, Corsaro RA, Andronico D (2006) Coupled textural and compositional characterization of basaltic scoria: Insights into the transition from Strombolian to fire fountain activity at Mount Etna, Italy. Geology 34:201–204. doi: 10.1130/G22318.1

Robson GR (1956) The volcanic geology of Vestur – Skaftarfellssysla Iceland. Doctoral, Durham University

Sable JE, Houghton BF, Del Carlo P, Coltelli M (2006) Changing conditions of magma ascent and fragmentation during the Etna 122 BC basaltic Plinian eruption: Evidence from clast microtextures. J Volcanol Geotherm Res 158:333–354. doi: 10.1016/j.jvolgeores.2006.07.006

Sable JE, Houghton BF, Wilson CJN, Carey RJ (2009) Eruption mechanisms during the climax of the Tarawera 1886 basaltic Plinian eruption inferred from microtextural characteristics of the deposits. Stud Volcanol Leg George Walk Geol Soc Lond 129–154.

Sahagian DL, Proussevitch AA (1998) 3D particle size distributions from 2D observations: stereology for natural applications. J Volcanol Geotherm Res 84:173–196. doi: 10.1016/S0377-0273(98)00043-2

Schneider CA, Rasband WS, Eliceiri KW (2012) NIH Image to ImageJ: 25 years of image analysis. Nat Methods 9:671–675. doi: 10.1038/nmeth.2089

Shea T, Houghton BF, Gurioli L, et al (2010) Textural studies of vesicles in volcanic rocks: An integrated methodology. J Volcanol Geotherm Res 190:271–289. doi: 10.1016/j.jvolgeores.2009.12.003

Sigl M, Winstrup M, McConnell JR, et al (2015) Timing and climate forcing of volcanic eruptions for the past 2,500 years. Nature 523:543–549. doi: 10.1038/nature14565

Sigurðardóttir SS, Gudmundsson MT, Hreinsdóttir S (2015) Mapping of the Eldgjá lava flow on Mýrdalssandur with magnetic surveying. Jökull 65:61–71.

Sparks RSJ (2003) Dynamics of magma degassing. Geol Soc Lond Spec Publ 213:5–22. doi: 10.1144/GSL.SP.2003.213.01.02

Stevenson JA, Loughlin SC, Font A, et al (2013) UK monitoring and deposition of tephra from the May 2011 eruption of Grímsvötn, Iceland. J Appl Volcanol 2:1–17. doi: 10.1186/2191-5040-2-3

Stovall WK, Houghton BF, Gonnermann H, et al (2011) Eruption dynamics of Hawaiian-style fountains: the case study of episode 1 of the Kīlauea Iki 1959 eruption. Bull Volcanol 73:511–529. doi: 10.1007/s00445-010-0426-z

Stovall WK, Houghton BF, Hammer JE, et al (2012) Vesiculation of high fountaining Hawaiian eruptions: episodes 15 and 16 of 1959 Kīlauea Iki. Bull Volcanol 74:441–455. doi: 10.1007/s00445-011-0531-7

Taddeucci J, Pompilio M, Scarlato P (2004) Conduit processes during the July–August 2001 explosive activity of Mt. Etna (Italy): inferences from glass chemistry and crystal size distribution of ash particles. J Volcanol Geotherm Res 137:33–54. doi: 10.1016/j.jvolgeores.2004.05.011

Thordarson T, Miller DJ, Larsen G, et al (2001) New estimates of sulfur degassing and atmospheric mass-loading by the 934 AD Eldgjá eruption, Iceland. J Volcanol Geotherm Res 108:33–54. doi: 10.1016/S0377-0273(00)00277-8

Thordarson T, Self S (1993) The Laki (Skaftár Fires) and Grímsvötn eruptions in 1783–1785. Bull Volcanol 55:233–263.

Thordarson T, Self S (2003) Atmospheric and environmental effects of the 1783–1784 Laki eruption: A review and reassessment. J Geophys Res. doi: 10.1029/2001JD002042

Thordarson T, Self S, Miller DJ, et al (2003) Sulphur release from flood lava eruptions in the Veidivotn, Grimsvotn and Katla volcanic systems, Iceland. Geol Soc Lond Spec Publ 213:103–121. doi: 10.1144/GSL.SP.2003.213.01.07

Thordarson T, Self S, Oskarsson N, Hulsebosch T (1996) Sulfur, chlorine, and fluorine degassing and atmospheric loading by the 1783–1784 AD Laki (Skaftár Fires) eruption in Iceland. Bull Volcanol 58:205–225.

Walker GPL, Croasdale R (1971) Characteristics of some basaltic pyroclastics. Bull Volcanol 35:303–317.

Wilson L, Head JW (1981) Ascent and eruption of basaltic magma on the Earth and Moon. J Geophys Res Solid Earth 86:2971–3001. doi: 10.1029/JB086iB04p02971

Wilson TM, Stewart C, Sword-Daniels V, et al (2012) Volcanic ash impacts on critical infrastructure. Phys Chem Earth Parts ABC 45–46:5–23. doi: 10.1016/j.pce.2011.06.006

Wohletz KH (1986) Explosive magma-water interactions: Thermodynamics, explosion mechanisms, and field studies. Bull Volcanol 48:245–264. doi: 10.1007/BF01081754

Wohletz KH, Zimanowski B, Büttner R (2013) Magma-water interactions. In: Fagents SA, Gregg TKP, Lopes RMC (eds) Modelling volcanic processes: the physics and mathematics of volcanism, 1st edn. Cambridge University Press, Cambridge, p 421

Zielinski GA, Germani MS, Larsen G, et al (1995) Evidence of the Eldgjá (Iceland) eruption in the GISP2 Greenland ice core: relationship to eruption processes and climatic conditions in the tenth century. The Holocene 5:129–140. doi: 10.1177/095968369500500201

Zielinski GA, Mayewski PA, Meeker LD, et al (1994) Record of Volcanism Since 7000 B.C. from the GISP2 Greenland Ice Core and Implications for the Volcano-Climate System. Science 264:948–952. doi: 10.1126/science.264.5161.948

Paper III

Variation of eruption style and magma composition during a fissure eruption

William M. Moreland[1, 2, *], Thorvaldur Thordarson[2], Bruce F. Houghton[3], Gudrun Larsen[1], D. Jay Miller[4]
* wmm2@hi.is
[1] Institute of Earth Sciences, University of Iceland, Askja, Sturlugata 7, 101 Reykjavík, Iceland
[2] Faculty of Earth Sciences, University of Iceland, Askja, Sturlugata 7, 101 Reykjavík, Iceland
[3] Department of Geology and Geophysics, SOEST, University of Hawai'i at Mānoa, Honolulu, HI 96822, USA
[4] International Ocean Drilling Program, Texas A & M University Research Park, 1000 Discovery Drive, College Station, Texas 77845–9547, USA

Abstract

The 10th century Eldgjá basaltic flood lava eruption in southern Iceland erupted up to 21.0 km^3 of magma, 1.3 km^3 dense rock equivalent (DRE) as tephra. Explosive activity took place in at least 16 discrete phases which produced a composite tephra stratigraphy. By mapping the individual deposits and chemically analysing this stratigraphy it has been possible to constrain the evolution of the magma source both temporally and spatially. The Eldgjá products are on the primitive end of the Katla volcanic system's (the system of which Eldgjá is included) compositional spectrum. The Eldgjá products show a compositional evolution with time, a trend which conflicts with the model of extracting magma from a compositionally-zoned magma chamber. Further, detailed isopach maps of the Eldgjá tephra deposits demonstrate that activity did not simply propagate along the fissure but instead focused around one spot and made repeated switches to and fro across this region.

Introduction

Large volume basaltic flood lava eruptions occur in Iceland roughly every couple hundred years (Thordarson and Höskuldsson 2008) and are defined as events producing more than 1 km^3 of lava. Although these events are often classed as effusive due to over 95% of the erupted magma forming lava (Thordarson and Larsen 2007), the sheer volume of these events means that just a few percent of tephra production can be significant (1.3 km^3 dense rock equivalent for Eldgjá tephra). They may also exhibit explosive phases which, in combination with the high thermal output of effusive volcanism (Stothers et al. 1986), produce eruption columns of up to 20 km (Stothers et al. 1986; Thordarson and Self 1993; Woods 1993). Previous studies have suggested that activity was confined to limited lengths of fissure at a time (Thordarson and Self 1998; Brown et al. 2014) and that magma discharge rates were similar to the maximum rates recorded for historical flood lava eruptions (1783 Laki eruption, ~4000 $m^3\ s^{-1}$, Thordarson and Self 1993; Self et al. 1998).

Basaltic flood lava eruptions have the potential to be major polluting events causing acid rain, climate change through the modification of cloud albedoes and lifetimes (Jones et al. 2001), and generation of fine particles which are hazardous to respiratory systems (Schmidt et

al. 2011). As flood lava eruptions can continue for months to years (Self et al. 1997), voluminous tephra production from these events could have significant impacts on both local and global society and environment. For this reason, it is important to fully understand how the explosive activity during these mostly effusive events takes place.

The Eldgjá fissures

The 10th century eruption of Eldgjá is here used as a case study of a large volume basaltic flood lava eruption. Eldgjá is the fissure system associated with the Katla volcanic system in southern Iceland. Its surface expression is a ~70-km-long mixed cone row, which stretches from

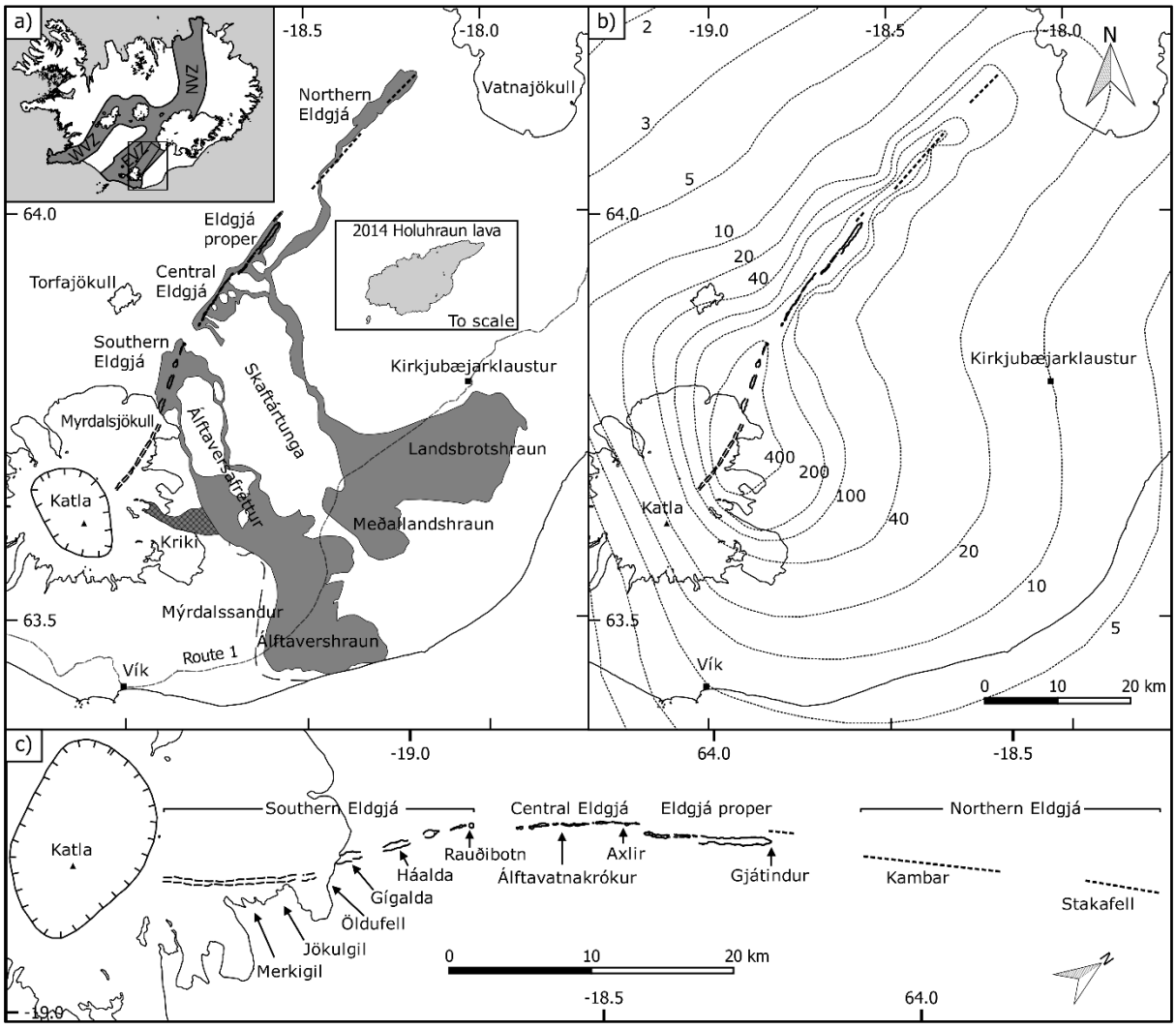

Figure 1 ***a)*** *Map of the Eldgjá fissure and lava fields and the names of surrounding areas. The dashed line to the west of Álftavershraun indicates the suspected buried margin of the lava beneath Mýrdalssandur as mapped by Sigurðardóttir et al. (2015). The outline of the 2014-15 Holuhraun lava, erupted in the north of Iceland, has been overlain for comparison of size. Its volume is 1.44 km^3 (Pedersen et al. 2017) compared to 1.3 km^3 DRE for the Eldgjá tephra alone.* ***b)*** *Isopach map for the entire tephra deposit of Eldgjá (Larsen 2000).* ***c)*** *Map of the Eldgjá fissure system with locality names. Outlines of the subaerial Southern, Central, and Eldgjá proper segments are after Robson (1956). The dashed outline of the subglacial Southern Eldgjá segment is inferred from radio-echo soundings (Björnsson et al. 2000)*

beneath Mýrdalsjökull in the southwest to Vatnajökull in the northeast (Figure 1). Eldgjá produced up to 19.7 km^3 of lava (Sigurðardóttir et al. 2015) including at least 0.5 km^3 of hyaloclastite flow at Kriki (Figure 1, Larsen 2000). It also produced 1.3 km^3 of tephra (dense rock equivalent, DRE; Larsen 2000) in over sixteen distinct explosive phases.

The Eldgjá fissure system is discontinuous and can be split into four fissure segments on this basis: 1) Southern Eldgjá, 2) Central Eldgjá, 3) Eldgjá proper, and 4) Northern Eldgjá. A detailed map of the Southern, Central, and Eldgjá proper segments was made by Robson (1956), which allows the segments to be split up into individual vents (Figure 1). The Northern fissure was not mapped as Eldgjá until later, by Miller (1989).

The Southern fissure disappears under Mýrdalsjökull near Öldufell and, as the glaciers of Iceland retreat, more of the fissure is being exposed. In the c.60 years since Robson mapped the Eldgjá fissures, another Southern vent has been uncovered from the ice. This vent has no name and given its proximity to Háalda (Robson's vent A) has been here labelled as Gígalda.

Although the Eldgjá fissure is known to continue a significant distance under the Mýrdalsjökull ice based upon whole-deposit isopach maps (Larsen 2000), it has been difficult to identify it definitively using land or satellite-based radar. By mapping the fallout from individual units of Eldgjá it is possible to distinguish two hotspots of explosive activity beneath the ice. These two subglacial segments are labelled here as Merkigil and Öldufell. Merkigil is the southwestern-most region, located directly west of Merkigil and Jökulgil. The Öldufell segment is west and southwest of the mountain Öldufell. For the purpose of describing large-scale activity the Merkigil and Öldufell segments are considered to be part of the Southern Eldgjá fissure.

Methods

The thickness of each tephra unit was mapped out in detail to create isopach maps. In addition to measuring the thickness, each unit was described in terms of grain-size, sorting, grading, morphological composition, and nature of the upper and lower contacts with adjacent units. Units with distinct characteristics, such as unusual lithic content or distinctive grading, were used to ease the tracking of more mundane units across the field area. Tephra thickness measurements were taken at a total of 141 locations, and the resulting isopach maps used to constrain the source of each tephra unit.

Eldgjá tephra samples from a range of localities and stratigraphic heights were collected for geochemical analysis (Figure 2). These samples expand a pre-existing sample suite of Eldgjá lava collected by Miller (1989). Major and trace element analysis of tephra and lava samples was carried out by X-ray fluorescence spectrometry. Samples were prepared for XRF by preparing fused glass discs for major element analysis and pressed powder pellets for trace elements. The methods used in the preparation followed those outlined by Fitton et al. (1998) with modifications noted by Fitton & Godard (2004). Analytical precision and accuracy are comparable to the values reported by Fitton et al. (1998).

Results

The sequence of explosive events

Explosive activity during the Eldgjá eruption occurred as a series of distinct phases originating from discrete segments of the fissure system. Although the locus of activity generally

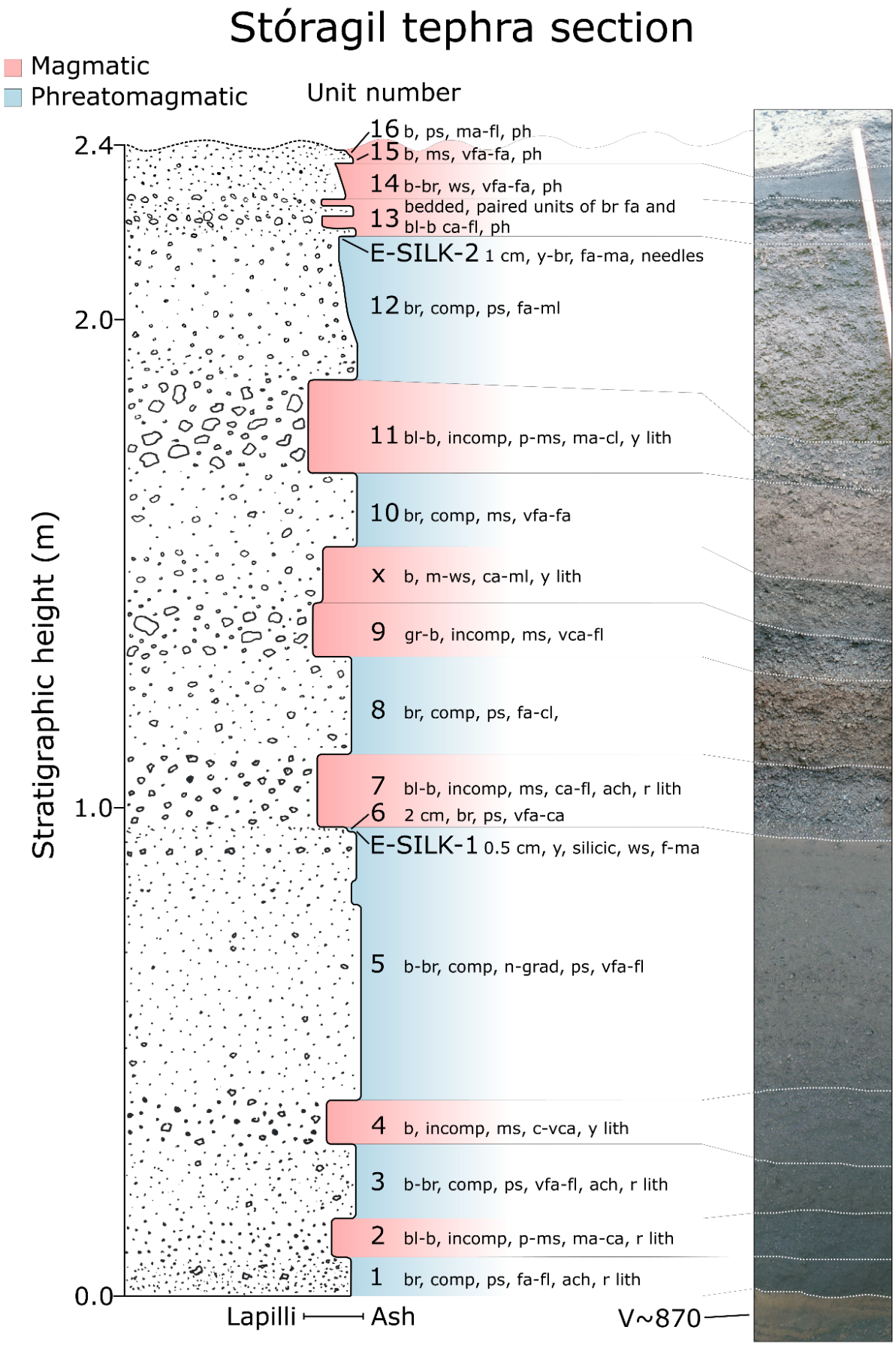
Stóragil tephra section
Magmatic
Phreatomagmatic
Unit number
16 b, ps, ma-fl, ph
15 b, ms, vfa-fa, ph
14 b-br, ws, vfa-fa, ph
13 bedded, paired units of br fa and bl-b ca-fl, ph
E-SILK-2 1 cm, y-br, fa-ma, needles
12 br, comp, ps, fa-ml
11 bl-b, incomp, p-ms, ma-cl, y lith
10 br, comp, ms, vfa-fa
x b, m-ws, ca-ml, y lith
9 gr-b, incomp, ms, vca-fl
8 br, comp, ps, fa-cl,
7 bl-b, incomp, ms, ca-fl, ach, r lith
6 2 cm, br, ps, vfa-ca
E-SILK-1 0.5 cm, y, silicic, ws, f-ma
5 b-br, comp, n-grad, ps, vfa-fl
4 b, incomp, ms, c-vca, y lith
3 b-br, comp, ps, vfa-fl, ach, r lith
2 bl-b, incomp, p-ms, ma-ca, r lith
1 br, comp, ps, fa-fl, ach, r lith
Stratigraphic height (m)
2.4
2.0
1.0
0.0
Lapilli
Ash
V~870

Figure 2 (overleaf) Tephra stratigraphy of Eldgjá showing the composite nature of the deposit. Red and blue colouring indicates the magmatic and phreatomagmatic units respectively. The photograph is a composite of four photos, split at the top of units 1, 5, 10, and 12. The unit shown in the photograph below Eldgjá and separated by soil is the ~870 CE deposit from Vatnaöldur (Larsen 1984). Abbreviations in the unit descriptions are as follows: b, black; br, brown; gr, grey; y, yellow; r, red; (in)comp, (in)competent; p/m/ws, poorly-/moderately-/well-sorted; vf/f/m/ca or l, very fine/fine/medium/coarse ash or lapilli; ach, achnelith; ph, Pele's hair; lith, lithic. E-SILK refers to Eldgjá silicic Katla. Unit x is a magmatic unit which appears in the Stóragil section but is not preserved in enough other locations to allow its source vent to be identified

progressed from southwest to northeast, activity recurred at several segments throughout the eruption. Evidence of the sequential explosive activity is preserved as units of tephra fall within the Eldgjá tephra deposit, with each unit generally recording a single explosive phase (Figure 2 and Figure 3).

Unit 1

The first explosive phase occurred at a fissure segment beneath Mýrdalsjökull, near to the present-day edge of the glacier. This phase is recorded in the stratigraphy as a brown, very poorly-sorted, very fine ash to lapilli fall deposit within 15 km of source. The colour is a result of the thin, translucent bubble walls which make up the ash component and the poor sorting results in a well-packed unit which is resistant to erosion. This unit features a sharp lower contact with soil, showing no sign of earlier explosive activity. This unit is categorized as phreatomagmatic and is the stereotype for such units within the Eldgjá tephra fall deposits. The volume of unit 1 is 0.012 km^3 (all volumes are given as dense rock equivalent, DRE).

Unit 2

The second phase recorded in the stratigraphy consists of a moderately- to poorly-sorted, coarse ash to medium lapilli within 15 km of source. This was a magmatic phase which originated from the Rauðibotn crater on the Southern Eldgjá fissure. Achneliths are a major component of this and all other Eldgjá magmatic units, and the metallic lustre of these clasts give the magmatic units a blue-black colour. The coarse grainsize of this unit, and other magmatic units of Eldgjá, means that it is unconsolidated and often weathers out. The volume of unit 2 is 0.042 km^3.

Units 3 and 4

These minor explosive phases produced deposits with limited dispersal and are only found in the northern end of the Hólmsá valley. It is possible that these two units represent a continuation of phase 2 due to similarities in composition and location of deposition.

Unit 5

Phase 5 is the most voluminous phreatomagmatic event of the Eldgjá eruption, producing 0.091 km^3 of tephra. This phase marks the first return to subglacial activity after activity had shifted to subaerial segments. It originates from a subglacial fissure segment southwest of Öldufellsjökull where radio echo soundings have revealed a depression flanked by a steep ridge striking N33°E (Björnsson et al. 2000). This is also the source of units 8 and 10. It is a moderately- to well-sorted deposit consisting of black fine to medium ash within 15 km of

source. It is normally graded with the exception of a distinctive, discontinuous medium lapilli layer near the top.

Unit 6

A minor phreatomagmatic phase, producing around 0.002 km^3 of tephra, occurred immediately after phase 5. This phase originated from near the source of phase 1, located between the previous phase 5 and the next phase 7 marking a relatively gradual transition of locus of activity. This deposit appears as a thin unit composed of poorly- to moderately-sorted, black, fine to coarse ash.

Unit 7

Phase 7 was a major subaerial magmatic explosive event which took place along the length of the Southern Eldgjá fissure from Gígalda to Rauðibotn. The result was a thick, widespread poly-lobate deposit consisting of moderately-sorted very coarse ash to lapilli which is black to metallic blue in colour. The deposit is dominantly juvenile tephra comprised of basaltic pumice clasts and achneliths. The volume of unit 7 is 0.024 km^3.

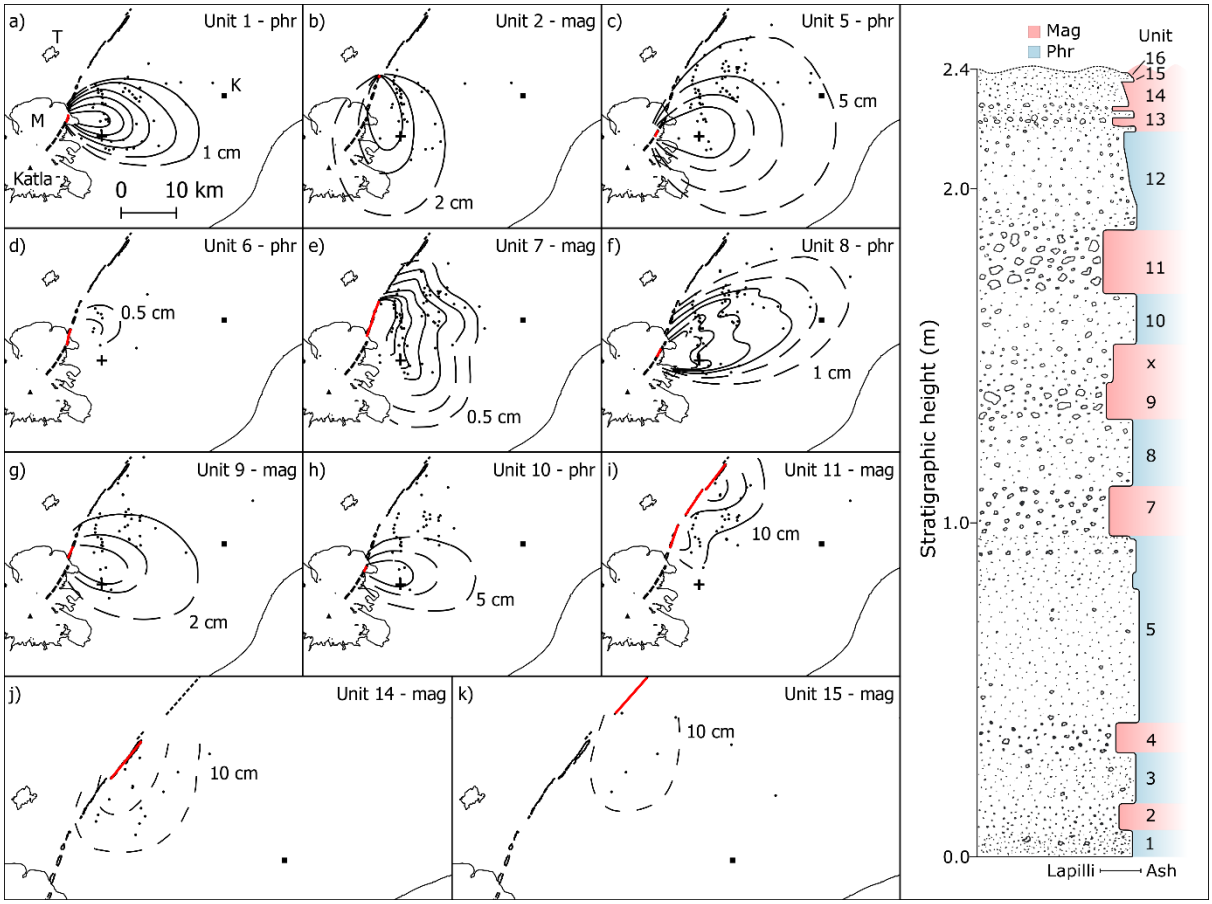

Figure 3 The sequence of explosive events as revealed by the Eldgjá tephra stratigraphy and shown using isopach maps. For the names of active vents (red lines) refer to Figure 1c. The location of the example stratigraphic section, Stóragil, is shown by a cross. The abbreviations in a) are: M, Mýrdalsjökull; K, Kirkjubæjarklaustur; T, Torfajökull. Dashed isopach lines indicate areas of inadequate data. Isopach maps with thickness labels are available in the supplementary material

Unit 8

Phase 8 marked the fourth recurrence of subglacial phreatomagmatic activity. This deposit consists of typical phreatomagmatic tephra as described above and its volume is 0.029 $km^{3.}$ This phase covered the area of Kirkjubæjarklaustur in nearly 2 cm of tephra.

Unit 9

This magmatic phase marked the end of activity on the southwestern end of the Southern Eldgjá fissure at Gígalda. It is a typical magmatic deposit in most respects except that it is greyer in appearance. The reason for this colour change is unclear. It contains a discontinuous layer of medium lapilli near the top. The volume of unit 9 is 0.043 km^3.

Unit 10

Phase 10 marked the fifth recurrence of subglacial activity and originates from the same length of subglacial fissure as phases 5 and 8, producing a 0.050 km^3 phreatomagmatic deposit. This unit is brown, well-packed, and reverse graded from moderately sorted fine- to medium-ash to medium- to coarse-ash at the top. There is a discontinuous layer of fine- to medium-lapilli at the top of this unit.

Unit 11

Phase 11 is the second major magmatic event which involved a significant length of subaerial fissure. It is composed of typical magmatic tephra which is poorly sorted and coarse ash to medium lapilli. There is at least one horizon composed of dominantly medium to coarse ash. In the upland areas of the Hólmsá valley (Álftaversafréttur) and Skaftártunga, the Eldgjá tephra is often without soil and vegetation cover. As a result of this Units 11 and 12, which are often the uppermost units present, are not always entirely preserved. It was not possible to calculate an accurate volume for unit 11.

Unit 12

Unit 12 is very rarely preserved in the stratigraphy given its position in the sequence and that it is rarely covered by soil or vegetation which would protect it from erosion. As a result of this there are not sufficient measurements to produce an isopach map. However, based upon the deposit characteristics it is possible to identify phase 12 as phreatomagmatic. It is brown in colour, poorly- to moderately-sorted and well packed.

Events inside the Katla caldera

The Kriki hyaloclastite, which is partially covered by ice to the east of Katla, (Figure 1) is thought to have been erupted from the Katla caldera during the Eldgjá eruption (Larsen 2000). It has a volume of at least 0.5 km^3 outside of the ice. There are also at least two one-millimetre-thick (in Skaftártunga) units of silicic tephra which are included within the Eldgjá stratigraphy (E-SILK in Figure 2). The lower silicic tephra unit occurs immediately above unit 5 and is of fine to medium ash. The upper silicic unit occurs immediately above unit 12 and is also fine to medium ash but also contains tube pumices of coarse ash size, characteristic of Katla silicic prehistoric units (Larsen 2000). The composition of the Eldgjá silicic units are typical of Katla SILK tephra with an andesite-dacite composition (Thordarson 2017 pers. comm.).

Jökulhlaups

At least three jökulhlaups are known to have occurred as a result of subglacial activity during Eldgjá. Two emerged from Sléttjökull and Öldufellsjökull to the north and northeast edges of Mýrdalsjökull respectively, either side of Öldufell, and one from Sandfellsjökull, south of Merkigil (Larsen 2000; Kjær et al. 2004). A thick jökulhlaup sequence is preserved within the Eldgjá stratigraphy at Loðnugil (63.73485°N, -18.72905°E) and appears above unit 1 and below unit 7. This sequence may preserve at least two individual jökulhlaups which would have originated from the Sléttjökull outlet glacier.

Petrology

The Eldgjá products are mildly alkalic and their bulk chemical composition defines them as alkali basalt on the classification scheme of Le Bas and Streckeisen (1991; Figure 5a). Whilst the alkali character is typical of mafic magma from the Katla volcanic system, the Eldgjá data is, on average, more primitive than other basalts from Katla (Figure 5d).

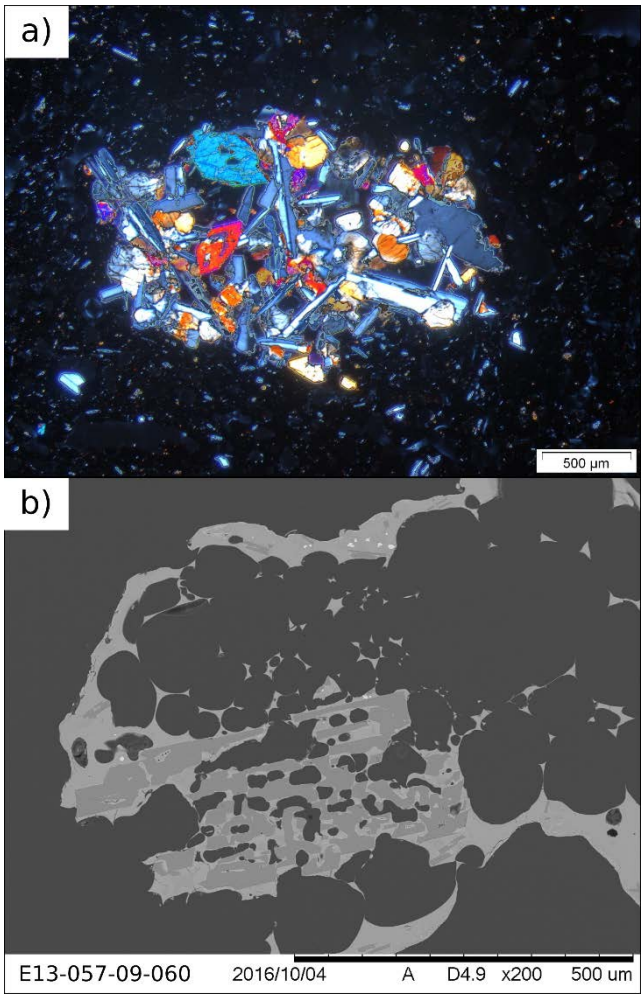

Figure 4 ***a)*** *Photomicrograph of a glomerocryst in Eldgjá tephra (sample E13-057-30-096);* ***b)*** *SEM image of a skeletal plagioclase phenocryst surrounded by vesicles in Eldgjá tephra (sample E13-057-09-060)*

The Eldgjá tephra and lavas are essentially aphyric, containing less than 2% phenocrysts by volume, with a macrocryst assemblage consisting of plagioclase (An_{65-92}), clinopyroxene ($En_{40}Fs_{17}Wo_{43}$–$En_{46}Fs_{8}Wo_{46}$), olivine (Fo_{70-89}), and magnetite (Thordarson et al. 2001). Most macrcrysts are euhedral except the plagioclase which are typically sieve-textured and are present as individual crystals and as glomerocrysts (Figure 4).

Selected major and trace element concentrations versus MgO content are shown in Figure 5. Whole-rock MgO contents vary from 5.0 to 5.7 wt.%. The CaO–MgO trend (Figure 5c) is entirely a positive linear correlation indicating that plagioclase and clinopyroxene were the controlling fractionating phases. Fractional crystallization calculations assuming 12% crystallization of 70% clinopyroxene and 30% plagioclase reproduce this trend (Figure 5c).

The chemical analyses of tephra from the stratigraphic section at Stóragil demonstrate how the chemical composition of the Eldgjá magma becomes more evolved with time (Figure 6). The concentration of MgO in early tephra units is between 5.6 and 5.7 wt.%, and drops to almost 5.0 wt.% with time. This pattern is also seen in FeO_T, and CaO. The remainder of the major elements show increasing concentrations with time; for example, TiO_2 increases from 4.3 to 4.7 wt.%. The incompatible trace element concentrations increase with time; for example, Ba increases from 161 to 210 ppm.

The ratio of Zr to Nb is effectively constant throughout the Stóragil stratigraphy, varying between 6.8 and 7.1. This demonstrates that the observed compositional range in the major and trace elements must be a result of fractional crystallization, and not magma mixing as that would require mixing a high MgO magma with a low MgO magma with both having identical incompatible element ratios.

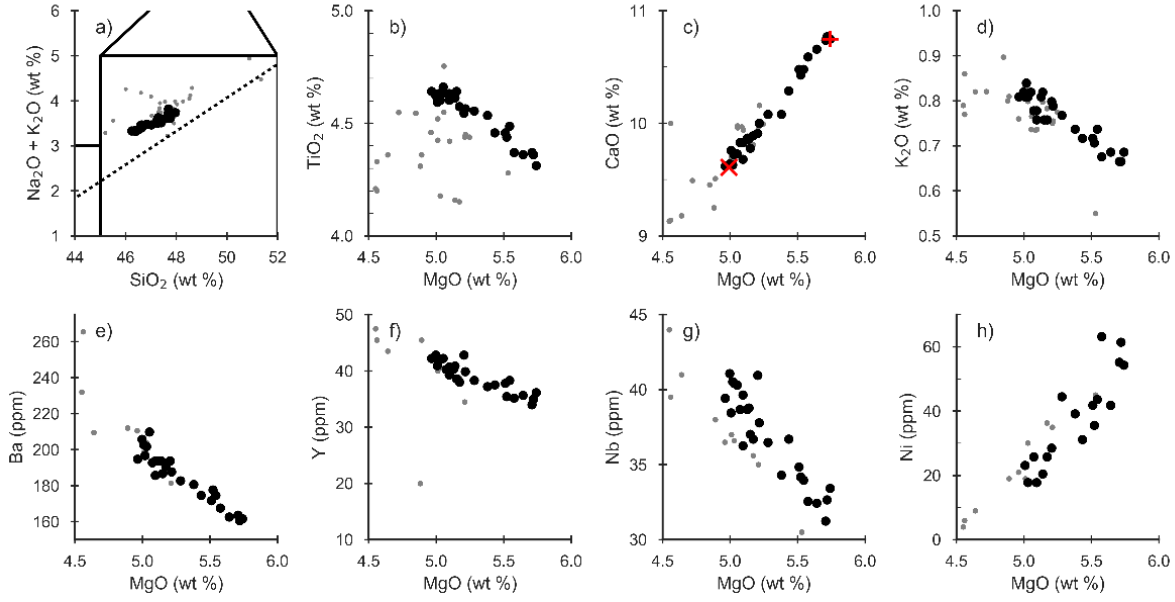

Figure 5 ***a)*** *Total-alkali – silica diagram showing the transitional alkali nature of the Eldgjá basalts. Black lines delineate the compositional fields of Le Bas and Streckeisen 1991, and the dotted line is the MacDonald and Katsura line (1964) separating alkaline (above) and tholeiitic basalts (below).* ***b) to h)*** *bivariate plots exhibiting the variation in major and trace element concentrations in the Eldgjá volcanic products. Red symbols in c) indicate starting composition (+) and modelled end composition (x) after 12% fractional crystallization of 70% clinopyroxene and 30% plagioclase. Grey circles represent Katla mafic products from the literature (Jakobsson 1979; Einarsson et al. 1980; Steinthorsson et al. 1985; Lacasse et al. 2007)*

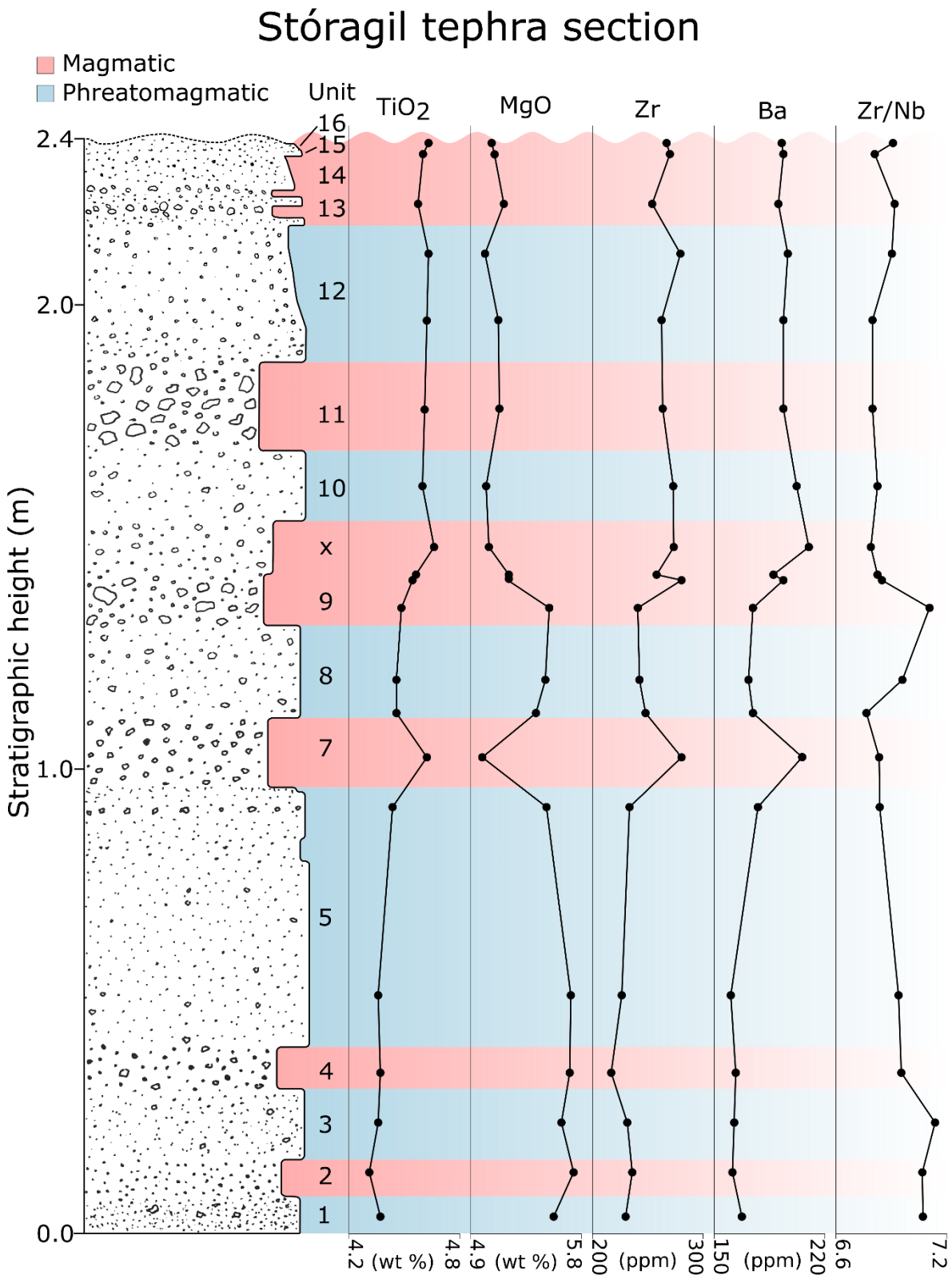

Figure 6 Element – profile plots for selected elements measured in tephra from the Stóragil section. Every plot demonstrates the magma composition evolving with time; incompatible elements increase and compatible elements decreases with stratigraphic height/time

Discussion

Sequence of activity

The evidence presented here demonstrates that the first explosive activity of the Eldgjá event occurred beneath Mýrdalsjökull on the Öldufell fissure with phase 1 (Figure 1c and Figure 3). This event would go on to typify the Eldgjá subglacial events in grain-size, colour, and volume. Explosive activity next took place from the subaerial Rauðibotn vent at the eastern-most end of the Southern Eldgjá segment. This phase 2 was markedly different to phase 1 in colour and grain-size but was a similar order of magnitude in terms of volume. Activity returned to beneath the glacier, this time taking place further southwest than the origin of phase 1, erupting from the Merkigil fissure segment. This was phase 5 and was the most voluminous explosive phase. The next significant explosive phase (phase 7) marked a return to subaerial activity, this time involving the entirety of the Southern Eldgjá fissure. Immediately after this was more subglacial activity, creating the phase 8 phreatomagmatic unit. Activity continues to become subaerial (phase 9 and 11) then subglacial (phase10 and 12) twice more before finally settling on subaerial segments and proceeding to the northeast with time (phases 13 to 16; Figure 3).

Length of fissures

A distinguishing feature of the eruptive styles of the subaerial and subglacial phases is that all of the magmatic phases involved long (>10 km) segments of the fissure system, with the exception of phase 2. The subglacial phases seem to have been concentrated on shorter lengths of the system. This may be a result of difficulties in breaking through the glacier ice to allow the eruption and deposition of tephra. Phase 2 is the exception to the magmatic case and this phase features one of the most distinctive vents of the entire system: Rauðibotn (Figure 1). Rauðibotn is a 300-m wide and 150 m deep circular volcanic crater which may predate Eldgjá (Robson 1956). The oxidised lava which form the sides of the crater give it its name – *red bottom*. It is suggested that phase 2 took advantage of this pre-existing structure and magma flow was concentrated here. That later phases make use of the entirety of the Southern Eldgjá segment suggests that magma flux rates increased.

The taking advantage of pre-existing features did not stop with Rauðibotn. When phase 11 begins erupting from the Central Eldgjá and Eldgjá proper segments, the latter is taking advantage of a pre-existing 270-m-deep depression which runs for 8 km to Gjátindur, where the segment terminates.

Variation in magma composition

Whole-rock composition of the tephra units at Stóragil show that the bulk chemical composition of the magma erupted during the Eldgjá eruption became more evolved with time. This trend holds even when the source of the tephra was moving to and fro along the Southern Eldgjá fissure. As an example, units 1 and 10 were both erupted from the Öldufell segment (Figure 1), are separated by units erupted from elsewhere along the fissure, and have MgO concentrations of 5.6 and 5.0 wt.% respectively. The trend continued to hold true when activity began to propagate away from the Southern Eldgjá fissure towards Central and then Eldgjá proper. The data indicate that the Eldgjá magma was not formed by magma mixing and instead

evolved by fractional crystallization. The aphyric nature of the products raises questions about the origin of the magma.

One possible magma source which explains the trend in composition may be a stratified magma chamber which is tapped to supply a changing magma composition. However, given that this typically means more evolved magma overlying more primitive magma, the chamber would have to either be tapped from below the level of evolved magma or have the more primitive magma extracted through the evolved magma. If the former scenario were the case, aphyric Eldgjá products would unlikely as crystals settling out of the magma chamber would be extracted along with the melt. The latter scenario is also unlikely as the data show no evidence of mixing which would be difficult to avoid while extracting one magma through another.

An alternative source of the magma is from a relatively deep storage region. If this region was situated beneath Öldufell, then the surface activity switching back and forth might reflect the early, primitive magma establishing a conduit. As the conduit was being established and began to extend to the northeast, crustal residence times increased for the magma which promoted crystallization. The crystals were left behind by settling out and the more evolved, aphyric magma was able to erupt at the surface.

Focus of activity

Although the explosive activity of Eldgjá progressed from southwest to northeast with time in general, the tephra stratigraphy demonstrates that this was not simply the case. Rather activity began at a location to northeast of Katla and behind Öldufell and fluctuated around this point before taking advantage of pre-existing upper crustal structures (the Álftavötn and Eldgjá grabens) and moving to the northeast.

It is difficult to reconcile this behaviour with the model put forward for the 2014-2015 Bárðarbunga–Holuhraun seismic event and fissure eruption (Sigmundsson et al. 2014; Gudmundsson et al. 2016; Pedersen et al. 2017; Reynolds et al. 2017) which involves a lateral dyke (identified by earthquakes) supplying basaltic magma from a magma chamber beneath Bárðarbunga to a fissure eruption at Holuhraun.

Conclusions

1) The Eldgjá basaltic fissure eruption consisted of over sixteen explosive phases individually producing volumes of tephra between 0.002 and 0.091 km^3 DRE.
2) The magma composition of Eldgjá varied through time with the earliest products being most primitive, irrespective of where along the fissure the magma was erupted from.
3) The data do not support a model of magma extraction from a chemically stratified magma chamber in which case the earliest products would be the least primitive.

References

Björnsson H, Pálsson F, Guðmundsson MT (2000) Surface and bedrock topography of the Mýrdalsjökull ice cap. Jökull 49:29–46.

Brown RJ, Blake S, Thordarson T, Self S (2014) Pyroclastic edifices record vigorous lava fountains during the emplacement of a flood basalt flow field, Roza Member, Columbia River Basalt Province, USA. Geol Soc Am Bull 126:875–891. doi: 10.1130/B30857.1

Einarsson EH, Larsen G, Thorarinsson S (1980) The Sólheimar tephra layer and the Katla eruption of ~1357. Acta Nat Isl 28:1–24.

Gudmundsson MT, Jónsdóttir K, Hooper A, et al (2016) Gradual caldera collapse at Bárdarbunga volcano, Iceland, regulated by lateral magma outflow. Science 353:aaf8988. doi: 10.1126/science.aaf8988

Jakobsson SP (1979) Petrology of recent basalts of the Eastern Volcanic Zone, Iceland. Icelandic Museum of Natural History

Jones A, Roberts DL, Woodage MJ, Johnson CE (2001) Indirect sulphate aerosol forcing in a climate model with an interactive sulphur cycle. J Geophys Res Atmospheres 106:20293–20310. doi: 10.1029/2000JD000089

Kjær KH, Sultan L, Krüger J, Schomacker A (2004) Architecture and sedimentation of outwash fans in front of the Mýrdalsjökull ice cap, Iceland. Sediment Geol 172:139–163. doi: 10.1016/j.sedgeo.2004.08.002

Lacasse C, Sigurdsson H, Carey SN, et al (2007) Bimodal volcanism at the Katla subglacial caldera, Iceland: insight into the geochemistry and petrogenesis of rhyolitic magmas. Bull Volcanol 69:373. doi: 10.1007/s00445-006-0082-5

Larsen G (1984) Recent volcanic history of the Veidivötn fissure swarm, southern Iceland — an approach to volcanic risk assessment. J Volcanol Geotherm Res 22:33–58. doi: 10.1016/0377-0273(84)90034-9

Larsen G (2000) Holocene eruptions within the Katla volcanic system, south Iceland: characteristics and environmental impact. Jökull 49:1–28.

Le Bas MJ, Streckeisen AL (1991) The IUGS systematics of igneous rocks. J Geol Soc 148:825–833. doi: 10.1144/gsjgs.148.5.0825

Macdonald GA, Katsura T (1964) Chemical Composition of Hawaiian Lavas. J Petrol 5:82–133. doi: 10.1093/petrology/5.1.82

Miller DJ (1989) The 10th Century eruption of Eldgjá, southern Iceland. Nordic Volcanological Institute, Reykjavík

Pedersen GBM, Höskuldsson A, Dürig T, et al (2017) Lava field evolution and emplacement dynamics of the 2014–2015 basaltic fissure eruption at Holuhraun, Iceland. J Volcanol Geotherm Res. doi: 10.1016/j.jvolgeores.2017.02.027

Reynolds HI, Gudmundsson MT, Högnadóttir T, et al (2017) Subglacial volcanic activity above a lateral dyke path during the 2014–2015 Bárdarbunga-Holuhraun rifting episode, Iceland. Bull Volcanol 79:38. doi: 10.1007/s00445-017-1122-z

Robson GR (1956) The volcanic geology of Vestur – Skaftarfellssysla Iceland. Doctoral, Durham University

Schmidt A, Ostro B, Carslaw KS, et al (2011) Excess mortality in Europe following a future Laki-style Icelandic eruption. Proc Natl Acad Sci 108:15710–15715.

Self S, Keszthelyi L, Thordarson T (1998) The Importance of Pāhoehoe. Annu Rev Earth Planet Sci 26:81–110. doi: 10.1146/annurev.earth.26.1.81

Self S, Thordarson T, Keszthelyi L (1997) Emplacement of Continental Flood Basalt Lava Flows. In: Large Igneous Provinces: Continental, Oceanic, and Planetary Flood Volcanism. American Geophysical Union, pp 381–410

Sigmundsson F, Hooper A, Hreinsdóttir S, et al (2014) Segmented lateral dyke growth in a rifting event at Bárðarbunga volcanic system, Iceland. Nature 517:191–195. doi: 10.1038/nature14111

Sigurðardóttir SS, Gudmundsson MT, Hreinsdóttir S (2015) Mapping of the Eldgjá lava flow on Mýrdalssandur with magnetic surveying. Jökull 65:61–71.

Steinthorsson S, Oskarsson N, Sigvaldason GE (1985) Origin of alkali basalts in Iceland: A plate tectonic model. J Geophys Res Solid Earth 90:10027–10042. doi: 10.1029/JB090iB12p10027

Thordarson T, Höskuldsson Á (2008) Postglacial volcanism in Iceland. Jökull 58:197–228.

Thordarson T, Larsen G (2007) Volcanism in Iceland in historical time: Volcano types, eruption styles and eruptive history. J Geodyn 43:118–152. doi: 10.1016/j.jog.2006.09.005

Thordarson T, Miller DJ, Larsen G, et al (2001) New estimates of sulfur degassing and atmospheric mass-loading by the 934 AD Eldgjá eruption, Iceland. J Volcanol Geotherm Res 108:33–54. doi: 10.1016/S0377-0273(00)00277-8

Thordarson T, Self S (1998) The Roza Member, Columbia River Basalt Group: A gigantic pahoehoe lava flow field formed by endogenous processes? J Geophys Res Solid Earth 103:27411–27445. doi: 10.1029/98JB01355

Thordarson T, Self S (1993) The Laki (Skaftár Fires) and Grímsvötn eruptions in 1783–1785. Bull Volcanol 55:233–263.